The Dissertation Committee for Caleb Vincent Funk Certifies that this is the approved version of the following dissertation

Microporous Mixed Matrix (ZeoTIPS) Membranes

Committee:

Douglas R. Lloyd, Supervisor

Steven L. Bryant

Robert B. Eldridge

Benny D. Freeman

C. Grant Willson

Microporous Mixed Matrix (ZeoTIPS) Membranes

by

Caleb Vincent Funk, B.S.

Dissertation

Presented to the Faculty of the Graduate School of

The University of Texas at Austin

in Partial Fulfillment

of the Requirements

for the Degree of

Doctor of Philosophy

The University of Texas at Austin

May 2008

Dedication

To my father

and

in memory of my grandfather,

the two greatest inspirations in my scientific and engineering endeavors.

Acknowledgements

I would like to thank by advisor, Douglas R. Lloyd, who gave me just enough free reign in the lab to learn to think on my own and learn from my mistakes while providing the encouragement, instruction, and advice I needed to become a better writer and a strong researcher. I would also like to thank the members of my Ph.D. committee, Steven L. Bryant, Robert B. Eldridge, Benny D. Freeman, and C. Grant Willson. Their input and advice helped make this research possible. In addition, David Furukawa, Robert Riley, and G. Glenn Lipscomb were important sources of guidance and support.

I also wish to thank the members of the Lloyd Group, all of which I considered friends before colleagues. Patrick Hanks was the first critic of every idea I had in my research, and was a strong supporter in every hurdle. His selfless assistance and brutal analysis of my ideas saved me countless hours of coding work and laboratory work, and his frequently-used ability to look the other way when the lab reached the "wallowing in our own filth" stage of tidiness was much appreciated. Jason Morehouse was also an important resource in the lab. Additionally, my undergraduate assistants Bonnie Beavers, Courtney Taylor, Kelsie Kaczorowski, and Caitlin Forschner were extremely valuable and were always ready to put my ideas into action. I hope they benefited as much as I did from their time in our labs.

The staff of the Chemical Engineering Department was also indispensable in my quest for a Ph.D. In particular, I'd like to thank "T" Stockman, Kay Swift, Jim Smitherman, and Butch Cunningham for always being ready to help when problems arose along the way.

I wish to thank my family for their support and encouragement, as well as my friends in Austin that helped me along the way. Finally, I'd like to thank my bride-to-be Christina for her constant support, for her willingness to listen to my frustrations every time I struck a wall in my research, and for helping to maintain my sanity through the latter half of my graduate school experience.

Microporous Mixed Matrix (ZeoTIPS) Membranes

Publication No._____

Caleb Vincent Funk, Ph.D.

The University of Texas at Austin, 2008

Supervisor: Douglas R. Lloyd

Recent work in the areas of zeolite membranes and mixed matrix membranes have inspired the development of isotropic microporous mixed matrix (ZeoTIPS) membranes, consisting of high-selectivity zeolite particles suspended in a cellular, microporous polymer matrix formed by thermally induced phase separation (TIPS). The particles form nanoporous connections between the cellular voids in the matrix, and can carry out separations independent of the choice of polymer matrix. Existing water purification and gas separation membranes have a variety of drawbacks, including durability, chemical instabilities, cost, flux, and formation difficulty. ZeoTIPS membranes address each of these drawbacks while yielding high selectivity.

Included in this work are theoretical predictions of ZeoTIPS membrane performance along with models and experiments designed to gain fundamental knowledge that can be used to develop these membranes. This dissertation discusses how zeolite particles influence the processes of droplet coarsening and pore formation in thermally induced phase separation by disrupting flow fields as well as changing local

compositions and viscosities. Additionally, a mathematical model is presented, leading to understanding of the ZeoTIPS formation process.

Polymers used in these membranes must have acceptable interactions with the zeolite particles and desired mechanical properties, but must also be able to undergo thermally induced phase separation with a non-hazardous diluent under reasonable processing conditions. Furthermore, processing conditions such as cooling rate are of vast importance in forming ZeoTIPS membranes, but the required conditions can be difficult to obtain. Thus, development of these membranes has required extensive experimental research to determine feasible polymer−diluent systems for forming the microporous matrix and to develop methods of formation.

Table of Contents

List of Tables xiii

List of Figures xiv

Chapter 1: Introduction 1

1.1 Current Membrane Technologies 1

1.1.1 Polymeric Membranes 1

1.1.2 Zeolite Membranes 3

1.1.3 Mixed Matrix Membranes 4

1.2 Thermally Induced Phase Separation 6

1.3 ZeoTIPS Membranes 9

1.4 Significance of this work 12

1.5 Structure of the dissertation 13

1.6 References 13

Chapter 2: ZeoTIPS Performance Modeling 18

2.1 Introduction 18

2.2 Parallel−Series Model Construction 21

2.3 ZeoTIPS Performance Predictions 24

2.4 Summary of Chapter 2 32

2.5 References 33

Chapter 3: TIPS Cell Size Analysis with Zeolite Filler 34

3.1 Introduction 34

3.2 Materials 35

3.3 Experimental Design 37

3.4 Experimental Procedure 38

3.5 Results and Discussion 42

3.5.1 Effects of Polymer Concentration, Cooling Rate, and Zeolite Loading on Cell Size 42

3.5.2 Effects of Initial Droplet Size and Polymer−Zeolite Affinity on Droplet Growth 48

3.6 Summary of Chapter 3 52
3.7 References 52
Chapter 4: ZeoTIPS Formation Modeling 54
4.1 Introduction 54
4.2 Cell Lattice Models 54
4.2.1 2-Dimensional Model 55
4.2.2 3-Dimensional Model 61
4.2.3 Lattice Model Conclusions 63
4.3 Random Droplet Placement Model 63
4.3.1 Model Construction 64
4.3.2 Connectivity Determination 69
4.3.3 Model Results and Discussion 69
4.3.4 Random Droplet Placement Model Conclusions 72
4.4 Summary of Chapter 4 73
4.5 References 73
Chapter 5: ZeoTIPS Formation Methods 75
5.1 Introduction 75
5.2 Materials 75
5.3 Experimental Methods 76
5.3.1 Extrusion 77
5.4 Polymer and Diluent Selection 82
5.4.1 Cell Size Control by Polymer and Diluent Selection 82
5.4.2 Polymer−Diluent−Zeolite Interaction Analysis 87
5.5 Zeolite Surface Modification 94
5.5.1 Literature overview 94
5.5.2 Experimental procedure 94
5.5.3 Results of the Zeolite Modification Studies 96
5.6 Effects of Cooling Rate on Polymer−Zeolite Adhesion 103
5.7 Summary of Chapter 5 107
5.8 References 107

Chapter 6: Liquid−Solid Thermally Induced Phase Separation for ZeoTIPS Membranes 110
6.1 Introduction....110
6.2 Materials and Methods....111
6.2.1 Materials 111
6.2.2 Membrane Systems and Phase Diagrams 112
6.2.3 Membrane Formation....114
6.3 Results and Discussion 115
6.3.1 Crystal and Pore Shape 116
6.3.2 Crystal Alignment....118
6.4 Processing Challenges 120
6.5 Application of L−S TIPS to ZeoTIPS Membranes....122
6.6 Summary of Chapter 6 127
6.7 References....128

Chapter 7: Conclusions and Recommendations 130
7.1 Conclusions....130
7.2 Recommendations for Future Work....132
7.2.1 ZeoTIPS Membrane Extrusion Downstream Processing Development....132
7.2.2 Liquid−Liquid ZeoTIPS Investigation....133
7.2.3 Liquid−Solid ZeoTIPS Investigation....134

Appendix A: Nomenclature 136

Appendix B: Matlab Code 138
B.1 2-Dimensional Lattice Model Code....138
B.2 3-Dimensional Lattice Model Code....138
B.3 3-Dimensional Random Droplet Placement Model Code 139

Appendix C: Compression Molding 141
C.1 Compression Molding Procedure 141
C.2 Compression Molding Membrane Images....142
C.3. References....144

Appendix D: TIPS Polymer−Diluent Systems Used in This Research 145
D.1 Liquid−Liquid Thermally Induced Phase Separation Systems.....145
D.2 Liquid−Solid Thermally Induced Phase Separation Systems.....148

References.....154

Vita 160

List of Tables

Table 2.1: Permeability data 25

Table 3.1: Cell size analysis experimental design 39

Table 5.1: Polymers and diluents used in the interaction strength analysis.....89

Table 6.1: Selected polar diluents for use in L−S ZeoTIPS membranes.....126

List of Figures

Figure 1.1: Schematic of a mixed matrix membrane. 4

Figure 1.2: Typical membranes made by L−L, S-L, and L−S TIPS 7

Figure 1.3: General liquid−liquid/solid−liquid TIPS phase diagram. 8

Figure 1.4: General liquid−solid/solid−liquid TIPS phase diagram....9

Figure 1.5: ZeoTIPS separation schematics 11

Figure 1.6: ZeoTIPS membrane formed from 4A zeolite, cellulose triacetate, and 2-ethyl-1,3-hexanediol. 12

Figure 2.1: Ideal and non-ideal ZeoTIPS membrane models....20

Figure 2.2: Selectivity of ideal and non-ideal ZeoTIPS membranes....26

Figure 2.3: Permeability of ideal and non-ideal ZeoTIPS membranes 26

Figure 2.4: Selectivity for ideal ZeoTIPS membranes, varying polymer permeability. 29

Figure 2.5: Performance of ideal ZeoTIPS membranes 30

Figure 2.6: Selectivity for ideal ZeoTIPS membranes, varying void permeability. 31

Figure 2.7: Selectivity for ideal ZeoTIPS membranes, varying void volume to polymer volume ratio. 32

Figure 3.1: Adjusted zeolite particle size distribution....36

Figure 3.2: SEM image of the 4A zeolite powder. 36

Figure 3.3: Test tube agitation assembly 40

Figure 3.4: Image analysis procedure....43

Figure 3.5: iPP−DPE cell size data with 20 wt-% zeolite loadings....43

Figure 3.6: iPP−DPE cell size data with 23.75 wt-% zeolite loadings 44

Figure 3.7: iPP−DPE cell size data with 27.5 wt-% zeolite loadings 44

Figure 3.8: iPP−DPE cell size data with 31.25 wt-% zeolite loadings 45

Figure 3.9: iPP−DPE cell size data with 35 wt-% zeolite loadings.....45

Figure 3.10: Cell sizes in iPP−DPE system with 27.5 wt-% polymer and cooling rate of 125ºC/min. 46

Figure 3.11: Effect of cooling rate and zeolite loading on iPP−DPE cell size 47

Figure 3.12: Typical PMMA−cyclohexanol membrane sample 49

Figure 3.13: Cell sizes in PMMA−cyclohexanol system. 49

Figure 3.14: Typical polystyrene−dodecanol ZeoTIPS sample. 51

Figure 3.15: Cell sizes in polystyrene−dodecanol system. 51

Figure 4.1: Cell structure in the 2-dimensional cell lattice model. 56

Figure 4.2: Portion of the 2-dimensional simulation 57

Figure 4.3: Results from the 2-dimensional lattice model for W/D = 1.....59

Figure 4.4: Examples of W/D ratios used in the 2-dimensional simulation.....59

Figure 4.5: Results from the 2-dimensional lattice model. 60

Figure 4.6: Normalized results from the 2-dimensional lattice model.....60

Figure 4.7: Results from the 3-dimensional pore blockage model.....62

Figure 4.8: Critical zeolite loading results from the 3-dimensional pore blockage model 62

Figure 4.9: Matlab plot of particle placements.....66

Figure 4.10: Example of droplet growth process 68

Figure 4.11: Matlab plot of particle placements with random orientation. 68

Figure 4.12: Random droplet placement pore prevention model results for the iPP−DPE system 70

Figure 4.13: Critical zeolite loading versus the number of allowed pores/cell 71

Figure 5.1: Downstream processing equipment for twin-screw extrusion.....78

Figure 5.2: SEM image of an extruded membrane surface 80

Figure 5.3: SEM image of a 30 wt-% polymer iPP−DPE membrane extruded on the fiberglass belt 81

Figure 5.4: SEM image of a 27.5 wt-% polymer PMMA−cyclohexanol membrane cooled at 125ºC/min. 85

Figure 5.5: SEM image of a 27.5 wt-% polymer PMMA−PEG200 membrane cooled at 125ºC/min. 85

Figure 5.6: SEM image of a 27.5 wt-% polymer PMMA−PEG600 membrane cooled at 125ºC/min. 86

Figure 5.7: SEM image of a 20 wt-% polymer EVAL44−glycerol membrane cooled at 125ºC/min. 86

Figure 5.8: SEM image of a 20 wt-% polymer EVAL38−glycerol membrane cooled at 125ºC/min. 87

Figure 5.9: Interaction strength behavior for various polymers and diluents.....90

Figure 5.10: Interaction strength behavior for all polymers and diluents investigated. 90

Figure 5.11: SEM image of a non-ideal EVAL44−glycerol membrane containing zeolite particles. 92

Figure 5.12: SEM image of an EVAL44−(90/10 glycerol/1,4-butanediol mixture) membrane containing zeolite particles. 92

Figure 5.13: SEM image of an EVAL38−glycerol membrane containing zeolite particles and cooled at 125ºC/min. 93

Figure 5.14: XPS spectrum showing the presence of carbon from silane additions 97

Figure 5.15: XPS spectrum showing the presence of nitrogen from the APDMES reaction. 98

Figure 5.16: EVAL44−glycerol membrane containing TMCS-modified zeolite particles 99

Figure 5.17: Polystyrene−dodecanol membranes containing unmodified and TMCS-modified zeolite particles. 100

Figure 5.18: PES−cyclohexanol membrane containing unmodified and TMCS-modified zeolite particles. 101

Figure 5.19: PMMA−cyclohexanol membranes containing unmodified and TMCS-modified zeolite particles. 102

Figure 5.20: SEM image of an extruded EVAL38−glycerol membrane containing zeolite particles 104

Figure 5.21: Extrdued iPP−DPE membranes cooled quickly and slowly 106

Figure 6.1: Phase diagram for the EVAc−benzoic acid system 113

Figure 6.2: Phase diagram for the PES−benzoic acid system 114

Figure 6.3: EVAc−benzoic acid membrane showing pores formed from crystals in a sheet morphology 117

Figure 6.4: PES−benzoic acid membrane cross section (break perpendicular to direction of crystal growth) 117

Figure 6.5: PES−benzoic acid flat sheet membrane cross section (break parallel to direction of crystal growth) 119

Figure 6.6: PES−benzoic acid hollow fiber membrane cross section (break perpendicular to the spinline) 120

Figure 6.7: Proposed structure of a L−S ZeoTIPS membrane 122

Figure 6.8: Benzoic acid crystals grown at 10ºC/min cooling 124

Figure 6.9: SEM image of a PES−resorcinol membrane 127

Figure C.1: SEM image of an EAA15−DPE ZeoTIPS membrane 142

Figure C.2: SEM image of a poly(methyl methacrylate)−1,4-butanediol ZeoTIPS membrane 143

Figure C.3: SEM image of a cellulose triacetate−2-ethyl-1,3-hexanediol ZeoTIPS membrane 144

Figure D.1: SEM image of an EAA(15 wt-% acrylic acid)−mineral oil membrane 146

Figure D.2: SEM image of a polyethersulfone−cyclohexanol membrane 146

Figure D.3: SEM image of a PMMA−PEG200 membrane 147

Figure D.4: SEM image of a PMMA−dioctyl phthalate membrane 148

Figure D.5: SEM image of a PES−benzoic acid membrane 149

Figure D.6: SEM images of a polyetherimide(Ultem)−benzoic acid membrane 151

Figure D.7: SEM image of an EVAc(26.7 wt-% vinyl acetate)−benzoic acid membrane 152

Figure D.8: SEM image of a PMMA−benzoic acid membrane. 152

Figure D.9: SEM image of a PES−resorcinol membrane 153

Chapter 1: Introduction

1.1 CURRENT MEMBRANE TECHNOLOGIES

1.1.1 Polymeric Membranes

Polymeric membranes made by interfacial polymerization [1], phase inversion [2, 3], and evaporative casting [4, 5] have long been used for separations applications that rely on nano-size pores; for example, gas separations, reverse osmosis, nanofiltration, and pervaporation. Unfortunately, these methods have not been able to yield membranes of narrow enough pore-size distributions required to achieve the efficient separation of chemical species of almost identical size. This inability to obtain refined size-based separations is partially due to inherent randomness chain packing and chain mobility in the polymer membranes prepared by these methods [6].

Membranes prepared by the methods listed above often show a flux/selectivity tradeoff in performance; that is, as flux through the membrane increases, the ability to separate species of similar size decreases. The flux/selectivity tradeoff was well documented by Robeson for gas separations using polymer membranes [7]. Through the extensive analysis of published data and in-house experimental results, Robeson showed that regardless of the polymeric material used, there exists an upper bound in the flux/selectivity relationship, and that this limit cannot be exceeded for a given separation, such as oxygen/nitrogen. While Robeson showed this upper bound to be true for gas separations, this phenomenon also applies to liquid separations such as reverse osmosis, nanofiltration, and pervaporation using polymeric membranes. Considerable research has been undertaken in recent years in an attempt to produce membranes that exceed the upper bound limitation [6, 8, 9].

Polymeric membranes have proven to be effective for the reverse osmosis (RO) removal of dissolved inorganic salts and low molecular weight organic impurities from water. RO is a pressure-driven process, in which the feed stream is forced onto the membrane at a pressure greater than the osmotic pressure of the feed solution. The components of the feed solution partition into the membrane to different extents and diffuse through the membrane at different rates. It is the differences in solubility and diffusivity that result in the permeate having a different composition than the feed stream [10]. For example, RO membranes can remove hydrated sodium and calcium ions of approximately 5 Å diameter and hydrated potassium ion of 5.8 Å diameter [11] from water (which has a kinetic diameter of 2.96 Å [12]). However, since almost all substances dissolve in and diffuse through the polymeric membrane materials to some extent, rarely is 100% rejection of the impurities achieved.

Pervaporation membranes have been shown to remove organics from aqueous solutions and can be useful for separation of close-boiling organic–organic mixtures [13]. Like RO membranes, pervaporation membranes separate components on the basis of different solubilities and diffusion rates across the membrane, and pervaporation membranes can separate molecules on a similar size scale to RO. Unlike RO, pervaporation includes an energy-intensive evaporative phase change in the permeate stream. However, pervaporation requires much less heat than traditional distillation, and can overcome problems faced by traditional distillation, such as azeotropes or degradation of heat-sensitive components.

Nanofiltration (NF) membranes have become significant in the realm of water treatment over the past decade [14]. They require lower pressures than RO membranes, and result in high water fluxes [15]. Compared to RO membranes, NF membranes show

an inability to reject some small ions, and like polymeric RO membranes they show some limitations in chemical, thermal, and mechanical stabilities [14].

1.1.2 Zeolite Membranes

Zeolites, from oxides of elements such as Si, Fe, Ge, P, and Al, have demonstrated capabilities for refined size-based separations [16, 17]. Zeolite membranes have been formed by depositing crystals onto a porous substrate from solution, with the resulting pore size depending on the types of atoms in the framework [16]. Typically these membranes have nano-pores ranging in size from 0.38 to 0.77 nm in diameter with extremely narrow pore size distributions due to their crystalline structure [18]. These zeolite membranes have been used for gas separations, such as separating O_2 (3.75 Å in length) from N_2 (4.07 Å in length) [6, 18], in which gas separation occurs by selective diffusion as a result of size exclusion. Zeolites are typically more chemically stable than polymeric membranes and can resist degradation even in harsh organic environments [11]. The characteristics of zeolites that make them useful in gas separation are also beneficial in liquid separations, including water treatment. However, the use of zeolite membranes for water treatment has been somewhat limited, as outlined below.

Recent attempts to use zeolite flat-sheet membranes for RO and pervaporation have shown potential [8, 18]. While many positive characteristics indicate a promising future for zeolite membranes, several drawbacks have limited their applicability: (i) continuous zeolite films are difficult and expensive to produce, (ii) the films are roughly 5 μm thick, and as the crystals grow, gaps can form between crystals that are larger than the zeolitic pores, causing a drop in rejection capability, and (iii) these membranes are fragile and inflexible and therefore require that the films be cast onto microporous supports and subsequently handled with extreme care [19].

1.1.3 Mixed Matrix Membranes

Over the past three decades, mixed matrix membranes have been proposed as an answer to the above membrane drawbacks [6, 8, 20-35]. Mixed matrix membranes consist of a low-permeability polymer matrix, usually composed of a selective polymer, which acts to make the effectiveness of the membrane at least as good as a traditional polymeric membrane. The improvement offered by mixed matrix membranes results from suspended zeolite particles dispersed in the polymer matrix. These particles are chosen to reject one chemical component while allowing passage of another because of their extremely narrow pore size distribution. Thus, the desired permeate component, component A in Figure 1.1, moves faster through a mixed matrix membrane than through a purely polymeric membrane made with the same polymer. Additionally, the undesired chemical component is forced to travel a more tortuous path around the zeolite particles, thus decreasing mobility for that component and increasing the overall selectivity for the desired component [6].

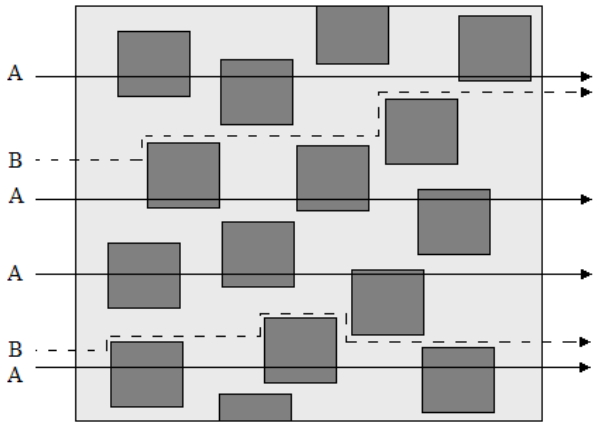

Figure 1.1: Schematic of a mixed matrix membrane. Component A, the desired, smaller component, moves faster through the membrane than component B.

Paul and Kemp suspended zeolite particles with pore diameters of 5 Å in a matrix of silicone rubber and documented increased adsorption of gaseous components such as CO_2 and CH_4 [36]. Kulprathipanja *et al.* used silicalite in cellulose acetate to increase the membrane selectivity of O_2 over N_2, noting small increases in selectivity over that of the pure polymer matrix [32]. Jia *et al.* and Suer *et al.* also found an increase in membrane selectivity by the addition of zeolite to polymers for gas separation [35, 37]. Koros used both zeolites and carbon molecular sieves within matrices of poly(vinyl acetate), Matrimid, and Ultem to improve O_2/N_2 separations [9, 22, 23].

Like zeolite films, mixed matrix membranes are not without drawbacks. The most important being the limit to their separation capabilities. Because the zeolite particles are by no means a continuous separation layer, only a small improvement over polymeric membranes can be achieved [6]. Furthermore, many researchers have dealt with poor polymer−zeolite adhesion, which results in decreased selectivity. Recent research has been performed regarding the modification of zeolite surfaces to improve the performance of mixed matrix membranes. Some of this research involved attaching long polymeric tethers to the zeolite via silane groups [22]. Other research, rather than modifying the zeolites to accommodate a specific polymer, has used polymers that will adhere well to the unmodified zeolite and modified the polymer's properties to suit the application [8].

Like polymeric and zeolite membranes, dense mixed matrix membranes have also been employed for pervaporation. For example, Chung and Kulprathipanja used cross-linked polyvinyl alcohol with zeolites for the removal of ethanol from water [8]. These membranes are similar to those used for RO, and thus they exhibit the same drawbacks listed above.

1.2 THERMALLY INDUCED PHASE SEPARATION

Thermally induced phase separation (TIPS) has been used to produce microporous materials and membranes for decades [38-48]. Depending on the polymer and diluent selected to form the membrane and the processing conditions, there are three types of thermally induced phase separation processes: liquid−liquid TIPS; solid−liquid TIPS; and liquid−solid TIPS. These different TIPS processes can lead to distinctive structures, as shown in Figure 1.2: liquid–liquid TIPS (Figure 1.2(a)), solid–liquid TIPS (Figure 1.2 (b)), and liquid–solid TIPS (Figure 1.2 (c)).

In general, a thermally induced phase separation (TIPS) membrane is formed by first mixing a polymer with a high boiling point diluent at high temperatures to melt-blend the two components into a homogeneous phase. The diluent acts as a solvent for the polymer only at high temperatures, and by cooling the homogeneous solution, phase separation occurs. In liquid−liquid TIPS (L–L TIPS), droplets of a polymer-lean phase form in a continuous polymer-rich phase. A phase diagram describing this phenomenon is shown in Figure 1.3. Factors controlling the size of the diluent-rich droplets include the polymer concentration in the homogeneous solution and the cooling rate. Following solidification of the polymer, extraction of the diluent, and drying of the membrane, the space formerly occupied by the diluent droplets forms the roughly spherical *cells* of the final membrane, and connecting these cells are circular *pores* [45].

In solid−liquid TIPS, phase separation occurs via the solidification of the polymer in a diluent-rich solution. The resulting morphology (Figure 1.2(b)) typically lacks the strength of a liquid−liquid TIPS membrane and is therefore not useful for ZeoTIPS membranes as discussed below.

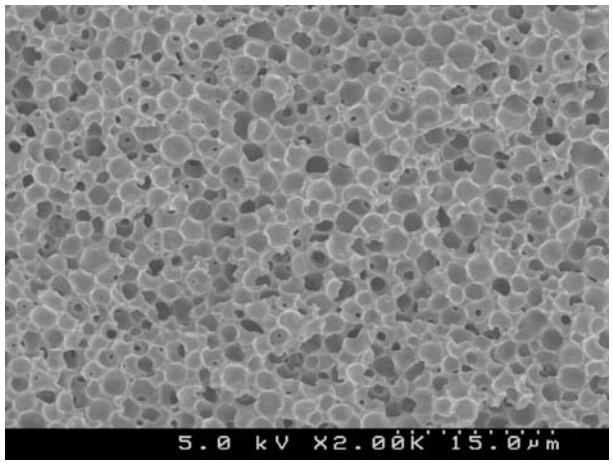

(a)

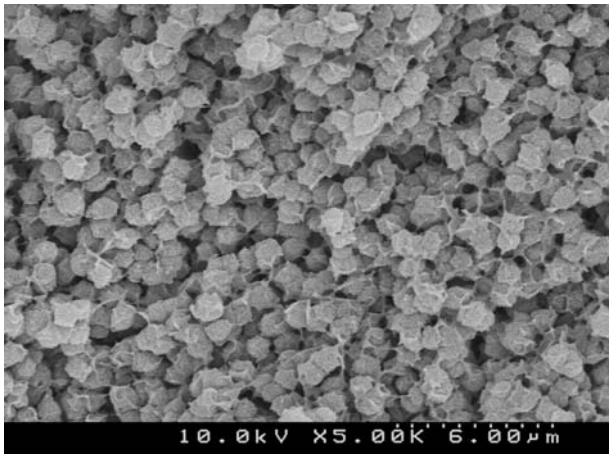

(b)

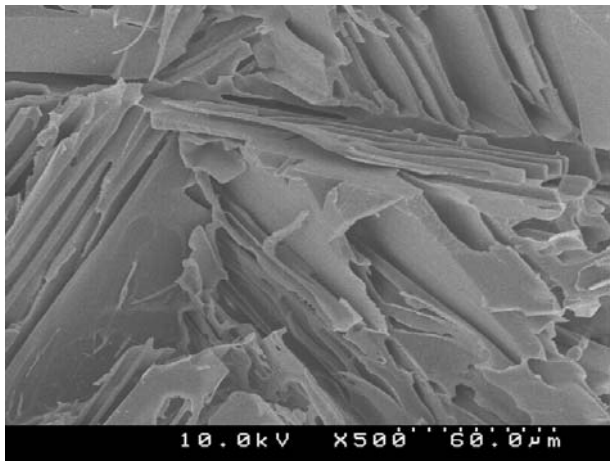

(c)

Figure 1.2: Typical membranes made by (a) L−L TIPS (made with 25 wt-% EVAL(32 mol-% ethylene) and 75 wt-% PEG400), (b) S-L TIPS (made with 25 wt-% EVAL(44 mol-% ethylene) and 75 wt-% PEG300), and (c) L−S TIPS (made with 25 wt-% LDPE and 70 wt-% hexamethylbenzene).

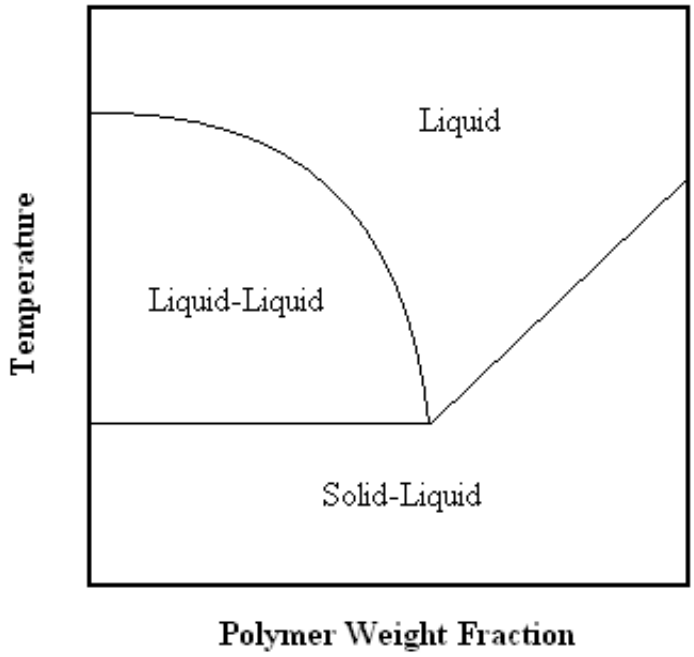

Figure 1.3: General form of a phase diagram for systems undergoing liquid−liquid/solid−liquid TIPS.

Liquid–solid (L–S) TIPS occurs when the diluent crystallizes in a polymer-rich liquid matrix. A general phase diagram for such a system is shown in Figure 1.4. Upon further cooling to solidify the polymer and subsequent extraction of the diluent, the nature of the resulting morphology depends upon the crystal structure and kinetics of crystal growth [49-54]. A typical structure resulting from L–S TIPS is shown in Figure 1.2(c). L–S TIPS provides several opportunities for controlling the microporous membrane morphology, including cooling rate, diluent concentration, and diluent crystal structure (*i.e.,* triclinic, monoclinic, orthorhombic, etc.). Consequently, when forming membranes via L–S TIPS, selection of the diluent requires careful consideration of the crystal form. Proper control of the kinetics of crystal growth may lead to a tight pore size distribution, indicating potential use in biological separations in which a narrow cut-off is needed. Furthermore, a L−S TIPS membrane can be made into hollow fiber form, an

important advantage over track-etch membranes, which characteristically have narrow pore size distributions useful for biological separations but cannot be formed as hollow fibers. L−S TIPS will be discussed further in Chapter 6.

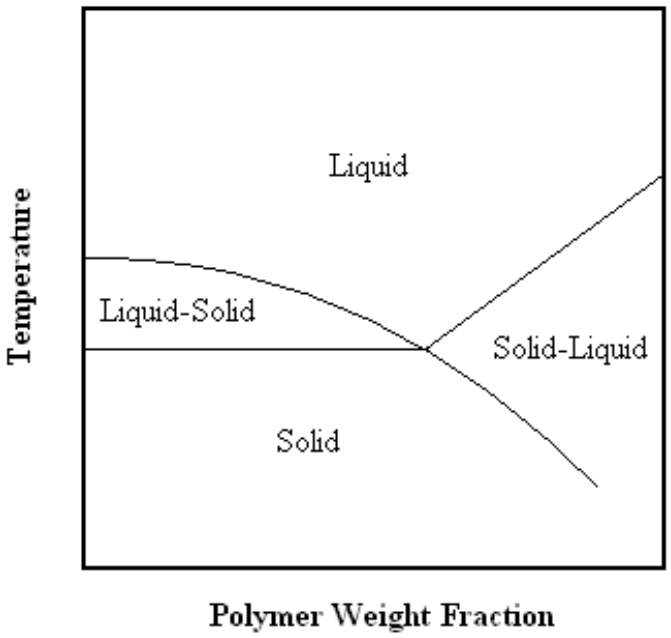

Figure 1.4: General form of a liquid−solid/solid−liquid TIPS phase diagram

1.3 ZEOTIPS MEMBRANES

Liquid−liquid thermally induced phase separation (L−L TIPS) is a viable method for making microporous polymer membranes, yielding the cellular structures shown in Figure 1.2(a) above. However, these membranes do not possess the small pore size needed to achieve the desired separations listed above. In the research reported here, it is proposed that by merging the mixed matrix concept with a L−L TIPS membrane, one can form a "microporous mixed matrix membrane" or "ZeoTIPS membrane" with small

nano-scale pores of narrow pore size distribution. Such a membrane addresses the drawbacks of both zeolite films and dense mixed matrix membranes by providing a micro-porous matrix with dispersed nano-porous zeolite particles distributed in such a way that only the particles participate in the separation. This unique structure will ideally give the same separation capabilities of the continuous film zeolite membrane with greater durability and flexibility.

Formation of a ZeoTIPS membrane begins with the suspension of zeolite particles in a homogeneous polymer−diluent solution at an elevated temperature. Upon cooling, diluent-rich liquid droplets form between the particles within a polymer-rich liquid phase. As the droplets continue to grow during the cooling of the liquid–liquid suspension, they come in contact with the zeolite particles. Following solidification of the polymer-rich phase, extraction of the diluent, and evaporation of the volatile extractant, one is left with a structure in which the zeolite particles are held in place by the polymer and connected by voids (represented schematically in Figure 1.5). In Figure 1.5, the white circles represent the void spaces, the light grey squares represent zeolite particles, and the darker grey areas represent the polymer matrix.

Figure 1.5(a) shows the result of adding an insufficient number of zeolite particles. In this case, microporous connectivity still exists, and no high selectivity separation is achieved as permeating species easily travel from the top of the membrane to the bottom. In contrast, Figure 1.5(b) illustrates the case when there are enough nano-porous zeolite particles dispersed throughout the microporous structure to prevent any permeating species from traversing the microporous membrane without encountering at least one nano-porous zeolite particle. That is, in Figure 1.5(b) the *critical zeolite loading* has been reached. Stated another way, while Figure 1.5(a) shows microporous connectivity, Figure 1.5(b) shows nano-porous connectivity is achieved when the

membrane contains zeolite loadings equal to or greater than the critical zeolite loading. In Figure 1.5(b), the smaller component (represented by the solid line) can traverse the membrane through the void space and the zeolite particles, but the larger component (represented by the dashed line) is rejected near the upper surface of the ZeoTIPS membrane. An actual ZeoTIPS membrane is shown in Figure 1.6 for comparison.

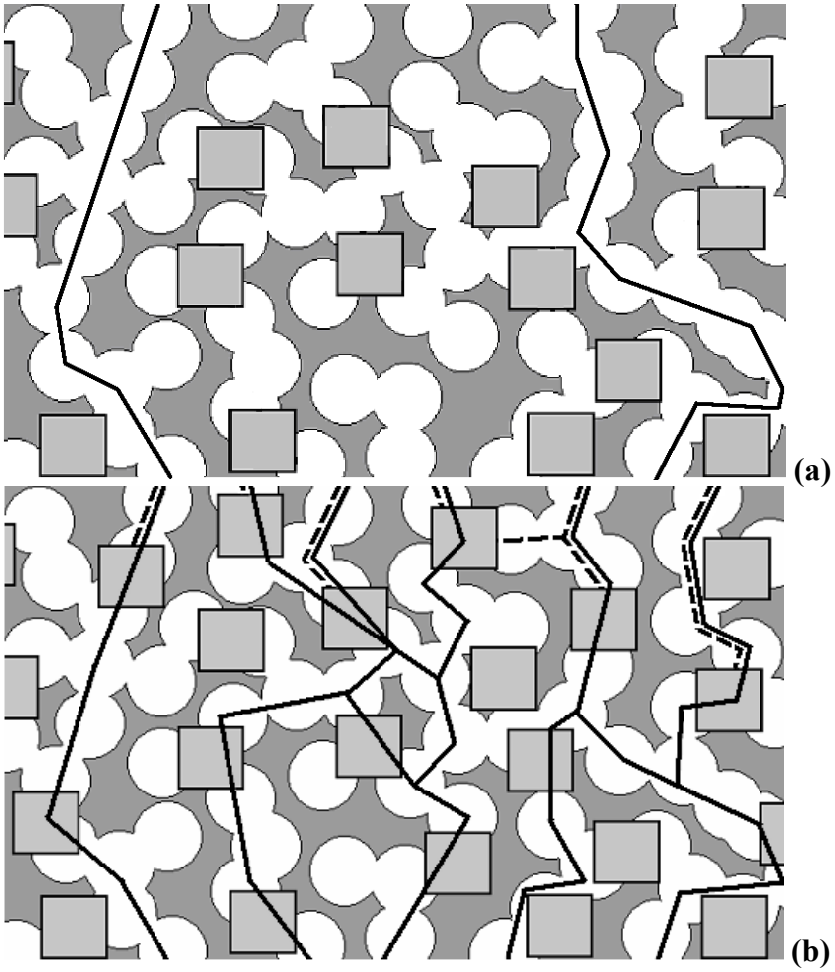

Figure 1.5: ZeoTIPS separation schematics. (a) When not enough zeolite is added, solution components can pass from top to bottom of the membrane shown without being sieved by a zeolite particle. (b) When the critical zeolite loading is reached, high selectivity is achieved. The dashed lines represent the path of the larger component. The solid lines represent the path of the smaller component.

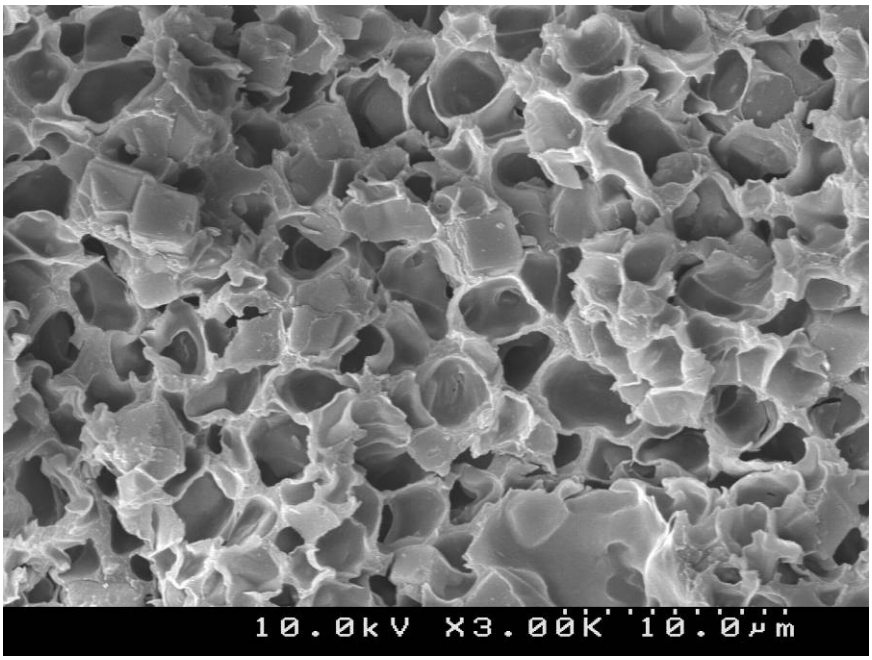

Figure 1.6: ZeoTIPS membrane formed from 4A zeolite, cellulose triacetate, and 2-ethyl-1,3-hexanediol.

Due to the wide range of available TIPS polymer–diluent systems, ZeoTIPS membranes can be made from a wide variety of polymers, many of which are quite durable, chemically resistant, and inexpensive. ZeoTIPS membranes can be extruded into flat sheet or hollow fiber form, and if the matrix is chosen properly, can be used for both gas separations and liquid separations. With these advantages, and because of theoretically high separation efficiencies discussed in Chapter 2, ZeoTIPS membranes have great potential to improve current industrial separation processes.

1.4 SIGNIFICANCE OF THIS WORK

This research is the first of its kind to combine the benefits of microporous polymeric membranes, zeolite particles, and dense mixed matrix membranes while avoiding many of their disadvantages. Furthermore, this work is the first to address the

growth of droplets in nascent liquid−liquid TIPS membranes in the presence of particulate filler, with application to both selective and adsorbent fillers [55]. An additional contribution of this work is a model that predicts the necessary zeolite loading in a ZeoTIPS system; this and other fundamental knowledge gained from the model are useful for future development of these membranes. Finally, in the process of developing liquid−solid ZeoTIPS membranes, the first proposed method of forming liquid−solid TIPS membranes with aligned crystals was developed. This may lead to high porosity, high selectivity microporous membranes.

1.5 STRUCTURE OF THE DISSERTATION

Chapter 2 compares ZeoTIPS membranes to dense mixed matrix membranes through theoretical performance predictions. An investigation on the effects of particulate fillers in liquid−liquid TIPS membranes is contained in Chapter 3. Chapter 4 presents a MATLAB model that helps to predict the necessary compositions for successful ZeoTIPS membranes. Chapter 5 includes methods of forming ZeoTIPS membranes, both the experimental methods and the factors to consider when choosing polymer, diluent, and zeolite. Also included are methods of zeolite surface modification. Chapter 6 introduces a different approach to ZeoTIPS membranes, liquid−solid TIPS, along with methods for aligning diluent crystals in L−S TIPS. Finally, Chapter 7 contains conclusions from this work and recommendations for future investigation.

1.6 REFERENCES

1 P.W. Morgan, *Interfacial Polymerization*, in: J.I. Kroschwitz (Ed.), Encyclopedia of Polymer Science and Engineering, 8, Wily, New York, 1987, pp. 221-237.

2 I.M. Wienk, R.M. Boom, M.A.M. Beerlage, A.M.W. Bulte, C.A. Smolders, and H. Strathmann, *Recent advances in the formation of phase inversion membranes made from amorphous or semi-crystalline polymers.*, Journal of Membrane Science, 113 (1996) 361-371.

3 I. Kim, K. Lee, and T. Tak, *Preparation and characterization of integrally skinned uncharged polyetherimide asymmetric nanofiltration membrane*, Journal of Membrane Science, 183 (2001) 235-247.

4 B. Kunst and S. Sourirajan, *Effect of casting conditions on the performance of porous cellulose acetate membranes in reverse osmosis*, Journal of Applied Polymer Science, 14 (1970) 723-733.

5 C.R. Cannon, *Cellulose acetate reverse osmosis desalination membranes*, United States Patent 3285765, 1966.

6 C.M. Zimmerman, A. Singh, and W.J. Koros, *Tailoring mixed matrix composite membranes for gas separations*, Journal of Membrane Science, 137 (1997) 145-154.

7 L.M. Robeson, *Correlation of separation factor versus permeability for polymeric membranes*, Journal of Membrane Science, 62 (1991) 165-185.

8 H.-M. Guan, T.-S. Chung, Z. Huang, M.L. Chng, and S. Kulprathipanja, *Poly(vinyl alcohol) multilayer mixed matrix membranes for the dehydration of ethanol-water mixture*, Journal of Membrane Science, 268 (2006) 113-122.

9 R. Mahajan and W.J. Koros, *Factors controlling successful formation of mixed-matrix gas separation materials*, Industrial & Engineering Chemistry Reasearch, 39 (2000) 2692-2696.

10 S. Obst and H. Bradaczek, *Molecular dynamics study of the structure and dynamics of the hydration shell of alkaline and alkaline-earth metal cations*, Journal of Physical Chemistry, 100 (1996) 15677-15687.

11 I. Kumakiri, T. Yamaguchi, and S. Nakao, *Application of a zeolite A membrane to reverse osmosis process*, Journal of Chemical Engineering of Japan, 33 (2000) 333-336.

12 M.E.v. Leeuwen, *Derivation of Stockmayer potential parameters for polar fluids*, Fluid Phase Equilibria, 99 (1994) 1.

13 P. Shao and R.Y.M. Huang, *Polymeric membrane pervaporation*, Journal of Membrane Science, 287 (2007) 162-179.

14 J.S. Taylor and E.P. Jacobs, *Reverse osmosis and nanofiltration*, in: J. Mallevialle, P.E. Odendaal, and M.R. Wiesner (Eds.), Water Treatment Membrane Processes, McGraw-Hill, New York, 1996.

15 Y. Song, F. Liu, and B. Sun, *Preparation, characterization, and application of thin film composite nanofiltration membranes*, Journal of Applied Polymer Science, 95 (2005) 1251-1261.

16 T. Bein, *Synthesis and Applications of Molecular Sieve Layers and Membranes*, Chemistry of Materials, 8 (1996) 1626-1653.

17 M. Noack, P. Kolsch, R. Schafer, P. Toussaint, and J. Caro, *Molecular Sieve Membranes for Industrial Application: Problems, Progress, Solutions*, Chemical Engineering Technology, 25 (2002) 221-230.

18 T.C. Bowen, R.D. Noble, and J.L. Falconer, *Fundamentals and applications of pervaporation through zeolite membranes*, Journal of Membrane Science, 245 (2004) 1-33.
19 L. Li, J. Dong, T.M. Nenoff, and R. Lee, *Reverse osmosis of ionic aqueous solutions on a MFI zeolite membrane*, Desalination, 70 (2004) 309-316.
20 T.T. Moore, R. Mahajan, D.Q. Vu, and W.J. Koros, *Hybrid membrane materials comprising organic polymers with rigid dispersed phases*, AIChE Journal, 50 (2004) 311-321.
21 Y. Li, T.-S. Chung, C. Cao, and S. Kulprathipanja, *The effects of polymer chain rigidification, zeolite pore size and pore blockage on polyethersulfone (PES)-zeolite A mixed matrix membranes*, Journal of Membrane Science, 260 (2005) 45-55.
22 R. Mahajan and W.J. Koros, *Mixed matrix membrane materials with glassy polymers. Part 1*, Polymer Engineering and Science, 42 (2002) 1420-1431.
23 R. Mahajan and W.J. Koros, *Mixed matrix membrane materials with glassy polymers. Part 2*, Polymer Engineering and Science, 42 (2003) 1432-1441.
24 T.T. Moore and W.J. Koros, *Non-ideal effects in orgain-inorganic materials for gas separation membranes*, Journal of Molecular Structure, 739 (2005) 87-96.
25 L.Y. Jiang, T.S. Chung, C. Cao, Z. Huang, and S. Kulprathipanja, *Fundamental understanding of nano-sized zeolite distribution in the formation of the mixed matrix single- and dual-layer asymmetric hollow fiber membranes*, Journal of Membrane Science, 252 (2005) 89-100.
26 S.B. Teli, G.S. Gokavi, M. Sairam, and T.M. Aminabhavi, *Mixed matrix membranes of poly(vinyl alcohol) loaded with phosphomolybdic heteropolyacid for the pervaporation separation of water-isopropanol mixtures*, Colloids and Surfaces A, 301 (2007) 55-62.
27 S. Kulprathipanja, *Mixed Matrix Membrane Development*, Annals of the New York Academy of Sciences, 984 (2003) 361-369.
28 J.A. Sheffel and M. Tsapatsis, *A model for the performance of microporous mixed matrix membranes with oriented selective flakes*, Journal of Membrane Science, 295 (2007) 50-70.
29 Z. Huang, Y. Li, R. Wen, M.m. Teoh, and S. Kulprathipanja, *Enhanced gas separation properties by using nanostructured PES-Zeolite 4A mixed matrix membranes*, Journal of Applied Polymer Science, 101 (2006) 3800-3805.
30 S. Husain and W.J. Koros, *Mixed matrix hollow fiber membranes made with modified HSSZ-13 zeolite in polyetherimide polymer matrix for gas separation*, Journal of Membrane Science, 288 (2007) 195-207.
31 C.-C. Hu, T.-C. Liu, K.-R. Lee, R.-C. Ruann, and J.-Y. Lai, *Zeolite-filled PMMA composite membranes: influence of coupling agent addition on gas separation properties*, Desalination, 193 (2006) 14-24.
32 S. Kulprathipanja, R.W. Neuzil, and N.N. Li, *Separation of fluids by means of mixed matrix membranes*, United States Patent 4740219, 1988.
33 S. Kulprathipanja, *Separation of gases by means of mixed matrix membranes*, United States Patent 5127925, 1988.

34 E. Okumus, T. Gurkan, and L. Yilmaz, *Development of a mixed-matrix membrane for pervaporation*, Separation Science and Technology, 29 (1994) 2451.
35 M.G. Suer., N. Bac, and L. Yilmaz, *Gas permeation properties of polymer-zeolite mixed matrix membranes*, Journal of Membrane Science, 91 (1994) 77.
36 D.R. Paul and D.R. Kemp, *The diffusion time lag in polymer membranes containing adsorptive fillers*, Journal of Polymer Science, 41 (1973) 79-93.
37 M. Jia, K.V. Peinemann, and R.D. Behling, *Molecular sieving effect of the zeolite-filled silicone rubber membranes in gas permeation*, Journal of Membrane Science, 57 (1991) 289-96.
38 A.J. Castro, *Methods for making microporous products*, US Patent 4,247,498, 1981.
39 H. Matsuyama, S. Berghmans, M.T. Batarseh, and D.R. Lloyd, *Formation of anisotropic and asymmetric membranes via thermally induced phase separation*, in: I. Pinnau and B.D. Freeman (Eds.), Membrane Formation and Modification, ACS Symposium Series, 744, ACS Press, Washington, DC, 2000, pp. 23-41.
40 S.S. Kim and D.R. Lloyd, *Microporous membrane formation via thermally-induced phase separation. III. Effect of thermodynamic interactions on the structure of isotactic polypropylene membranes*, Journal of Membrane Science, 64 (1991) 13-29.
41 S.S. Kim, G.B.A. Lim, A.A. Alwattari, Y.F. Wang, and D.R. Lloyd, *Microporous membrane formation via thermally-induced phase separation. V. Effect of diluent mobility and crystallization on the structure of isotactic polypropylene membranes*, Journal of Membrane Science, 64 (1991) 41-53.
42 G.B.A. Lim, S.S. Kim, Q. Ye, Y.F. Wang, and D.R. Lloyd, *Microporous membrane formation via thermally-induced phase separation. IV. Effect of isotactic polypropylene crystallization kinetics on membrane structure*, Journal of Membrane Science, 64 (1991) 31-40.
43 D.R. Lloyd, J.W. Barlow, and K.E. Kinzer, *Microporous membrane formation via thermally-induced phase separation*, in: K.K. Sirkar and D.R. Lloyd (Eds.), New Membrane Materials and Processes for Separation, AIChE Symposium Series 261, New York, 1988.
44 D.R. Lloyd, K.E. Kinzer, and H.S. Tseng, *Microporous membrane formation via thermally-induced phase separation. I. Solid-liquid phase separation*, Journal of Membrane Science, 52 (1990) 239-261.
45 D.R. Lloyd, S.S. Kim, and K.E. Kinzer, *Microporous membrane formation via thermally-induced phase separation. II. Liquid-liquid phase separation*, Journal of Membrane Science, 64 (1991) 1-11.
46 K.S. McGuire, D.R. Lloyd, and G.B.A. Lim, *Microporous membrane formation via thermally-induced phase separation. VII. Effect of dilution, cooling rate, and nucleating agent addition on morphology*, Journal of Membrane Science, 79 (1993) 27-34.
47 P.D. Graham, A.J. Pervan, and A.J. McHugh, *The dynamics of Thermal-Induced Phase Separation in PMMA solutions*, Macromolecules, 30 (1997) 1651-1655.
48 B. Liu, Q. Du, and Y. Yang, *The phase diagrams of EVAL and PEG in relation to membrane formation*, Journal of Membrane Science, 180 (2000) 81-92.

49 P. Smith and A.J. Pennings, *Eutectic crystallization of pseudo binary systems of polyethylene and high melting diluents*, Polymer, 15 (1974) 413-419.
50 A.A. Alwattari and D.R. Lloyd, *Microporous membrane formation via thermally-induced phase separation. VI. Effect of diluent morphology and relative crystallization kinetics on polypropylene membrane structure*, Journal of Membrane Science, 64 (1991) 55-68.
51 A.A. Alwattari and D.R. Lloyd, *Isothermal crystallization of isotactic polypropylene-hexamethylbenzene blends: crystal morphology*, Polymer, 35 (1994) 2710-2715.
52 A.A. Alwattari and D.R. Lloyd, *Isothermal crystallization of isotactic polypropylene - hexamethylbenzene blends: kinetics analysis*, Polymer, 39 (1998) 1129-1137.
53 A. Alwattari, *Thermally induced phase separation of isotactic polyproylene and hexamethylbenzene*, Dissertation, The University of Texas at Austin, 1990.
54 R.J.M. Zwiers, S. Gogolewski, and A.J. Pennings, *General crystallization behavior of poly(L-lactic acid) PLLA. 2. Eutectic crystallization of PLLA*, Polymer, 24 (1983) 167-174.
55 J.M. Larson and S.H. Gryska, *Sorbent-filled polyolefin/wax membranes made via thermally induced phase separation process and adsorption properties.*, Polymer Materials Science and Engineering, 77 (1997) 361-362.

Chapter 2: ZeoTIPS Performance Modeling [1]

2.1 INTRODUCTION

The modeling of permeation through traditional or dense mixed matrix membranes has taken on various forms. Most significant was a modified Maxwell model developed by Koros to describe dense mixed matrix performance in which zeolite particles were approximated as spheres [1]. The 2-dimensional Maxwell model upon which Koros based his approximation is only valid for low particulate loadings, and therefore cannot be used to model ZeoTIPS membranes [2], which require greater than ~25 vol-% zeolite loading (Loading limits are discussed in Chapters 3 and 4). However, parallel−series models give a different depiction of mixed matrix performance [1] and can be applied to the ZeoTIPS concept after some modifications.

Modeling of the irregular structure shown in Figure 1.5 would be difficult and beyond the scope of this work. Instead, the membrane structure is modeled in terms of a mixture of regular shaped polymer regions, voids, and zeolite particles in a parallel–series arrangement. Figure 2.1(a) shows a schematic representation of an *ideal* ZeoTIPS membrane. Consider permeation from the top to the bottom of Figure 2.1(a) (Permeation from left to right in Figure 2.1 is not considered because diffusion of any species through a void is orders of magnitude greater than diffusion through a dense polymer.). A permeating molecule can pass through the dark grey polymer region (path I) via diffusion. An alternative or parallel path (path II) is for the molecule to pass through the void–zeolite–void sequence in series. That is, transport through the membrane can be modeled in a parallel–series fashion. Of course, producing an ideal membrane such as

[1] This chapter is based on: Funk, C.V., and D.R. Lloyd, *Zeolite-filled microporous mixed matrix (ZeoTIPS) membranes: prediction of gas separation performance*, J. Membrane Sci., 313 (2008), 224-231.

that shown in Figure 2.1(a) is not trivial since it has been documented in the literature that the zeolite particle is often coated with a layer of polymer. Furthermore, it has been shown that the particles can be surrounded on all sides by void [3], which is not useful for dense mixed matrix membranes or ZeoTIPS membranes.

It is well documented that the formation of dense mixed matrix membranes can lead to an interphase region at the surface of the zeolite particles [4]. The polymer in this interphase can be denser or less dense than the bulk polymer. The case of a denser polymer near the zeolite surface is not a concern in the ideal ZeoTIPS membrane represented in Figure 2.1(a), since the diffusion of permeating molecules through the polymer phase is much less than through the void and the zeolite. The case of a less dense polymer region near the zeolite surface is a result of stresses occurring during formation and is less of a concern in ZeoTIPS membranes due to the method of formation of these membranes. ZeoTIPS membranes are formed not by solvent casting, as are many dense mixed matrix membranes, but by thermally induced phase separation, and the stresses involved in diluent expulsion during polymer solidification are significantly less than those occurring when solvent evaporation is the method of membrane formation. Additionally, due to the high temperatures used during membrane formation, large stresses are unlikely to occur in the formation of ZeoTIPS membranes like those in dense mixed matrix membrane formation. Since these interphase regions are unlikely to be significant in ZeoTIPS membranes they are not included in the model discussed here.

Consequently, Figure 2.1(b) shows a schematic representation of a more realistic *non-ideal* ZeoTIPS membrane in which the zeolite particle is coated with a polymer layer of uniform thickness on all sides. The different shading for the sections of the polymer coating is used to distinguish the parallel and series paths associated with the void−zeolite−void arrangement. The 2-dimensional model presented below is developed

for *non-ideal* membranes (Figure 2.1(b)), and it is then shown that the model can be reduced to the *ideal* case (Figure 2.1(a)).

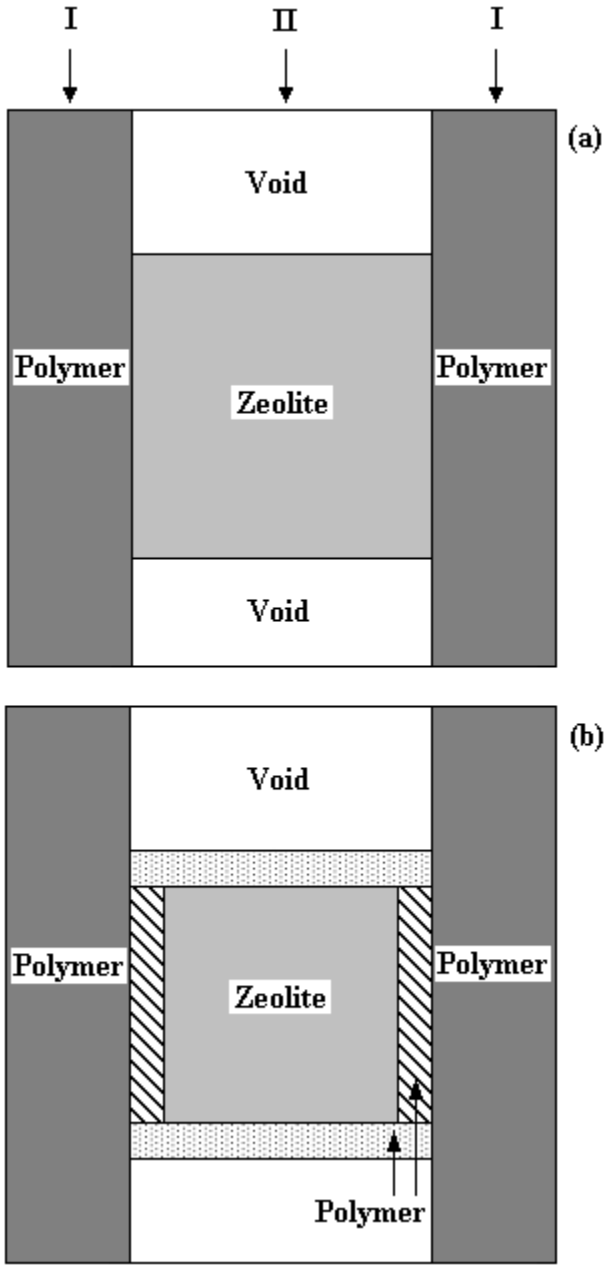

Figure 2.1: ZeoTIPS membranes can be modeled as (a) a polymer phase in parallel with a void and uncoated zeolite in series, or as (b) a polymer phase in parallel with void and polymer-coated zeolite in series. Membrane transport occurs from top to bottom of diagrams via Path I or II.

2.2 PARALLEL−SERIES MODEL CONSTRUCTION

In a non-ideal ZeoTIPS membrane, as represented in Figure 2.1(b), each zeolite particle has a polymer coating of uniform thickness. This coating forms when the zeolite affinity for the polymer surpasses its affinity for the diluent. As shown in Figure 2.1(b), the coated zeolite itself is represented by a parallel−series arrangement, with polymer in series and in parallel with the zeolite. Path II contains region III, the parallel zeolite−polymer portion. In the development that follows, the variables P and ϕ represent permeabilities and volume fractions, respectively. The superscripts *o*, *I*, *II*, and *III* represent the overall membrane, the polymer in path I, the entirety of path II (including region III), and region III, respectively. Subscripts *P*, *V*, and *Z* refer to the polymer, void, and zeolite components. Permeation through path II in Figure 2.1(b) is described by Equation (2.1).

$$P^{II} = \frac{P_V P_P P^{III}}{\left(1-\phi_V^{II}-\frac{\phi_P^{II}}{2}\right)P_V P_P + \phi_V^{II} P_P P^{III} + \frac{\phi_P^{II}}{2} P_V P^{III}} \tag{2.1}$$

P^{III} denotes the permeability of the parallel component of path II as represented by the zeolite and cross-hatched polymer in Figure 2.1(b) and is defined in Equation (2.2).

$$P^{III} = \phi_Z^{III} P_Z + \phi_P^{III} P_P \tag{2.2}$$

The variables ϕ_Z^{III} and ϕ_P^{III} defined in Equations (2.3) and (2.4) denote the volume fractions of the zeolite and polymer within the parallel portion of path II in Figure 2.1(b).

$$\phi_Z^{III} = \frac{\phi_Z^{II}}{\phi_Z^{II} + \frac{\phi_P^{II}}{2}} \tag{2.3}$$

$$\phi_P^{III} = \frac{\phi_P^{II}}{2} \tag{2.4}$$

The variables $\phi_Z{}^{II}$ and $\phi_P{}^{II}$ defined in Equations (2.5) and (2.6) refer to the volume fractions of the zeolite and polymer (both the cross-hatched and dotted polymer regions) in the entire path II portion of the membrane.

$$\phi_Z^{II} = \frac{\phi_Z^o}{\phi_Z^o + \phi_V^o + \beta\phi_P^o} \tag{2.5}$$

$$\phi_P^{II} = \frac{\beta\phi_P^o}{\phi_Z^o + \phi_V^o + \beta\phi_P^o} \tag{2.6}$$

In Equations (2.5) and (2.6), the factor β refers to the percentage of the total polymer in the membrane that contributes to the coating of the zeolite particles. In Equations (2.5) and (2.6), the $\phi_P{}^o$ and $\phi_V{}^o$ refer to overall volume fractions of the polymer and void (volume fractions in the original suspension of polymer, diluent (void), and zeolite), as defined below in Equations (2.7) and (2.8).

$$\phi_P^o = \left(1 - \phi_Z^o\right)\phi_P^* \tag{2.7}$$

$$\phi_V^o = \left(1 - \phi_Z^o\right)\phi_V^* \tag{2.8}$$

The volume fractions of the polymer and void without taking into account the presence of zeolite (volume fractions in the original solution of polymer and diluent (void)) are denoted by ϕ_P* and ϕ_V*. In Equation (2.9), $\phi_V{}^{II}$ refers to the volume fraction of the void within the path II portion of the membrane.

$$\phi_V^{II} = \frac{\phi_V^o}{\phi_Z^o + \phi_V^o + \beta\phi_P^o} \tag{2.9}$$

The total membrane permeability is the arithmetic average of the polymer (path I) and the void−polymer−zeolite series (path II) permeabilities, as shown in Equation (2.10).

$$P_{Total} = \phi^I P_P + \phi^{II} P^{II} = (\phi_P^o(1-\beta))P_P + (1-(\phi_P^o(1-\beta)))P^{II} \tag{2.10}$$

An *ideal* ZeoTIPS membrane would have no polymer coating around the zeolite, resulting in an essentially co-continuous structure as shown in Figures 1.5 and 2.1(a). This structure can be achieved in membrane production by balancing of polymer−zeolite and diluent−zeolite affinities, as discussed in Section 5.4. To represent the *ideal* ZeoTIPS membrane, one sets $\beta = 0$ in Equations (2.5), (2.6), and (2.10). Recall that β represents the fraction of the total polymer in the membrane that coats the zeolite particles; therefore, $\beta = 0$ corresponds to a zero thickness of the cross-hatched and dotted polymer regions of Figure 2.1(b), resulting in Figure 2.1(a). The resulting equations are (2.11) and (2.12), which describe this ideal membrane.

$$P^{II} = \frac{P_V P_Z}{\phi_Z^{II} P_V + \phi_V^{II} P_Z} \tag{2.11}$$

$$P_{Total} = \phi^{II} P^{II} + \phi^I P_P \tag{2.12}$$

In Equations (2.11) and (2.12), the terms P_V, P_P, and P_Z refer to the permeabilities of the void, polymer, and zeolite, respectively, and P_{Total} refers to the average

permeability of the entire membrane. The volume fractions of the membrane components are denoted by ϕ_V^o, ϕ_P^o, and ϕ_Z^o. Equations (2.11) and (2.12) are equivalent to those in a previous analysis presented by Robeson [5]. The results discussed below involve membranes with a constant void to polymer ratio of $\phi_P^*:\phi_V^* = 3:1$; changes in zeolite loading do not affect this ratio.

Membrane selectivity is defined in Equation (2.13) in the standard way as the ratio of the permeabilities of the components to be separated, oxygen and nitrogen in the analysis that follows.

$$Selectivity = \frac{P_{O_2}}{P_{N_2}} \tag{2.13}$$

Zeolite loading is defined in Equation (2.14) as the ratio of the zeolite volume percent ϕ_Z^o to the total membrane volume.

$$Zeolite\ Loading = \frac{\phi_Z^o}{\phi_V^o + \phi_P^o + \phi_Z^o} \tag{2.14}$$

It appears from membranes produced in this research (see Figures 1.6, 5.21(b), C.1, C.2, and C.3) that at a zeolite loading of at least ~25 vol-% is needed to prevent microporous connectivity through a membrane. This must be taken into account when analyzing the performance predictions presented in the following section.

2.3 ZEOTIPS PERFORMANCE PREDICTIONS

Using the polymer permeability data presented by Mahajan and Koros [3] and the zeolite 4A data calculated by Zimmerman and Koros [1] from data taken previously

[6, 7] and summarized in Table 2.1, the above model for ZeoTIPS membranes was compared with dense mixed matrix membranes for oxygen / nitrogen separation. The polymer used for comparison is poly(vinyl acetate), and the void permeability is arbitrarily set at 100 barrers.

Table 2.1: Permeability data (barrers):

	Oxygen	**Nitrogen**	**Oxygen/Nitrogen**
PVAc	0.5	0.083	5.9
Void	100	100	1
Zeolite	0.77	0.021	37

The results of the ideal and non-ideal versions of the model, along with dense mixed matrix membrane results for comparison, are presented in Figures 2.2 and 2.3. The data for dense mixed matrix membranes is obtained by setting $\beta = 0$ and $\phi_V^* = 0$ in the non-ideal ZeoTIPS equations and is similar to the data obtained by Mahajan and Koros using a modified Maxwell model [3]. ZeoTIPS membranes modeled in both figures contain a 3:1 void to polymer ratio. In Figures 2.2 and 2.3, the solid and dashed lines represent the range of useful ZeoTIPS membranes in terms of polymer–diluent–zeolite affinity. The solid line represents equal polymer–zeolite and diluent–zeolite affinity − leading to the ideal ZeoTIPS structure. The dashed lines represent strong polymer–zeolite affinity and weak diluent–zeolite affinity, with varying values of β, corresponding to varying thicknesses of the polymer coating on the zeolite surfaces.

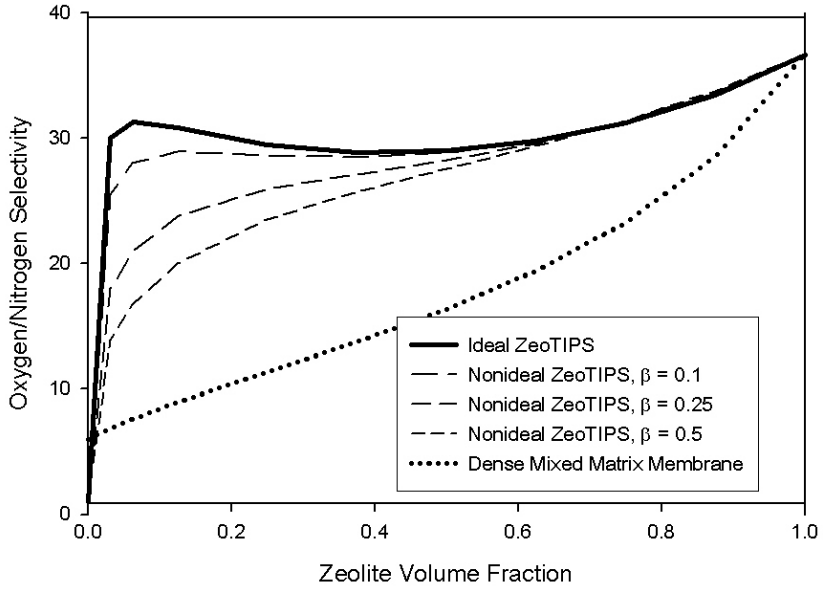

Figure 2.2: Selectivity of ideal and non-ideal ZeoTIPS membranes (with 3:1 void to polymer ratios) and dense mixed matrix membranes using data stated in Table 2.1.

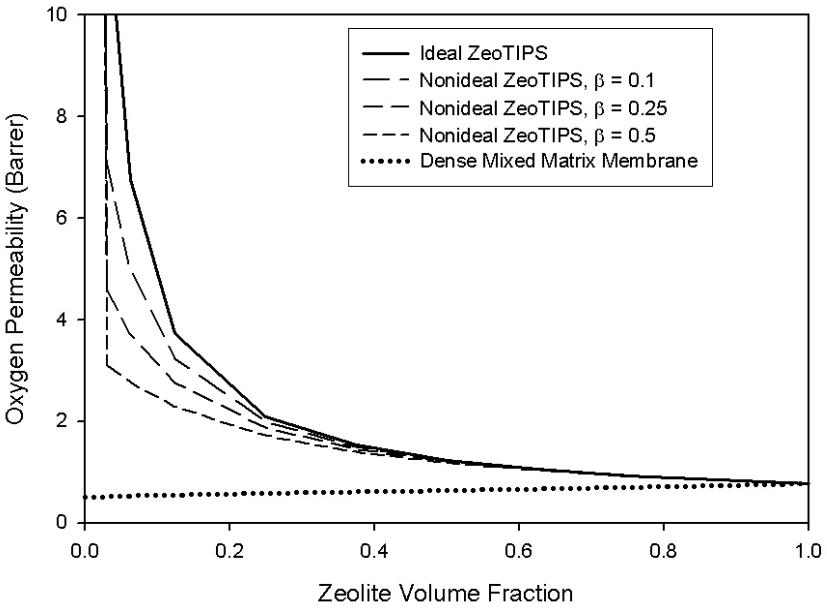

Figure 2.3: Permeability of ideal and non-ideal ZeoTIPS membranes (with 3:1 void to polymer ratios) and dense mixed matrix membranes using data stated in Table 2.1.

As shown in Figures 2.2 and 2.3, for the dense mixed matrix membrane, selectivity increases with increased zeolite loading and permeability increases slightly with increased loading. In reality, the loading cannot approach 100%, and so the selectivity cannot increase much beyond two to three times the selectivity of the matrix polymer (approximately 5.9, according to Table 2.1) within a reasonable range of zeolite loading (see Figure 2.2).

In the ideal parallel−series model (solid lines), expected optimal membrane performance is shown in Figures 2.2 and 2.3. As a reminder, the low zeolite loading data is not meaningful, since it has been shown in our laboratory that at least ~25 vol-% zeolite is needed to prevent microporous connectivity through the membrane. However, the increase from zero to ~25% loading does show that there is an immense increase in selectivity from one to about 29 as soon as the critical zeolite loading is reached. This dramatic increase in selectivity results from the fact that the gas molecules can move more quickly through the voids to the zeolites than through the polymer. Thus, the highly oxygen-selective zeolites perform the bulk of the separation, resulting in selectivities near that of the zeolite particles themselves. Permeability drops off with increased loading, but it always remains higher than that of a dense mixed matrix membrane since the oxygen does not have to pass through the lower permeability polymer matrix.

The non-ideal parallel series model (dashed lines in Figures 2.2 and 2.3) also shows significant improvement over dense mixed matrix membranes, due to the fact that species need diffuse through only a small amount of polymer to traverse the membrane, reducing the resistance to permeation. Even when half of the total polymer in the membrane contributes to coating the zeolite particles (an unrealistic worst-case scenario),

there is still favorable selectivity and permeability. As β approaches one, the ZeoTIPS predictions approach those for dense mixed matrix membranes.

The goal in producing membranes is to approach the ideal case represented by the solid lines in Figures 2.2 and 2.3. This can be accomplished by selecting appropriate polymer–diluent systems that have equal polymer–zeolite and diluent–zeolite affinity *or* by chemically modifying the zeolite surface prior to membrane formation to balance the zeolite affinity for the polymer and diluent. The balancing of polymer−zeolite and diluent−zeolite affinity is discussed extensively in Chapter 5. The remaining discussion in this chapter focuses on the ideal case.

Direct contact of the voids with the zeolite particles is essential to an ideal ZeoTIPS membrane, which makes the balancing of polymer−zeolite and diluent−zeolite interactions important in the formation process. In the case of strong polymer−zeolite interaction, as mentioned in Chapter 5, zeolite surface modifications may be performed to shift this interaction toward equal affinity of the zeolite for polymer and diluent. Several such modifications have been cited in the literature [3, 8].

Figure 2.4 shows the increase in selectivity of the ideal ZeoTIPS membrane as the permeability of the polymer decreases to zero. In the case of the polymer with zero permeability, once the critical zeolite loading has been added, the selectivity with a polymer permeability of zero is approximately that of the zeolite since the zeolite is the only selective component of the membrane.

For the ideal ZeoTIPS membranes with polymers of some permeability, Figure 2.4 shows that a ZeoTIPS membrane is still useful even when the matrix polymer has a higher permeability than the zeolite filler, as is the case where $P_{O2} = 2.0$. This is a result of the high permeability voids in series with the zeolite particles. This result is in contrast to dense mixed matrix membranes, which have shown less improvement over the

polymer matrix when the polymer has a higher permeability than the zeolite [3]. In such a case, the oxygen permeability is reduced whereas the selectivity is increased only slightly.

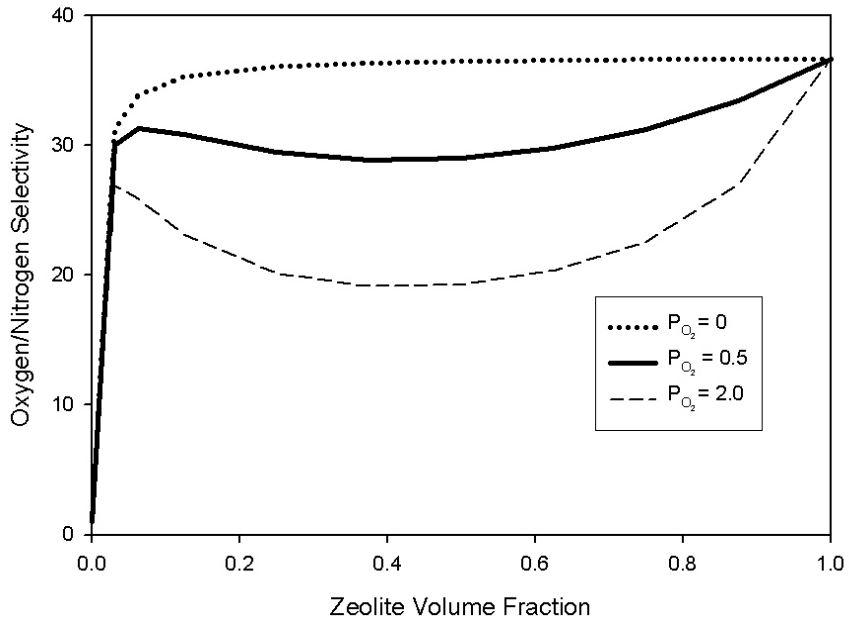

Figure 2.4: Selectivity for ideal ZeoTIPS membranes (3:1 void volume to polymer volume ratio, P_V = 100 Barrers), varying polymer permeability.

To best understand the magnitude of performance enhancement with ZeoTIPS membranes, it is useful to consider the well-documented upper bound proposed by Robeson [9]. Ideal ZeoTIPS membranes produce a combination of selectivity and permeability significantly higher than the upper bound. All data points in Figure 2.5 represent ZeoTIPS membranes with 25 vol-% zeolite loading. The solid dots (•) represent the ideal ZeoTIPS membranes of different polymer permeability. As the polymer permeability increases for zero (uppermost dot) the selectivity of the membrane decreases accompanied by an increase in permeability. As the amount of polymer coating the zeolite surfaces increases in the non-ideal ZeoTIPS case (□), the selectivity

and permeability both decrease, but the values still remain well above the upper bound. Dense mixed matrix membranes (▲) with a 25 vol-% zeolite loading remain below the upper bound for all values of polymer permeability investigated. Note: the case of $P_{O2} = 0$ was not included for dense mixed matrix membranes or for non-ideal ZeoTIPS membranes.

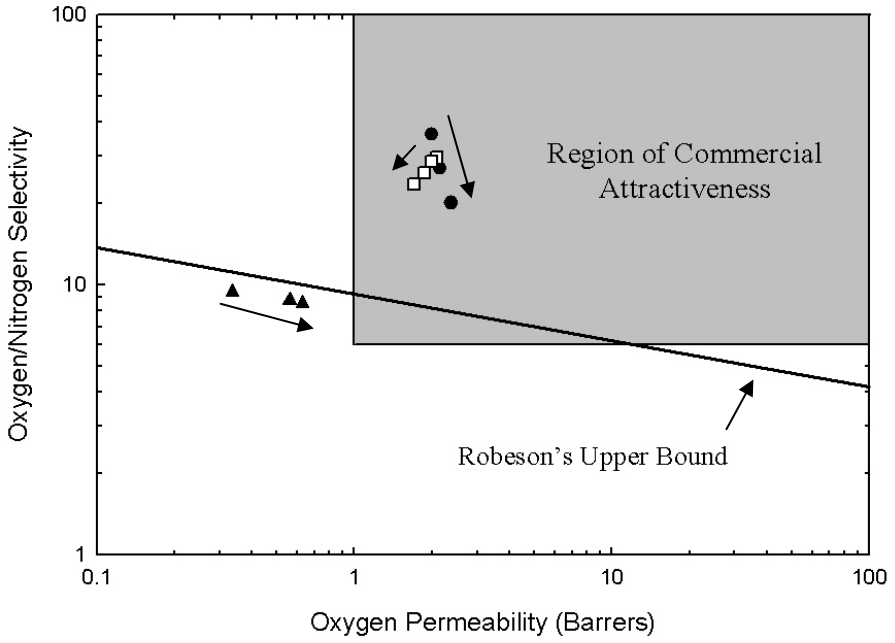

Figure 2.5: Performance of ideal ZeoTIPS membranes, with arrow indicating increasing polymer permeability (●), non-ideal ZeoTIPS membranes, with arrow indicating increasing β (□), and dense mixed matrix membranes, with arrow indicating increasing polymer permeability (▲), plotted with Robeson's 1991 upper bound and region of commercial attractiveness [3]. All points correspond to 25 vol-% zeolite loading, and all ZeoTIPS membrane points correspond to a 3:1 void volume to polymer volume ratio.

Since the voids in a ZeoTIPS membrane can have a variety of permeabilities if the diluent is not extracted, the change in selectivity with decreasing void permeability is shown in Figure 2.6 below. Even if the diluent is a permeable polymer, the increase in

selectivity is still significant compared to other mixed matrix membranes as long as the permeability is higher than that of the polymer matrix, as shown in Figure 2.6.

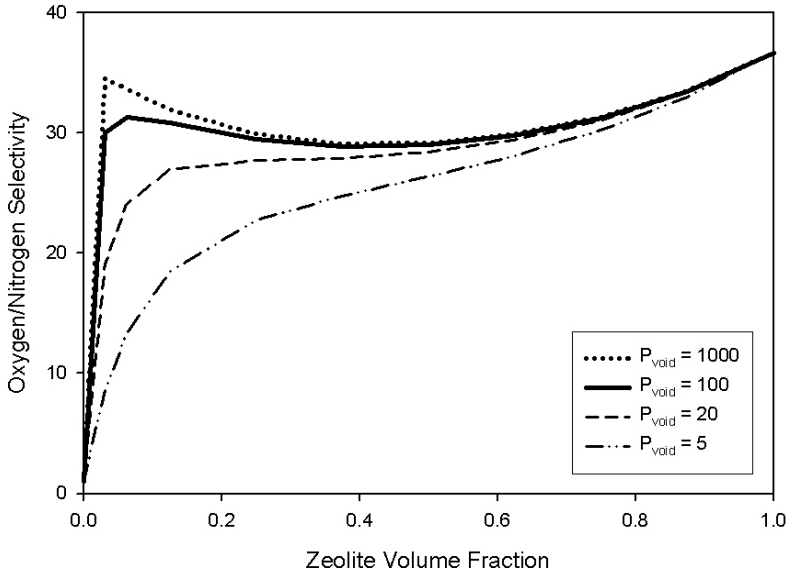

Figure 2.6: Selectivity for ideal ZeoTIPS membranes (3:1 void volume to polymer volume ratio, matrix of PVAc), varying void permeability.

Figure 2.7 shows the effect of void volume to polymer volume ratio in a ZeoTIPS membrane. The greater the void:polymer ratio, the greater the selectivity due to the increased microscopic porosity of the membrane. Since the polymer is permeable, the greater this ratio, the greater the ratio of zeolite to polymer in the membranes, and thus, the greater the average selectivity of the membrane. However, ratios greater than 3:1 can lead to viscosities that are too low for extrusion and polymer concentrations that are too low for structural integrity in the solidified membrane.

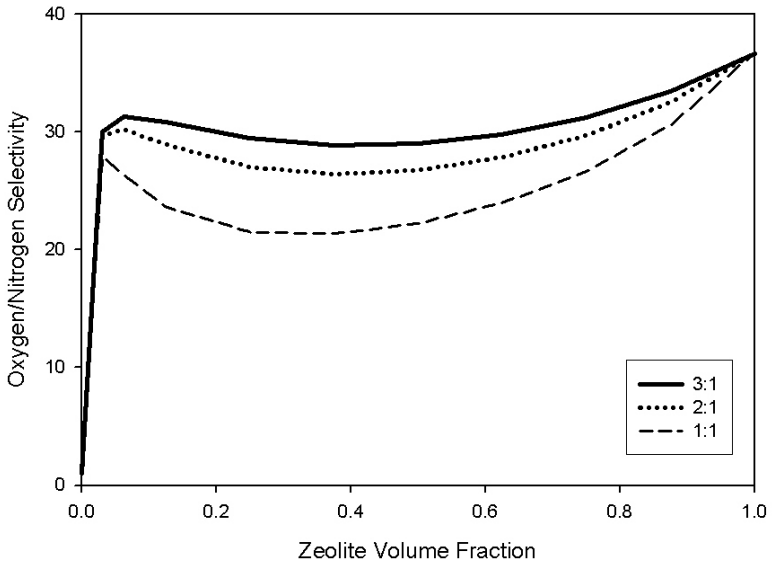

Figure 2.7: Selectivity for ideal ZeoTIPS membranes (matrix of PVAc, P_V = 100 Barrers), varying void volume to polymer volume ratio.

2.4 SUMMARY OF CHAPTER 2

Permeation modeling of ZeoTIPS membranes shows potential for improvement over dense mixed matrix membrane performance when the ZeoTIPS membrane is modeled as polymer in parallel with zeolite and void in series. The membrane performance is predicted to surpass Robeson's upper bound for gas separation polymers. The greatest improvement is exhibited when the polymer in an ideal ZeoTIPS membrane is impermeable to the species to be separated, in contrast to a mixed matrix membrane, which requires permeability of the polymer. An ideal ZeoTIPS membrane is, however, still predicted to improve on mixed matrix membrane performance when the polymer has a higher permeability than the zeolite itself. Furthermore, when the permeability of the void is maximized, and when the ratio of void volume to polymer volume is the greatest

that still leaves each microporous path blocked by at least one zeolite particle, the membrane efficiency is maximized. Finally, even when the ZeoTIPS membrane structure is non-ideal, as is the case when polymer coats the zeolite particles, there is a significant increase in selectivity and permeability compared to dense mixed matrix membranes.

Before attempting extensive experiments, it is important to have a grasp of the ZeoTIPS membrane formation process. Chapters 3 and 4 involve an analysis of that process using experimental results and theoretical modeling together to explain what occurs during the formation of ZeoTIPS membranes.

2.5 REFERENCES

1 C.M. Zimmerman, A. Singh, and W.J. Koros, *Tailoring mixed matrix composite membranes for gas separations*, Journal of Membrane Science, 137 (1997) 145-154.

2 C. Maxwell, *Treatise on Electricity and Magnetism*, 1, Oxford University Press, London, 1873.

3 R. Mahajan and W.J. Koros, *Factors controlling successful formation of mixed-matrix gas separation materials*, Industrial & Engineering Chemistry Reasearch, 39 (2000) 2692-2696.

4 T.T. Moore and W.J. Koros, *Non-ideal effects in organic-inorganic materials for gas separation membranes*, Journal of Molecular Structure, 739 (2005) 87-96.

5 L.M. Robeson, A. Noshay, M. Matzner, and C.N. Merriam, *Physical property characteristics of pulysulfone/poly(dimethylsiloxane) block copolymers*, Angewandte Makromolekulare Chemie, 29 (1973) 47-62.

6 D.M. Ruthven and R.I. Derrah, *Diffusion of Monatomic and Diatomic Gases in 4A and 5A Zeolites*, Journal of the Chemical Society, Faraday Transactions, 71 (1975) 2031.

7 J. Karger and D.M. Ruthven, *Diffusion in zeolites and other microporous solids*, Wiley-Interscience Publications, New York, 1992.

8 S. Husain and W.J. Koros, *Mixed matrix hollow fiber membranes made with modified HSSZ-13 zeolite in polyetherimide polymer matrix for gas separation*, Journal of Membrane Science, 288 (2007) 195-207.

9 L.M. Robeson, *Correlation of separation factor versus permeability for polymeric membranes*, Journal of Membrane Science, 62 (1991) 165-185.

Chapter 3: Thermally Induced Phase Separation Cell Size Analysis with Zeolite Filler[2]

3.1 INTRODUCTION

It is clear from Chapter 2 that ZeoTIPS membranes are promising for high selectivity gas separations. However, before forming membranes and performing experimental measurements, it is necessary to gain fundamental understanding of the membrane formation process. This information will be useful in scaling up the formation process from small scale to a large enough scale for performing permeation experiments.

There has been a great deal of work completed on the growth of diluent droplets in liquid−liquid thermally induced phase separation [1-8]. A number of mechanisms have been proposed for droplet growth in TIPS systems, including Brownian coagulation [9], Ostwald ripening [10], and coalescence-induced coalescence [1, 11]. The two main factors affecting each of these mechanisms, coarsening time and system viscosity, are of interest in this research.

None of the mechanisms for droplet coarsening involve instantaneous growth, and the longer a L−L TIPS system remains in the liquid−liquid state, the larger the average droplet size. Thus, the size of the liquid−liquid region on the phase diagram (see Figure 1.3) and the rate at which the nascent membrane cools combine to influence the size of droplets in the two-phase suspension. Additionally, diluent droplet growth depends on the viscosity of the polymer solution and the phase separated suspension, both of which depend on the polymer molecular weight and, more importantly, the solution

[2] Portions of this chapter are based on: C.V. Funk, B.L. Beavers, and D.R. Lloyd, *Effect of particulate filler on cell size in membranes formed via liquid−liquid thermally induced phase separation*, J. Membrane Sci., (2008) submitted.

composition. These properties determine the ease with which neighboring droplets coalesce.

The addition of zeolite particles complicates the L−L TIPS process. A system with equal affinity of the polymer and diluent with the zeolite surfaces would be ideal. Since it is not a simple task to produce a membrane with perfectly equal interactions, the effects of zeolite particles on TIPS droplet growth in an ideal case can be predicted by looking at various non-ideal cases. These include systems with strong and weak polymer−zeolite interaction and systems with varying particle width to droplet diameter ratios (W/D).

3.2 MATERIALS

Type 4A Zeolite powder was purchased from Advanced Specialty Gas Equipment with a particle size distribution shown in Figure 3.1. The size distribution was measured using a Beckman-Coulter Multisizer 3 (www.beckmancoulter.com) and was adjusted for the cubic shape of the individual particles, since the Coulter Counter assumes the particles are spheres when determining particle volume and diameter. The average particle size was found to be 3.5 μm. Type 4A zeolite is inexpensive, and its 4 angstrom pore size is useful in a variety of separations, such as water purification and some gas separations. A scanning electron micrograph (SEM) image of the powder is shown in Figure 3.2.

Steps must be taken to ensure the zeolite powder is completely dry before forming the membranes, as adsorbed water can affect the interaction of polymer and diluent with the zeolite surface. The powder was held at 200ºC in a vacuum oven at 25 inHg vacuum for 48 hours while sweeping periodically with dry air, which is sufficient to remove

adsorbed water from the particle surfaces [12]. The powder was then stored under 25 inHg vacuum at room temperature until it was used in membrane formation.

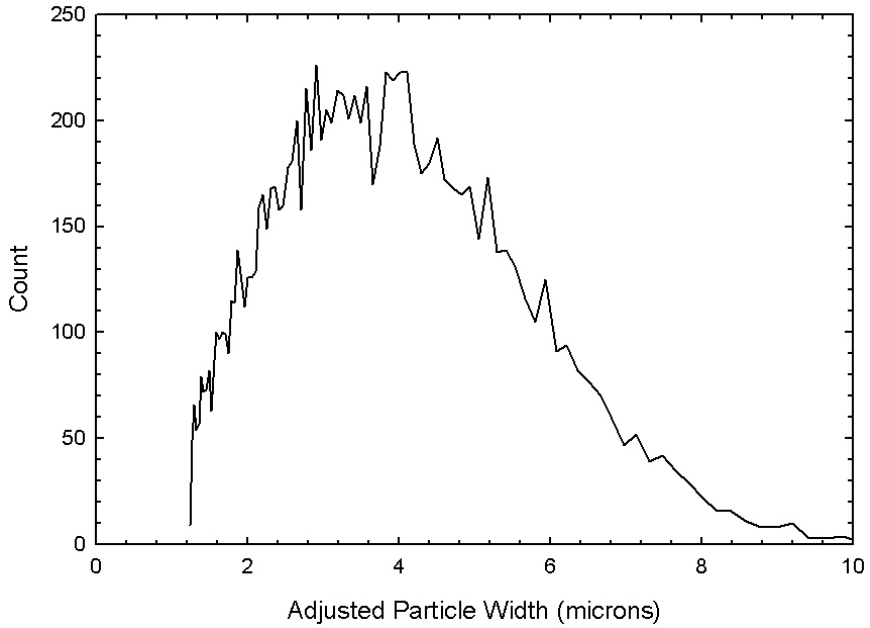

Figure 3.1: Adjusted particle size distribution measured with Coulter Counter.

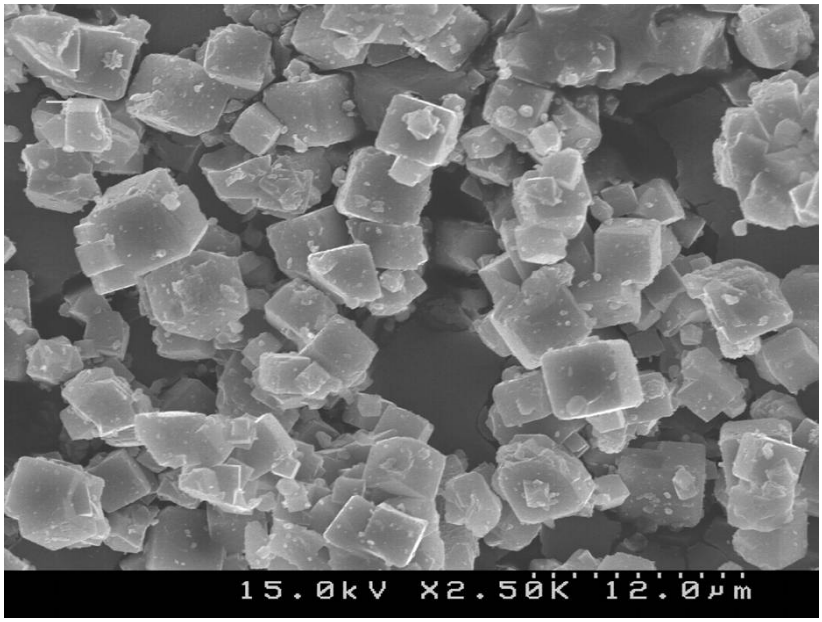

Figure 3.2: SEM image of the 4A zeolite powder.

Isotactic polypropylene (iPP) with a reported weight average molecular weight M_w of 340,000 g/mole was obtained from ExxonMobil Chemical (Houston, TX). Polystyrene (M_n = 170,000 g/mol, M_w = 350,000 g/mil) was purchased from Sigma-Aldrich (St. Louis, MO). Poly(methyl methacrylate) (PMMA, M_n = 32,900 g/mol, M_w = 105,400 g/mol) was obtained in the form of Plexiglas (product code V(811)100) from Rohm & Haas (Philadelphia, PA). Diphenyl ether, cyclohexanol, dodecanol, methanol, and isopropyl alcohol were purchased from Fischer Scientific (Pittsburgh, PA) and were used as received.

3.3 EXPERIMENTAL DESIGN

Three factors were anticipated to effect the growth of droplets in ZeoTIPS membrane formation: cooling rate, polymer concentration, and zeolite loading. The system of isotactic polypropylene−diphenyl ether (iPP−DPE) was chosen for the analysis because it has been the most characterized system in our laboratory [2, 3, 7, 13-16]. Preliminary experiments showed that a cooling rate range of 50 to 125ºC/min (the maximum rate possible using the Linkham hot stage) included all rates that would lead to useful cell sizes. Cells resulting from rates slower than 50ºC/min were so large that zeolite particles were not easily viewed in SEM images of the membranes. The range of 20 to 35 wt-% polymer was chosen because excessively large cells formed in solutions of less than 20 wt-% polymer and solutions of greater than 35 wt-% polymer were too viscous to incorporate the zeolite powder. A range of 20 to 35 wt-% zeolite was chosen because SEM images from preliminary experiments exhibiting numerous unobstructed pores showed zeolite loadings below 20 wt-% were too low to prevent a connected microporous structure. Furthermore, it was difficult to mix large concentrations of zeolite (greater than 35 wt-%) into the polymer−diluent solutions.

Using the JMP-IN statistical analysis software, a design of experiments of 32 membranes (including duplicates) was constructed. A central composite response surface design, useful for non-linear systems, was used to characterize the system. This design of experiments, which includes three levels of the above three factors and is randomized to prevent experimental bias, is shown in Table 3.1.

3.4 EXPERIMENTAL PROCEDURE

Typical small scale methods for producing liquid−liquid thermally induced phase separation samples [3] were not sufficient for forming ZeoTIPS membranes. The additional factors to be addressed begin with particle settling and subsequent clumping. Traditional methods of small scale formation do not require constant agitation, and in the case of high viscosity solutions, it is necessary to undertake more rigorous mixing methods to obtain the necessary dispersion of particles.

To form the samples for this study, glass test tubes were first filled with the necessary amounts of polymer and diluent. The test tubes were then purged with nitrogen and heat sealed. In systems where the viscosity was low enough to suspend zeolites without manual mixing, it was possible to add the zeolite powder to this inhomogeneous mixture before purging and heat sealing as long as constant agitation could be achieved during the dissolution process. To accomplish the necessary agitation to prevent clumping of the zeolite particles and achieve proper dispersal, a rotisserie spinning at 1 to 5 rpm inside an oven was used. Figure 3.3 is an illustration of this assembly, although the wire clamps used to immobilize the test tubes are not shown.

Table 3.1: Cell size analysis experimental design

Membrane	Cooling Rate (°C/min)	Polymer wt-%	Zeolite wt-%	Droplet Size (μm^2)
1	50	20	20	48.1
2	87.5	20	27.5	18.7
3	125	20	35	26.8
4	50	27.5	27.5	15.9
5	87.5	20	27.5	28.2
6	87.5	35	27.5	8.0
7	125	27.5	27.5	9.8
8	125	35	20	15.3
9	87.5	27.5	27.5	16.7
10	87.5	35	27.5	12.4
11	125	35	20	10.9
12	87.5	27.5	27.5	17.2
13	125	27.5	27.5	7.9
14	125	35	35	16.3
15	50	35	35	27.1
16	125	20	35	21.8
17	50	20	35	78.9
18	50	35	35	34.5
19	87.5	27.5	35	29.2
20	87.5	27.5	35	34.9
21	50	35	20	36.4
22	87.5	27.5	27.5	16.7
23	50	20	20	36.4
24	125	20	20	19.5
25	50	35	20	22.3
26	50	27.5	27.5	15.7
27	125	35	35	19.6
28	125	20	20	15.0
29	87.5	27.5	20	12.2
30	87.5	27.5	27.5	18.8
31	50	20	35	76.3
32	87.5	27.5	20	9.1

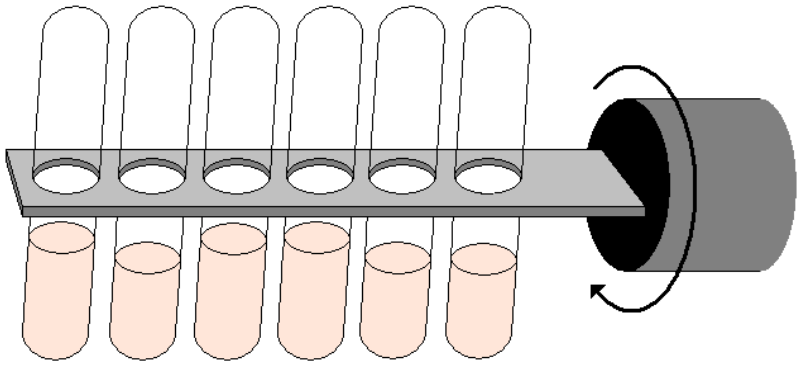

Figure 3.3: Test tube agitation assembly

After 24 hours of constant agitation at high temperature (>20ºC above the system phase separation temperature), the test tube containing the solution/suspension was removed from the oven and frozen in liquid nitrogen, after which the sample was removed from the liquid nitrogen. When the test tube reached room temperature (cold samples lead to water vapor condensation), the test tube was broken and a small slice of the solid sample was placed between two glass slides of dimensions 22 x 22 x 0.17 mm with a 0.13 mm Teflon spacer and vacuum grease applied to seal the edges. The sample was then heated using a Linkam TMS 91 hot stage at a rate of 125ºC/min to a temperature roughly 20ºC above the system phase separation temperature. The sample was held at this temperature for 10 minutes to erase the thermal history and was then cooled at the desired rate (50−125ºC/min).

If a polymer−diluent solution has a high viscosity, as is the case with the isotactic polypropylene−diphenyl ether system, the solution must be homogeneous before adding the zeolite. If not, the zeolite increases the system viscosity to such an extent as to prevent proper mixing of the polymer and diluent. Therefore, once the polymer solution had been solidified and brought to room temperature, the test tube was broken, and a portion of the sample was placed into a new test tube and weighed. The necessary

amount of zeolite powder was then added to the test tube, along with a 0.25 inch steel screw. The test tube was then purged and sealed, and upon melting of the sample in an oven, the sample was briefly removed and agitated using a strong magnet to move the screw. This process was repeated 3 or 4 times to ensure proper mixing, since the sample viscosity increases quickly upon removal from the oven. The same process for hot stage sample formation explained above then applies.

Upon solidification, the membranes were removed from the glass slides and extracted in a volatile solvent (methanol or isopropyl alcohol, depending on the solubility of the polymer) for 24 hours. The membranes were then dried under ambient conditions without restraint.

The iPP−DPE membranes were produced by heating on the hot stage to 160°C and holding for 10 minutes. Subsequent cooling rates are described in Table 3.1. An additional iPP−DPE experimental set was produced using 27.5 wt-% polymer, cooling at 125ºC/min, and zeolite loadings of 0 and 10 wt-%.

Poly(methyl methacrylate)−cyclohexanol samples were formed similarly, but only using 27.5 wt-% polymer and cooling rates of 125°C/min after heating to 160°C and holding at that temperature for 10 minutes to achieve homogeneity. Polystyrene−dodecanol samples were made from 27.5 wt-% polymer, and were formed by adding all components to a sealed test tube and heating with constant agitation at 200°C. When forming polystyrene−dodecanol samples by the hot stage method, large amounts of diluent migrated out of the sample, changing the polymer concentration by an unknown amount; therefore this method was not repeatable enough for this study. Instead, once homogeneous, the test tube samples were cooled in ice water, the samples were removed from the test tubes, and a slice of each was taken from the center of the

cylindrical sample one centimeter from the bottom. These samples were imaged following extraction and drying without using the hot stage for further processing.

Isotactic polypropylene and polystyrene samples were extracted in isopropyl alcohol (IPA) and poly(methyl methacrylate) (PMMA) samples were extracted in methanol (IPA greatly softens PMMA that is plasticized by cyclohexanol), all for 24 hours before drying. After freeze fracturing with liquid nitrogen, a minimum of four SEM images were taken of each sample to ensure a good average of cell sizes. From these four images, the cross sectional area of 50 easily discernable cells were measured (with duplicates included, 100 cells were measured for each type of sample). Image analysis was performed using Image-Pro Plus Version 3.5.1. Figure 3.4 illustrates the measuring procedure. Image-Pro determines the number of pixels in each enclosed shape and translates it into an area based on a calibration measurement from the scale bar in each SEM image.

3.5 RESULTS AND DISCUSSION

3.5.1 Effects of Polymer Concentration, Cooling Rate, and Zeolite Loading on Cell Size

The first system investigated consisted of iPP, DPE, and 4A zeolite. In this system, the polymer–zeolite affinity is greater than the diluent–zeolite affinity, resulting in polymer-coated particles. The results from the experimental design were input into JMP and formed into a 4-dimensional relationship for cell size as a function of polymer content, cooling rate, and zeolite loading, shown in Figures 3.5 to 3.9. Each of the plots shows cell size as a function of polymer wt-% and cooling rate. The zeolite loading varies from plot to plot.

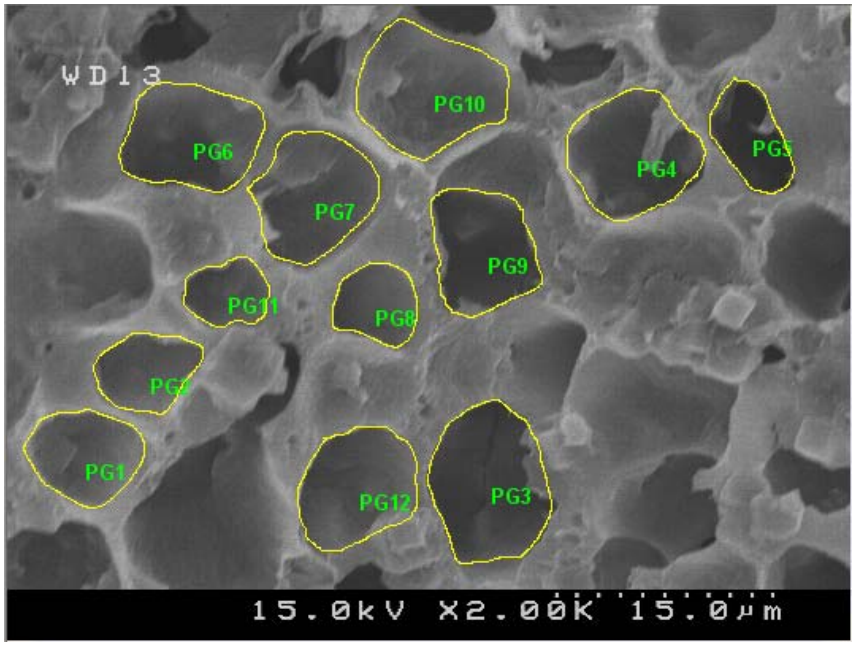

Figure 3.4: Sample SEM showing image analysis procedure with iPP−DPE sample made from 27.5 wt-% polymer and cooled at 50°C/min. Pixels in each enclosed shape translate to cell cross sectional area.

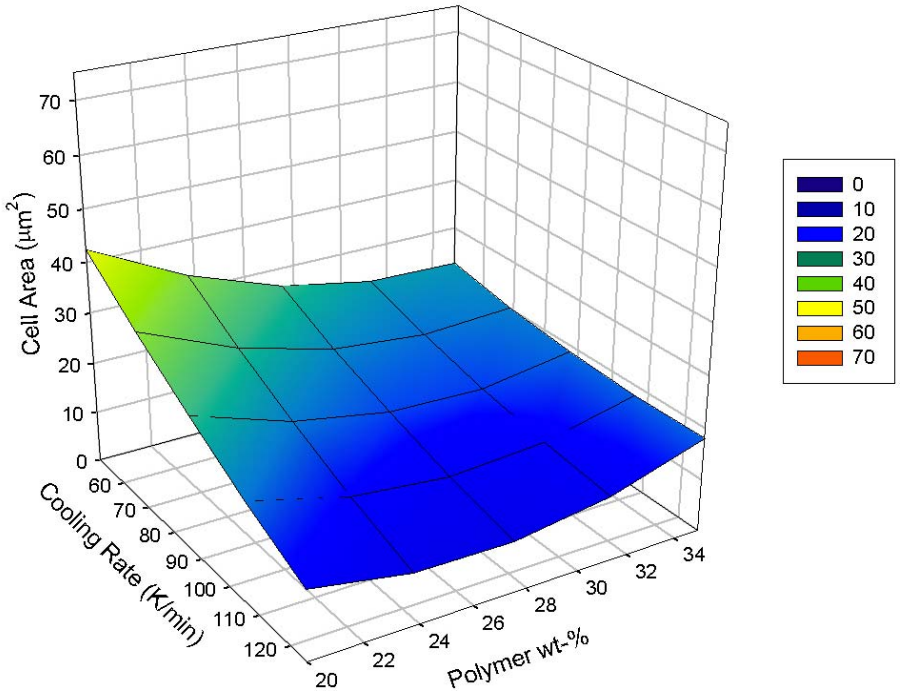

Figure 3.5: Cell size data with 20 wt-% zeolite loadings

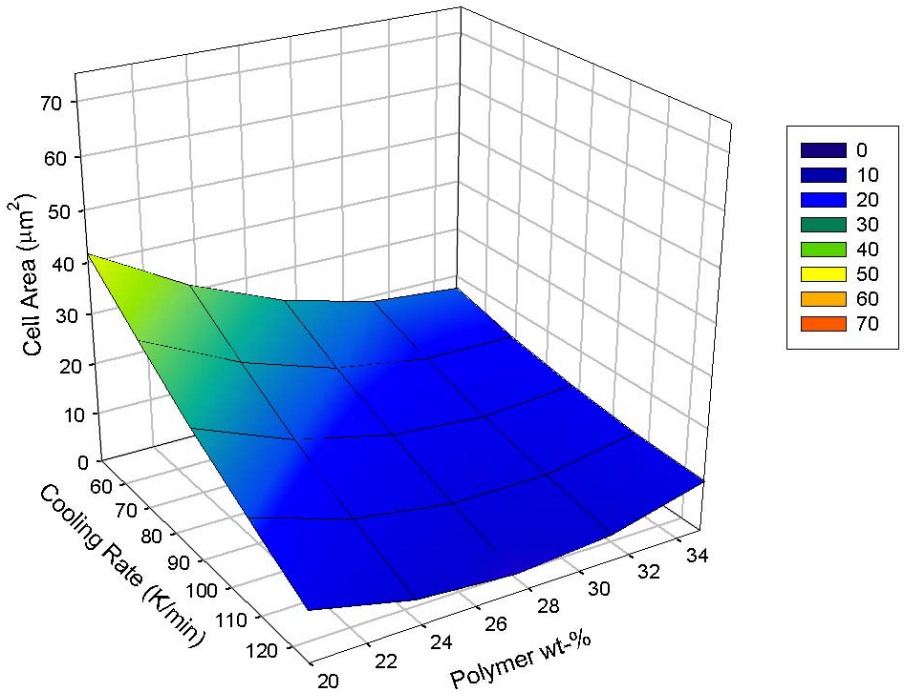

Figure 3.6: Cell size data with 23.75 wt-% zeolite loadings

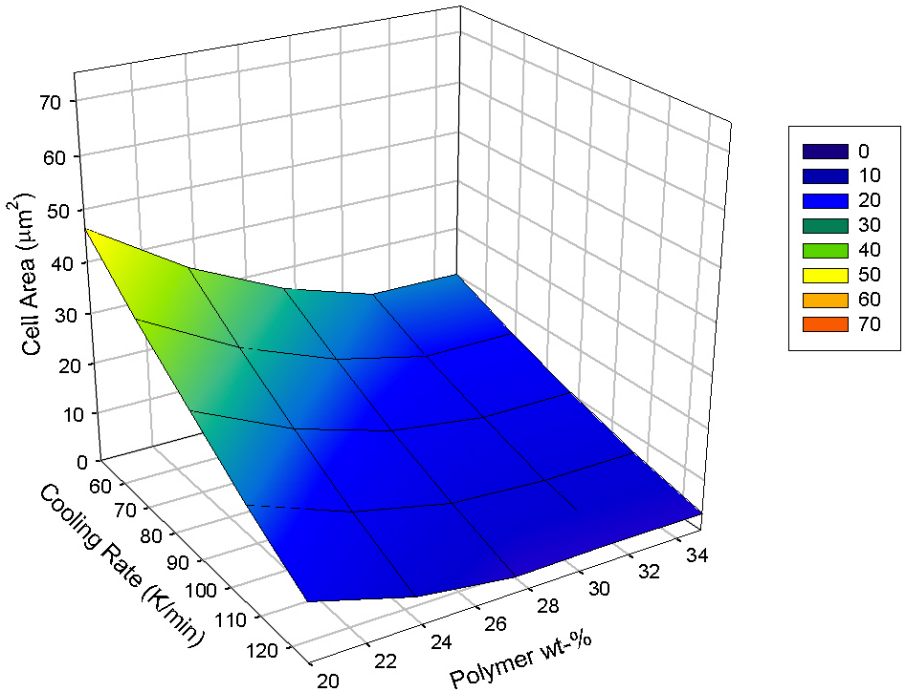

Figure 3.7: Cell size data with 27.5 wt-% zeolite loadings

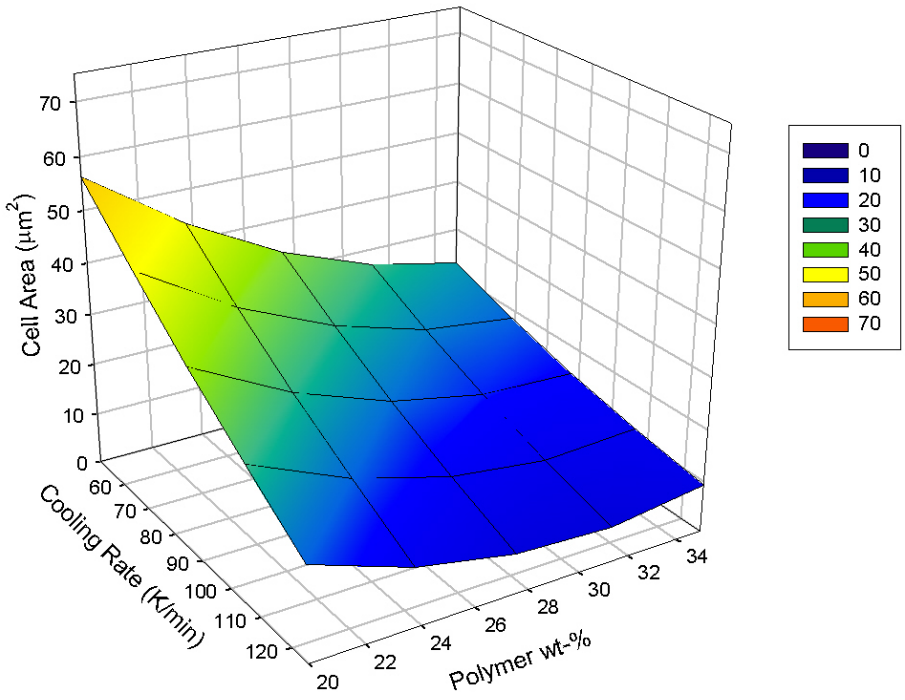

Figure 3.8: Cell size data with 31.25 wt-% zeolite loadings

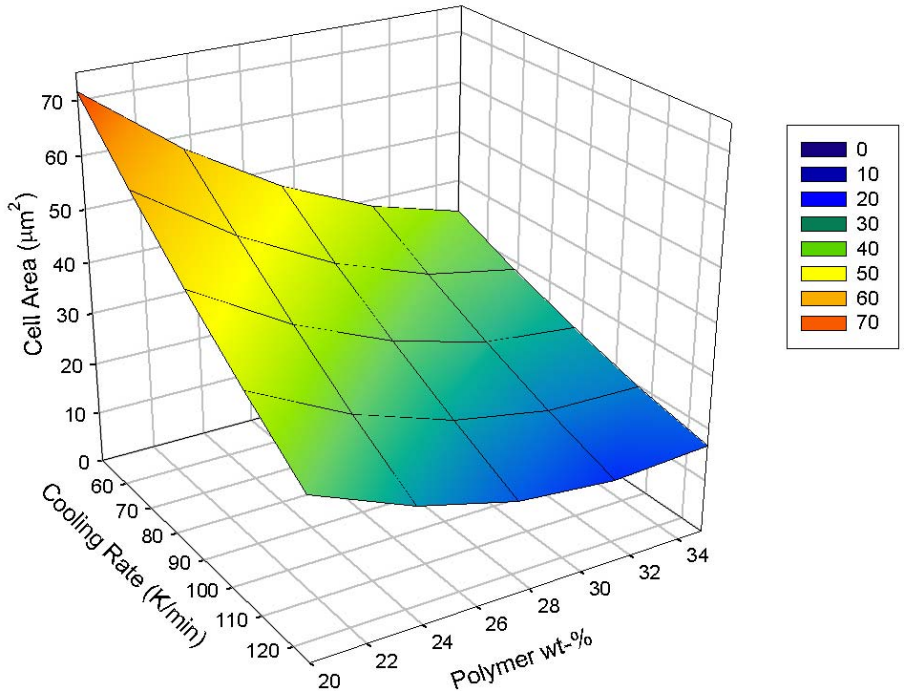

Figure 3.9: Cell size data with 35 wt-% zeolite loadings

In general, at any given combination of polymer wt-% and cooling rate, the cell sizes decreased, passed through a minimum, and then increased with increasing zeolite loading. This is illustrated by the experimental fit shown in Figure 3.10 (with additional data included and to be discussed below).

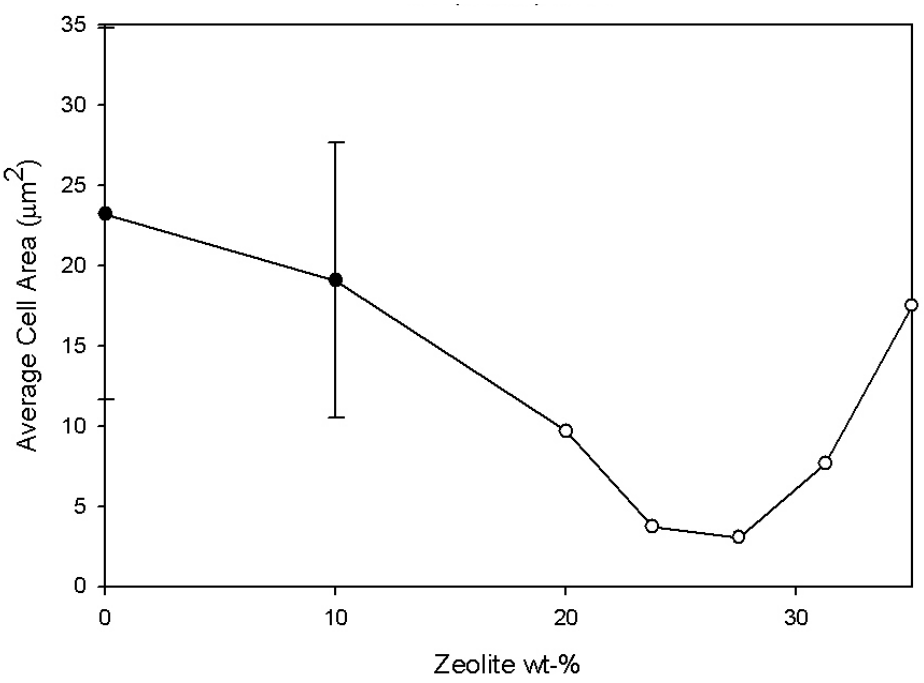

Figure 3.10: Cell sizes in iPP−DPE system with 27.5 wt-% polymer and cooling rate of 125°C/min. Open circles represent data extracted from Figures 3.5-3.9. Solid circles represent direct experimental data. Error bars indicate ± 1 standard deviation.

Analysis of Figures 3.5 through 3.9 indicates that at a fixed polymer composition increased cooling rate led to smaller cells. This observation is true for all zeolite loadings, as shown in Figure 3.11.

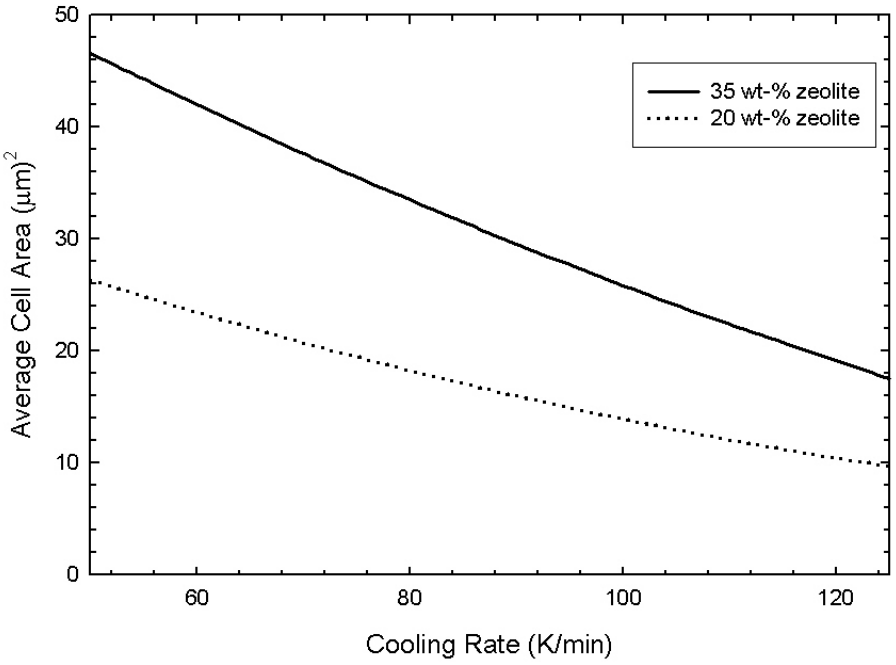

Figure 3.11: Effect of cooling rate and zeolite loading on iPP−DPE cell size at constant 27.5 wt-% polymer composition.

Slower cooling rates allow a greater amount of time for polymer to migrate and adhere to the zeolite surfaces. With increased zeolite loadings, more polymer acts in this way, resulting in the large differences in cell size over the experimental range of cooling rates. In an extreme case, it was shown in experiments discussed in Section 5.6 that extruded membranes cooled too quickly resulted in poor polymer−zeolite adhesion for the iPP−DPE system. Thus, the slower the cooling rate, the better the polymer−zeolite adhesion.

Since the expected result was a decrease in cell size over the entire range of zeolite loading due to the inhibition of droplet coalescence, the result was intriguing. It was hypothesized that the strong polymer−zeolite interaction resulted in a decreasing polymer concentration in the bulk solution with increasing zeolite loading, becoming significant where the cell sizes began to bottom out. Less polymer in solution leads to

larger diluent droplets since it becomes easier for droplets to grow and coalesce with decreased solution viscosity. These changes, combined with coalescence inhibition over the entire range of zeolite loading, were hypothesized to have resulted in the minimum.

3.5.2 Effects of Initial Droplet Size and Polymer−Zeolite Affinity on Droplet Growth

Further experimental sets were chosen to verify the hypothesis stated above regarding the effect of polymer−zeolite interaction on droplet growth. The first set involved PMMA and cyclohexanol with zeolite. This system also has a strong polymer−zeolite interaction due to the hydrophilicity of PMMA, but has very small droplets compared with iPP−DPE (see Figures 3.4 at 2,000X magnification and 3.12 at 15,000X magnification). The large particle width to droplet diameter W/D ratio was intended to eliminate the coalescence inhibition shown in the first experimental set. The samples were formed in the same manner, but only using 27.5 wt-% polymer and a cooling rate of 125°C/min. The fact that the droplets were so small compared to the particles allowed them to grow with minimal coalescence inhibition caused by the particles. Consequently, the average droplet size continued to increase with increasing zeolite loading throughout the range of experimental conditions studied, as shown in Figure 3.13.

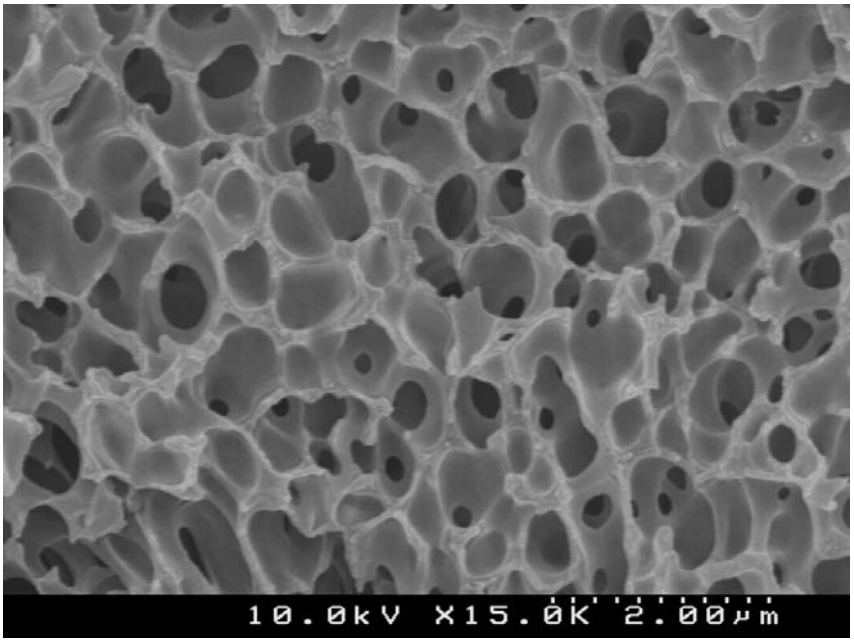

Figure 3.12: Typical PMMA−cyclohexanol sample made with 27.5 wt-% polymer and cooled at 125ºC/min.

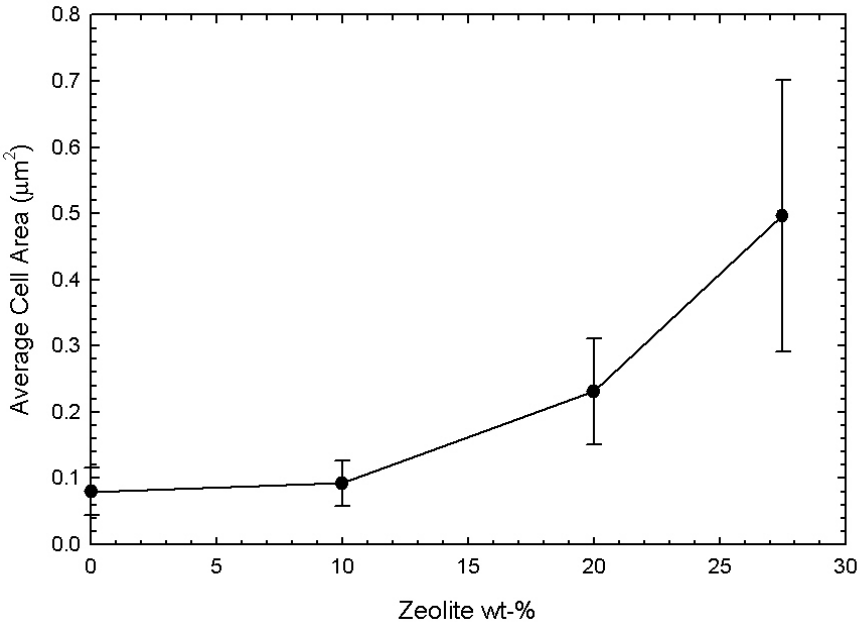

Figure 3.13: Cell sizes in PMMA−cyclohexanol system with 27.5 wt-% polymer and cooling rate of 125ºC/min. Error bars indicated ± 1 standard deviation.

Figure 3.10 shows additional iPP−DPE results (for comparison to those taken from the data in Figure 3.5-3.9) where zeolite loadings of 0 and 10 wt-% were added to the previous analysis to understand fully the extent of coalescence inhibition at low zeolite loadings. As predicted, because of droplet coalescence inhibition by the particles, the cell size decreases as zeolite loading increases for low zeolite loadings. The experimental fit shown in Figure 3.10 has no error bars because it is the mathematical trend produced from the first experimental data set, meaning none of the points shown in the fit were actually determined experimentally.

The third system investigated was polystyrene−dodecanol, a system with weak polymer−zeolite interaction resulting from the use of a hydrophilic diluent with a hydrophobic polymer. This set was intended to produce cells that were much smaller than the particles, but resulted in cells much larger than the particles due to the very large 2-phase region of the phase diagram for this system [17] (see Figure 3.14). The system was analyzed nonetheless, and the result shown in Figure 3.15 was as expected. Because there is an affinity of the diluent for the zeolite particles, the particles in the 2-phase solution tend to reside in the diluent droplets. This affinity results in an increase in volume of all droplets containing particles, and the outcome is not particularly useful, since a useful membrane would not have such a small W/D ratio (Figure 3.14 shows a range of 100−300 μm^2 cell areas, whereas Figures 3.4 and 3.12 show much smaller cell sizes). Zeolite loadings of greater than 20% were not included because the overall morphology of these membranes deviates from a cellular nature.

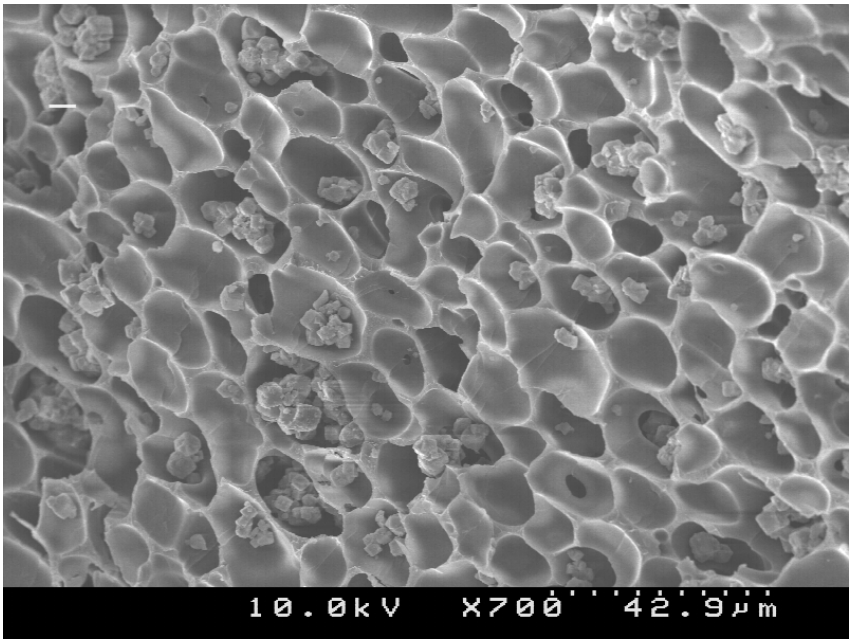

Figure 3.14: Typical polystyrene−dodecanol ZeoTIPS sample made with 27.5 wt-% polymer and 10 wt-% zeolite loading, cooled in ice water.

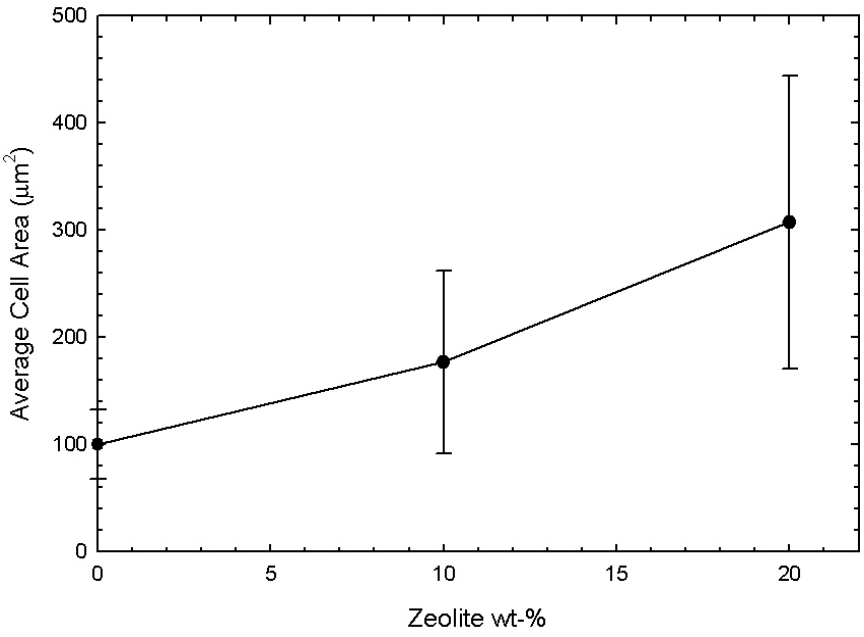

Figure 3.15: Cell sizes in polystyrene−dodecanol system with 27.5 wt-% polymer after quenching in ice water. Error bars indicate ± 1 standard deviation.

The latter experimental sets verify the hypothesis stated with regard to the iPP−DPE system. Combined, the results predict that with an ideal system (having equal interaction of polymer and diluent with the zeolite surfaces and having a W/D~1) the cell size will decrease with increasing zeolite loading solely as a result of coalescence inhibition. The extent to which this will occur depends on the cooling rate and polymer composition, as shown by the initial analysis.

3.6 SUMMARY OF CHAPTER 3

Adding zeolite powder to liquid−liquid thermally induced phase separation membranes complicates the droplet growth behavior. It was found that coalescence inhibition due to the presence of particles decreases the average droplet size. However, when strong polymer−zeolite interaction occurs, coalescence inhibition, if present, is counteracted by an increase in bulk diluent concentration. When producing ZeoTIPS membranes, these observations should be taken into account to reach the desired cell size.

3.7 REFERENCES

1 D.S. Martula, T. Hasegawa, D.R. Lloyd, and R.T. Bonnecaze, *Coalescence-induced coalescence of inviscid droplets in a viscous fluid*, Journal of Colloid and Interface Science, 232 (2000) 241-253.

2 K.S. McGuire, D.R. Lloyd, and G.B.A. Lim, *Microporous membrane formation via thermally-induced phase separation. VII. Effect of dilution, cooling rate, and nucleating agent addition on morphology*, Journal of Membrane Science, 79 (1993) 27-34.

3 D.R. Lloyd, S.S. Kim, and K.E. Kinzer, *Microporous membrane formation via thermally-induced phase separation. II. Liquid-liquid phase separation*, Journal of Membrane Science, 64 (1991) 1-11.

4 H. Matsuyama, S. Berghmans, M.T. Batarseh, and D.R. Lloyd, *Effects of thermal history on anisotropic and asymmetric membranes formed by thermally induced phase separation*, Journal of Membrane Science, 142 (1998) 27-42.

5 S.S. Kim and D.R. Lloyd, *Thermodynamics of polymer–diluent systems for TIPS. III. Liquid–liquid phase separation systems*, Polymer, 33 (1992) 1047-1057.
6 T. Hasegawa, D.S. Martula, D.R. Lloyd, and R.T. Bonnecaze, *Coalescence-induced coalescence: calculation of the velocity field*, Physics of Fluids, in preparation (2000).
7 K.S. McGuire, A. Laxminarayan, D.S. Martula, and D.R. Lloyd, *Kinetics of droplet growth in liquid-liquid phase separation of polymer-diluent systems: model development*, Journal of Colloid and Interface Science, 182 (1996) 46-58.
8 A. Laxminarayan, K.S. McGuire, S.S. Kim, and D.R. Lloyd, *Effect of initial composition, phase separation temperature, and polymer crystallization on the formation of microcellular structures via TIPS*, Polymer, 35 (1994) 3060-3068.
9 H. Wang and R.H. Davis, *Droplet growth due to Brownian, Gravitational, or Thermocapillary motion and coalescence in dilute dispersions*, Journal of Colloid and Interface Science, 159 (1993) 108-118.
10 P.W. Voorhees, *Ostwald ripening of two-phase mixtures*, Annual Reviews of Materials Science, 22 (1992) 197-215.
11 D.S. Martula, R.T. Bonnecaze, and D.R. Lloyd, *The effects of viscosity on coalescence-induced coalescence*, International Journal of Multiphase Flow, 29 (2003) 1265-1282.
12 T.T. Moore, R. Mahajan, D.Q. Vu, and W.J. Koros, *Hybrid membrane materials comprising organic polymers with rigid dispersed phases*, AIChE Journal, 50 (2004) 311-321.
13 K.S. McGuire, A. Laxminarayan, and D.R. Lloyd, *Kinetics of droplet growth in liquid-liquid phase separation of polymer-diluent systems: experimental results*, Polymer, 36 (1995) 4951-4960.
14 S.S. Kim and D.R. Lloyd, *Microporous membrane formation via thermally-induced phase separation. III. Effect of thermodynamic interactions on the structure of isotactic polypropylene membranes*, Journal of Membrane Science, 64 (1991) 13-29.
15 G.B.A. Lim, S.S. Kim, Q. Ye, Y.F. Wang, and D.R. Lloyd, *Microporous membrane formation via thermally-induced phase separation. IV. Effect of isotactic polypropylene crystallization kinetics on membrane structure*, Journal of Membrane Science, 64 (1991) 31-40.
16 S.S. Kim, G.B.A. Lim, A.A. Alwattari, Y.F. Wang, and D.R. Lloyd, *Microporous membrane formation via thermally-induced phase separation. V. Effect of diluent mobility and crystallization on the structure of isotactic polypropylene membranes*, Journal of Membrane Science, 64 (1991) 41-53.
17 P.C.v.d. Heijden, M.H.V. Mulder, and M. Wessling, *Phase behavior of polymer-diluent systems characterized by temperature modulated differential scanning calorimetry*, Thermochimica Acta, 378 (2001) 27-34.

Chapter 4: ZeoTIPS Formation Modeling

4.1 INTRODUCTION

Modeling of membrane formation via thermally induced phase separation has been undertaken previously [1-7]. In particular, the growth of droplets during the phase separation has been studied and modeled in an attempt to understand and control structure development. However, none of the models developed to date have taken into account the presence of particulate fillers, which certainly have major effects on the kinetics of droplet growth and the size of the cells in TIPS membranes, as discussed in Chapter 3.

Two goals exist in modeling ZeoTIPS membrane formation. The first is to develop a fundamental understanding of the membrane formation process, including determining the mechanism by which microporous connectivity across the membrane is prohibited by the zeolite particles. The second goal is to produce a predictive tool that can be used to calculate the amount of zeolite that needs to be added to a polymer−diluent solution to prevent microporous connectivity across the membrane.

In this chapter two mathematical approaches are used in an attempt to satisfy the stated goals. The first approach (Section 4.2) relies on classical percolation theory; the second approach (Section 4.3) depends on Monte Carlo calculations. Both approaches were designed to shed light on basic phenomena affecting membrane structure formation, which in turn serves as the basis for more complex models.

4.2 CELL LATTICE MODELS

A ZeoTIPS membrane, as shown in Figure 1.5, is somewhat analogous to a

porous structure that is often described by classical bond percolation theory; therefore, the model described in this section is based upon that theory [8]. Bond percolation theory states that when bonds are randomly placed between nodes of a regular lattice, there is a critical number of bonds or a "percolation threshold" below which it is impossible for connected bonds to traverse the membrane. This percolation threshold is dependent on Z, the number of bonds that connect to each node in the lattice. For a 2-dimensional hexagonal packing (Z = 6), the percolation threshold is 0.35, meaning 35% of the lattice must be connected with randomly-placed bonds in order for connectivity to be possible [8]. The cells of a ZeoTIPS membrane are analogous to the lattice points in classical bond percolation theory, and the micropores between cells are analogous to the bonds, although bonds (micropores) are removed in the ZeoTIPS membrane simulation, whereas they are added in classical theory. Thus, as a starting point for modeling the ZeoTIPS membrane, a 2-dimensional hexagonal lattice was first set up as an approximation of the cell packing in ZeoTIPS membranes.

4.2.1 2-Dimensional Model

The 2-dimensional model was developed as a stepping stone toward developing the 3-dimensional model described in Section 4.2.2. In constructing the 2-D model, the first step was to define a lattice on which the cells are located in a hexagonal lattice so that each cell has six open pores leading to neighbors, as shown in Figure 4.1. Each cell has an arbitrary diameter of two units. The overall lattice measures 50 by 36 units and contains a total of 520 cells.

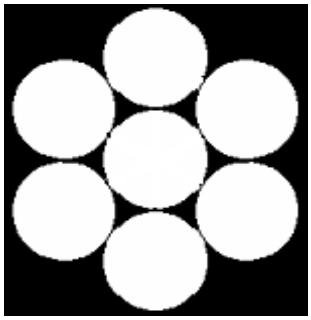

Figure 4.1: Cell structure in the 2-dimensional cell lattice model.

Both the cells and the pores in the lattice are numbered and corresponding cells and pores are related to each other via an array (# of cells by # of pores) of ones and zeroes.

While the idea of each cell connected to six nearest neighbors via pores is ideal, upon examination of numerous electron micrographs of microporous membranes formed via L–L TIPS, it is evident that each cell is not linked via pores to six neighbors. Indeed, micrographs indicate that on average there are between two and three pores per cell. For a membrane to be useful and allow good permeation from one membrane surface to the other surface, the structure should have on average at least two pores per cell. Consequently, the 2-D lattice structure constructed above was modified by randomly closing pores until each cell is left with three open pores.

Having defined the size and location of the cells and having "closed" the desired number of pores, the next step is to insert the zeolite particles into the lattice structure. Particle size is important: the larger a particle is, the better the chance of blocking one or more pores. As a starting point, the model uses a square particle of width W equal to the cell diameter D; that is, W/D = 1. (Subsequent analysis to determine the impact of modifying W/D is reported below.) A specified number of particles (for example, 100 particles) are randomly placed into the lattice one at a time. If a newly placed particle

overlaps with one of the previously place particles, it is repositioned. Once the desired number of particles has been added to the lattice, the program determines which pores have been "blocked" by using the definition that an "open" pore becomes "blocked" if it falls within the bounds of a particle. The resulting structure looks similar to Figure 4.2.

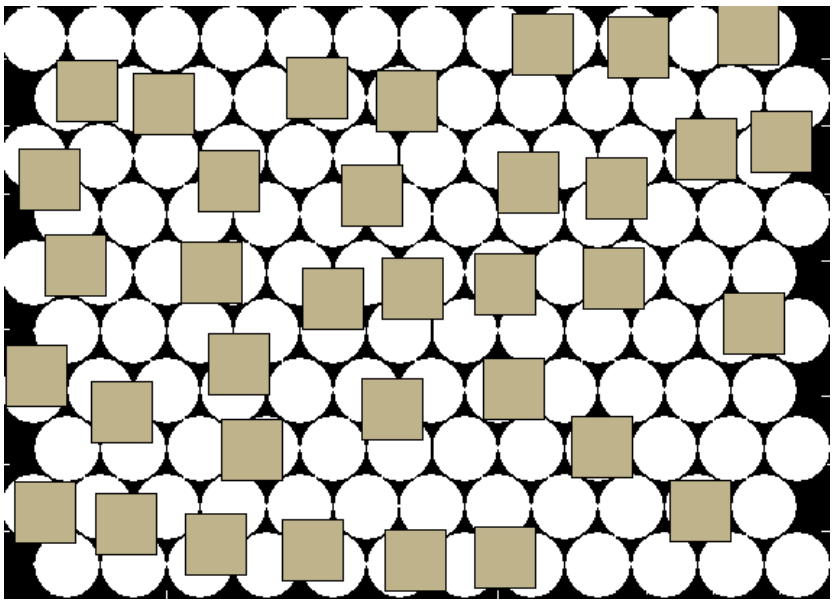

Figure 4.2: Portion of the 2-dimensional simulation showing structure of cells and particles.

Once the desired number of particles has been added, determination of microporous connectivity across the lattice involves application of bond percolation theory. Specifically, the ratio of "open" pores to the "total" number of pores (open plus closed plus blocked) is calculated. This ratio is compared to the theoretical percolation threshold of 0.35, and if the calculated value is greater than 0.35, the system is said to be connected. Otherwise, enough particles have been added to block microporous connectivity across the membrane. To improve the statistical reliability of this method, the entire process is repeated 500 times, with each repetition representing a different random placement of the "closed" pores, "open" pores, and particles. Each repetition

yields a value of the ratio of open pores to total pores. It was determined that 500 repetitions yielded nearly the same result as 250 repetitions, and is therefore statistically reliable for the purposes of this model. The results of all 500 repetitions are combined and output as the percent of the total repetitions that resulted in connected microporous structures. This point is then plotted on Figure 4.3.

The program then resets, adds a different number of zeolite particles, checks 500 times for microporous connectivity, and adds another point to Figure 4.3. After repeating this procedure for a variety of numbers of particles, one obtains a complete curve such that shown in Figure 4.3. The "critical zeolite loading" is defined as the point where the number of particles is sufficient that none of the 500 runs resulted in connected structures (that is, 0% of the "membranes" are below the critical zeolite loading level) and the curve reaches the x-axis. The critical zeolite loading is not analogous to the percolation threshold, but represents the smallest number of particles needed to reach the percolation threshold.

Figure 4.4 demonstrates that changing the ratio of particle width W to cell diameter D changes the number of pores a single particle can block. To determine the impact that changing W/D has on the shape and location of the curve shown in Figure 4.3, the procedure outlined above was repeated for a variety of W/D values. The results are presented in Figure 4.5. The smaller the particles, the more particles are needed to block all paths.

The results presented in Figure 4.5 are re-plotted in Figure 4.6 in terms of particle area-%, the 2-dimensional corollary to volume-%, which is useful in making membranes experimentally. According to these curves, the W/D ratio does not have a large effect on the critical zeolite loading, although results discussed in Section 4.2.2 show that the W/D ratio becomes more important in 3-dimensional space.

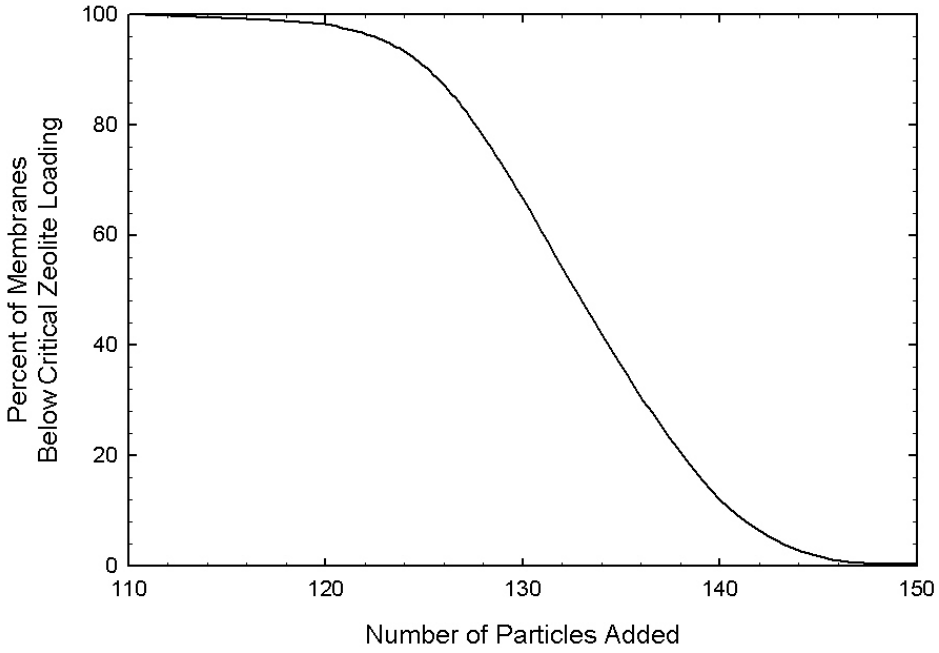

Figure 4.3: Results from the 2-dimensional lattice model for W/D = 1.

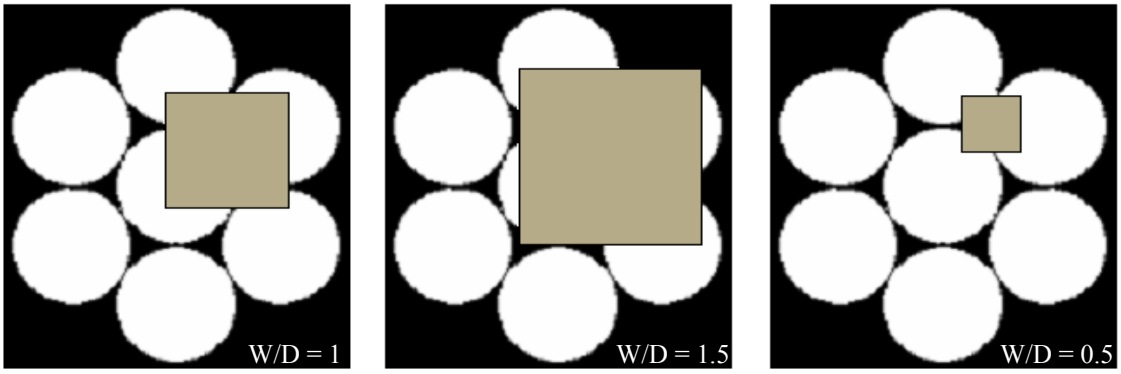

Figure 4.4: Examples of W/D ratios used in the 2-dimensional simulation.

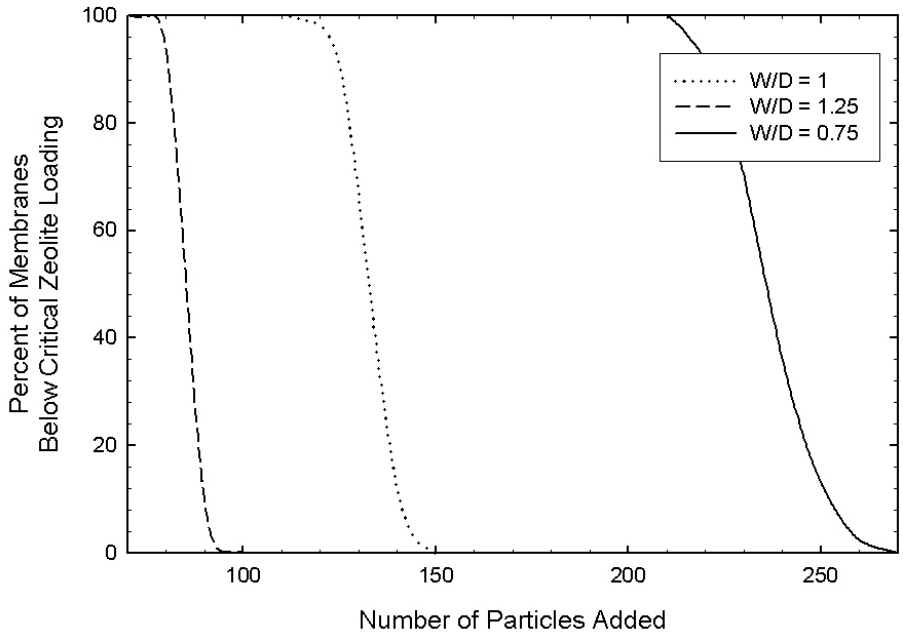

Figure 4.5: Results from the 2-dimensional lattice model.

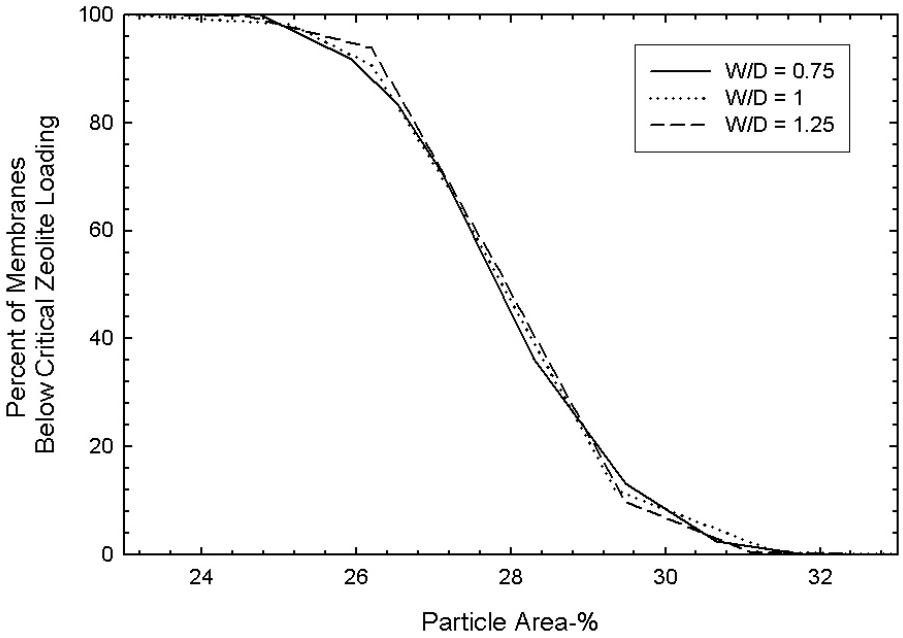

Figure 4.6: Normalized results from the 2-dimensional lattice model. The three W/D ratios examined showed little variation in critical loading.

4.2.2 3-Dimensional Model

Building upon the 2-dimensional model described above, a 3-dimensional lattice model was constructed in a similar manner. The cells and pores were placed into a simple cubic lattice (Z = 6) of 1000 cells (10 x 10 x 10 cells) with six open pores per cell. Experimental evidence using an iPP−DPE membrane formed with 27.5 vol-% polymer and cooled at 125ºC/min indicated that each cell has on average 2.3 pores connecting to neighboring cells. Consequently, the pores within the simulated membrane were randomly closed until the average of 2.3 open pores per cell was reached. The 3-D zeolite particles were randomly added to the structure in a fashion similar to that used in the 2-D model, and the program determined which pores remained open and which pores were "blocked" by the particles. The same method of connectivity determination was used as before, using a percolation threshold of 25% [8].

The results for a variety of W/D values are presented in Figure 4.6, where the results are presented in terms of volume-% zeolite particles, the 3-dimensional corollary to the area-% used in the 2-D model. While the W/D value does not significantly influence the shape of the curve, it does influence the critical zeolite loading value, the point where a curve reaches the x-axis (the percolation threshold remains unchanged at 0.25). To more clearly demonstrate the impact of W/D on the critical zeolite loading, the critical zeolite loading values of Figure 4.7 are re-plotted in Figure 4.8.

According to Figure 4.8 the lowest required particle loading occurs when the particle size is the same as the cell diameter (W/D = 1). As explained in the following sub-section, this result will have a significant impact on the formation of ZeoTIPS membranes.

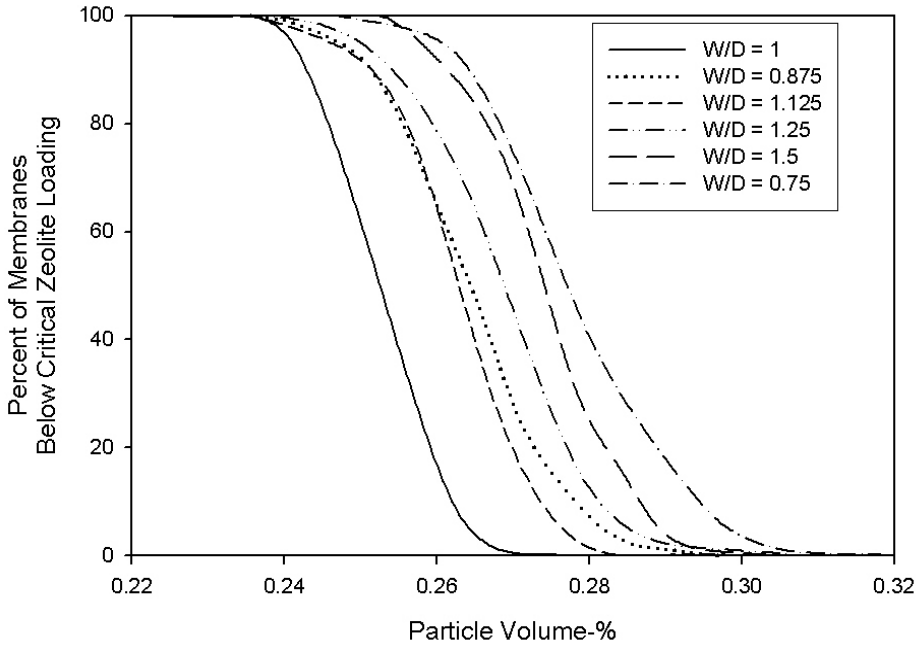

Figure 4.7: Results from the 3-dimensional pore blockage model show that the W/D ratio in 3-D has a greater effect on critical loading than in 2-D.

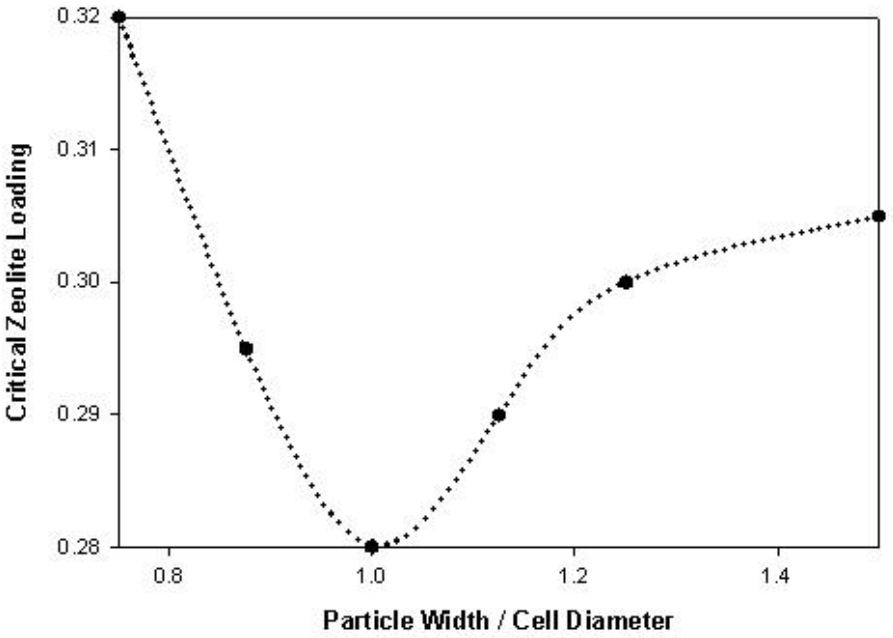

Figure 4.8: Critical zeolite loading results from the 3-dimensional pore blockage model. The minimum required zeolite loading occurs when W/D = 1.

4.2.3 Lattice Model Conclusions

The main conclusion to the lattice models is that a minimum in required zeolite loading occurs when the particle width is the same as the cell diameter. This result is quite useful in relation to the results in Chapter 3. If one is preparing ZeoTIPS membranes with a specific zeolite particle size, one should use the knowledge gained in Chapter 3 to control the phase separation kinetics and achieve the desired cell size.

There are a variety of drawbacks to the 2-D and 3-D lattice models presented above. First, both models have a set area or volume of cells that cannot be changed by the user, and neither is remotely close to the 70−80 vol-% that the cells occupy in real membranes. Second, there are a limited number of locations in which a pore can lie, making it much more likely that a single zeolite particle will block multiple pores, possibly skewing the critical zeolite loading data. Cells in real membranes have an infinite number of possible locations for pores on their surfaces. Finally, there is no cell size distribution, particle size distribution, or random orientation of particles, which also does not mimic reality. These drawbacks are addressed in further model development discussed below.

4.3 RANDOM DROPLET PLACEMENT MODEL

There are two random droplet placement models discussed in this section: a pore blockage model and a pore prevention model. Both models are designed to address the main drawbacks of the cell lattice models. Removing the lattice and placing droplets one by one allows the user to define the void volume in the membrane, to better mimic reality. Furthermore, by placing droplets randomly, an infinite number of possible pore positions arises, eliminating the common occurrence in the lattice models where a single zeolite particle blocks three or more pores.

The two random placement models check for connectivity mathematically, but without the use of percolation theory. Once a microporous connectivity determination has been performed, a nanoporous connectivity determination is undertaken, whereby the programs check to see if the membrane will have the desired high selectivity. This is also an advantage over the lattice models.

4.3.1 Model Construction

The random droplet placement models described below both begin with the user-defined variables of number of runs, diluent volume percent, particle volume percent, number of pores per cell, average cell size, and average particle size. The distributions of the cells and particles must also be described, and the variances of the distributions, along with minimum and maximum values are also user-defined.

4.3.1.1 Pore Blockage Model

In the pore blockage model, cells two units in diameter are placed into the 3-D space (20 x 20 x 20 units) first in random positions until a desired volume-% is reached. The overlapping cells result in pores at the location of the overlap. Initially, three pores per cell are allowed, as in the 3-D lattice model, and pores are randomly closed to reach this value. Zeolite particles of uniform distribution are then placed into the 3-D space in the same manner as that of the 3-D lattice model. If a particle encloses a pore, the pore is considered to be blocked. After the pre-determined particle volume-% has been reached, a connectivity determination (described in Section 4.3.2) is performed to see if the critical zeolite loading has been reached. This method was deemed inaccurate because it required greater than 50 vol-% zeolite to block enough pores, which are 2-dimensional,

unlike those in the regular lattice models. It will not be discussed further.

4.3.1.2 Pore Prevention Model

This section presents a new hypothesis for membrane formation in which it is postulated that the particles "prevent" the formation of pores in the membrane. The particles are present in the suspension before the droplets form. As they grow, the droplets are kept from their neighbors by the particles in two ways. First, the particles physically get in the way of droplets meeting. Second, it is known that when droplets coalesce, flow patterns are induced that can lead to further coalescence of droplets [9]. The particles disrupt flow patterns that occur during coalescence of smaller droplets, reducing the chances that a droplet will be pushed toward another droplet. With this hypothesis in mind, the model places the particles first, followed by placement and growth of droplets.

This model includes a new user-defined option, pores/cell, which is inputted in the form of a linear equation giving pores/cell in terms of zeolite loading. This equation is obtained by performing an image analysis on a membrane with no zeolite added, and one with a sufficiently large amount of zeolite (~25%) to describe the reasonable range of zeolite loadings. In these analyses, the number of pores in each cell of an SEM image is counted and doubled (one only sees on average half of the cell in an SEM image). This count also includes "half pores" which appear on the edge of a cell in the image. A linear fit is then applied to these points, giving a simplified relationship for how the number of pores/cell changes as more particles are added. This number is the basis for the model's accuracy. There are many more intersections of cells in the program than there are pores in a real membrane. This is because real membrane droplets are able to deform, while

this model only allows cells to be represented as spheres. Thus, the program must limit the number of pores each cell has. If the program does not know how many pores should be left after the membrane is formed, it cannot accurately determine the critical zeolite loading.

First, a pre-determined volume-% of particles of a uniform size are placed one at a time into the 3-D space in such a way that the sides of the particles are parallel to the sides of the 3-D space representing an elemental volume of membrane formation suspension. As with the previous models, if a particle overlaps with a particle already in the membrane, it is repositioned. The method for determining the particle overlap is more complex in this model, and the details are explained in the code commentary in Appendix B [10]. The program adds each particle's volume to a volume counter, and the total volume of particles is divided by the volume of the membrane. Once that volume percent reaches the user-defined particle volume percent, the loop ends and no more particles are added. A typical result is illustrated in Figure 4.9.

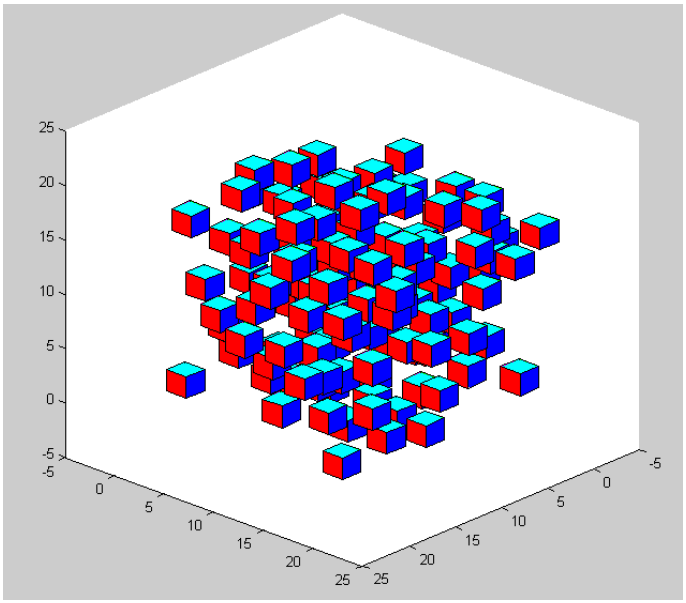

Figure 4.9: Matlab plot of particle placements.

A user-defined number of droplets of a uniform arbitrarily small size, $1/8^{th}$ the size of the average particle, are then placed into the 3-D space. There are two overlap constraints for the droplets. The first states that the center of a droplet cannot be inside a particle. The second constraint states that no two droplets can overlap. If either constraint is not met, the droplet is repositioned. Once all of the droplets have been placed, the droplets are allowed to grow, and the above overlap constraints still apply. The radius of each droplet is increased by 5%, and each droplet is checked for unacceptable overlaps. If an unacceptable overlap occurs, the droplet is "jiggled", or moved a random distance between zero and 0.1 in the x-, y-, and z-directions where it is again checked for unacceptable overlaps. The "jiggling" process repeats until no unacceptable overlaps occur, and then the rest of the droplets are checked in the same manner. The droplets continue to grow in steps of 5%, and the overlap check is repeated. Once the program reaches the point where any one droplet cannot be successfully repositioned via 100 jiggle movements the program is shifted to a second growth simulation described in the next paragraph.

At this point, the droplets are grown in a single step to reach the pre-determined cell volume. However, each droplet grows by a different amount in a manner similar to the "sphere of influence" method developed by Hanks and Lloyd [4]. It is this growth step that leads to a droplet size distribution. The details of this growth mechanism are explained in the code commentary in Appendix B. Figure 4.10 shows the starting and ending points of this droplet placement and growth.

The user also has the ability to apply random orientation to the zeolite particles in the program, as shown in Figure 4.11. A distribution of particle sizes can also be applied. The results for these variations will be discussed in Section 4.3.3.

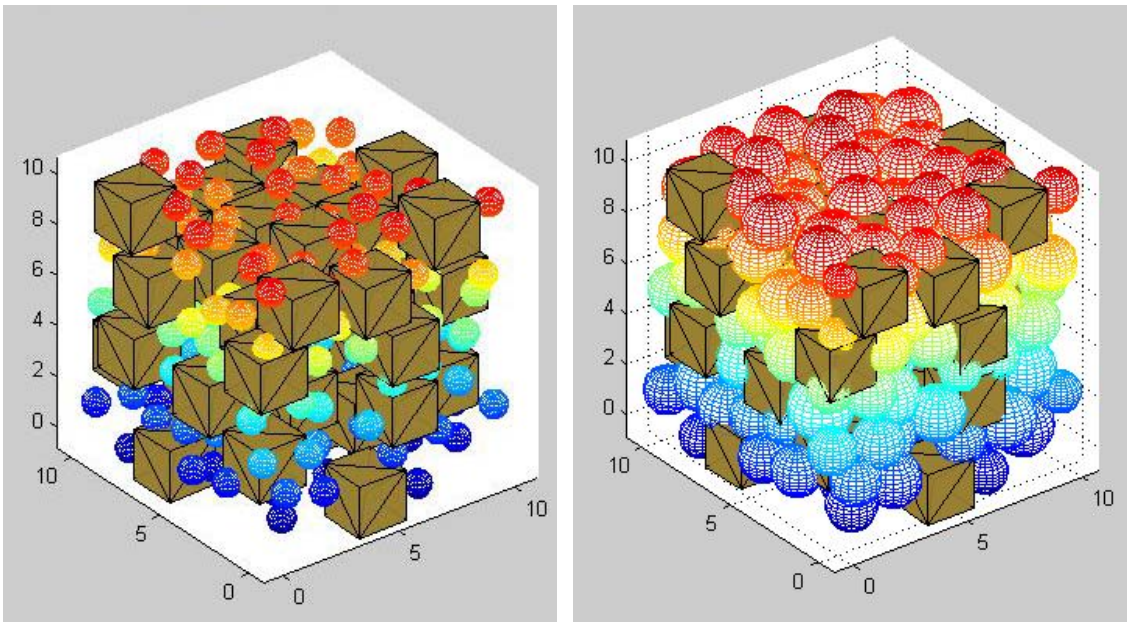

Figure 4.10: Example of droplet growth process. (a) small droplets are placed, and (b) droplets are grown by the "sphere of influence" method, producing a distribution of sizes.

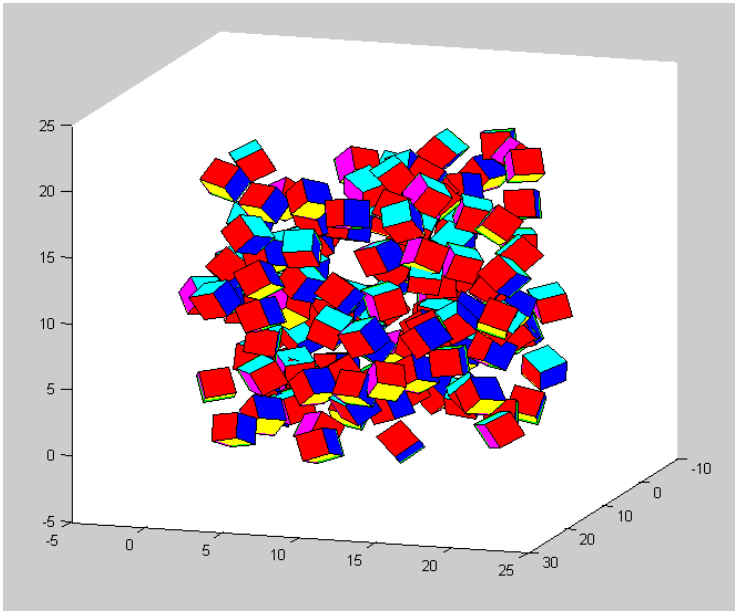

Figure 4.11: Matlab plot of particle placements with random orientation.

4.3.2 Connectivity Determination

The model code presented in Appendix B contains a variety of subroutines that are used sequentially to check for microporous connectivity. The first subroutine relates each cell to each of its neighbors by finding the coordinates of the pores that connect them. Next, start and end points of the simulation are determined. These include all cells that overlap with the edge of the 3-D space. Beginning with the x-direction, the third subroutine looks for a connected path across the membrane. Each direction is checked independently, and data from each is taken into account. The program ends by checking to be sure that any membrane that lacked microporous connectivity has enough particles in it to yield nanoporous connectivity, which is necessary for high-selectivity separations. When these routines are completed, the data is stored and the program repeats by placing new particles and droplets randomly into the 3-D space and checking for connectivity in the new membrane, as described above.

4.3.3 Model Results and Discussion

To investigate the effects of particle orientation and distribution, the iPP−DPE system was used to establish the pores/cell relationship. It was found that a 27.5 vol-% polymer iPP−DPE membrane cooled at 125ºC/min had 2.3 pores/cell, whereas the same membrane with 27.5 vol-% zeolite loading exhibited 0.75 pores/cell. These numbers were obtained by looking at 50 randomly selected cells in the membranes. It was also found that the W/D ratio of these membranes was approximately 1.5. The resulting relationship was approximated as linear for simplicity and was inputted into the Matlab program. Three sets of data were obtained, all with the same W/D ratio. The first was produced using a uniform particle orientation, the second with a random orientation, and the last with a particle size distribution and uniform orientation. The results are shown in Figure 4.12.

From this figure it appears that although the particle orientation and size distribution have an effect on the shape of the curve, their effect on the critical zeolite loading (the point at which the curves reach the x-axis) is negligible. This is a reasonable result, since the zeolite particles on average should contact the same number of cells regardless of their angle of orientation. Thus, the particles will prevent roughly the same number of pores between cells.

Figure 4.13 shows the effect of changing the pores/cell relationship in the model. As the number of pores/cell decreases from 1 to 0.5, the critical zeolite loading decreases from about 40 vol-% to about 25 vol-%. Obviously there is a strong correlation between the two variables, and for the model to work properly, the pores/cell relationship must be well-defined. This relationship is most likely not linear in reality, due to the number of factors that affect it, but for simplicity it was allowed to be linear, as explained in Section 4.3.1.2

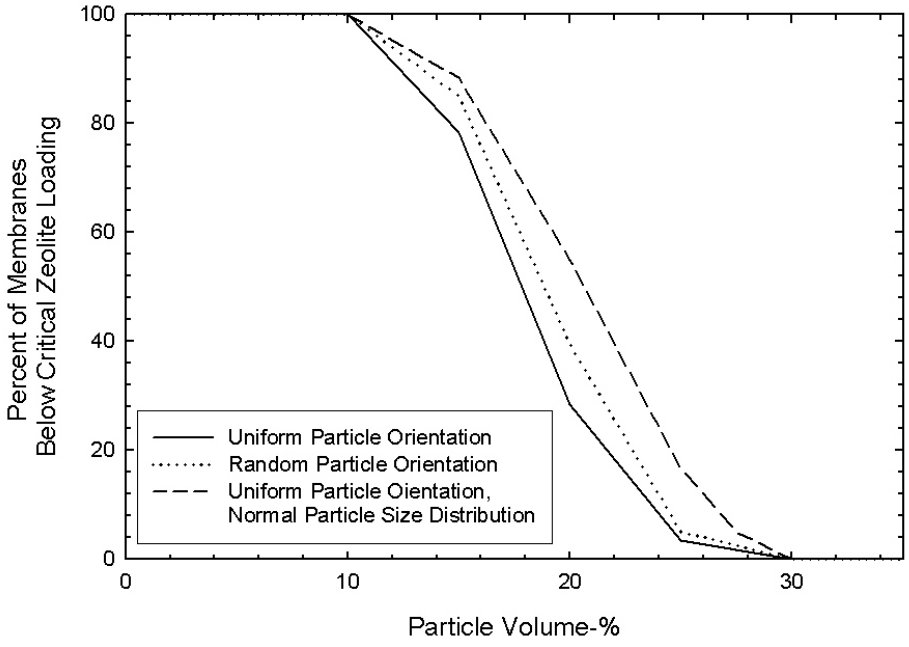

Figure 4.12: Random droplet placement pore prevention model results for the iPP−DPE system with a W/D ratio of 1.5.

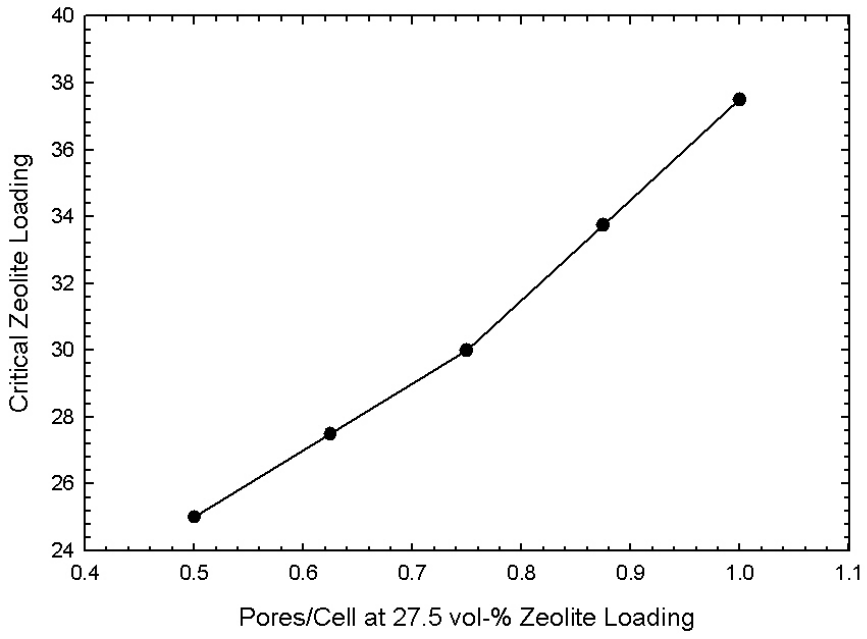

Figure 4.13: Model results showing the increase in critical zeolite loading as the number of allowed pores/cell at 27.5 vol-% loading increases.

Unfortunately, because the literature does not provide a way to predict the number of pores/cell in a membrane accurately, the model is not of great use as a predictive tool. In a particular polymer−diluent system, changing the polymer concentration changes the average inter-droplet distance, changing the likelihood that two droplets will merge upon solidification to form a pore. At this critical distance, the van der Waals forces between the droplets become large enough to break the fluid film separating the two [11]. Equation (4.1) describes the relationship between the critical inter-droplet distance at which two droplets will begin to merge, h_{cr}, the droplet size, and the system surface tension, γ [12].

$$h_{cr} = (Aa_{eq} / 8\pi\gamma)^{1/3} \tag{4.1}$$

where A is the Hamaker constant, and $a_{eq} = 2/(a_1^{-1} + a_2^{-1})$ is the equivalent radius of two neighboring, merging droplets with radii a_1 and a_2. Changing the cooling rate changes

the droplet size, which also affects the inter-droplet distance, according to Equation (4.1). Changing polymer−diluent systems affects a variety of variables such as solution viscosity, surface tension, polymer−diluent−zeolite interaction, and phase separation behavior, all of which affect either cell size, pore formation, or both. Finally, droplets in real membranes have the ability to deform from the ideal spherical shape, allowing them to come into contact with a greater number of neighbors, but also preventing the formation of pores in some cases by preventing overlaps with neighboring cells. All of these factors must be taken into account to predict the number of pores/cell in a membrane and the ability to make such predictions has not been attained in the literature to date due to the complexity of the physics involved.

4.3.4 Random Droplet Placement Model Conclusions

The random droplet placement model is useful in illustrating how the zeolite particles in a real membrane lead to a lack of microporous connectivity. Pores are not blocked by zeolite particles in a membrane; zeolite particles do not move within the suspension independent of the droplets. The pores are in fact prevented, as zeolite particles inhibit cells from meeting and coalescing during solidification.

Much like in the cell lattice model, there is a threshold in the random droplet placement model where the number of pores becomes too low for connectivity, and that threshold is reached by the addition of zeolite particles. However, unlike the cell lattice model, the random droplet placement model has a threshold that changes as the system it is used to simulated changes. Each polymer−diluent system will have different characteristics, and the number of particles and the size of particles added will have differing effects on the threshold for each system. Thus it was determined that there is no simple method for modeling the formation of ZeoTIPS membranes or for predicting the

necessary zeolite loading to produce one. Further efforts in modeling L−L TIPS pore formation would be required to accurately model ZeoTIPS membrane formation.

4.4 SUMMARY OF CHAPTER 4

The cell lattice models showed that the W/D ratio within a ZeoTIPS membrane is the most important factor leading to connectivity. The random droplet placement model showed that the most important factor is actually the number of pores per cell in the membrane, and how this number changes with increased zeolite loading. This number is related to the W/D ratio, since very small cells will not be influenced by large zeolite particles and very large cells will not be influenced by small zeolite particles in their relationships with neighboring cells. However, more important than the W/D ratio is the system's characteristics themselves. The system's viscosity, surface tension, polymer−diluent−zeolite interaction, and phase separation characteristics all play important roles in determining how many pores will be left in a membrane after a certain amount of zeolite has been added.

Although the program is not useful as a predictive tool without the use of extensive experimentation, these results are important in understanding the mechanism by which a successful ZeoTIPS membrane is formed. They may also provide a basis for future modeling of ZeoTIPS membrane formation.

4.5 REFERENCES

1 K.S. McGuire, A. Laxminarayan, D.S. Martula, and D.R. Lloyd, *Kinetics of droplet growth in liquid-liquid phase separation of polymer-diluent systems: model development*, Journal of Colloid and Interface Science, 182 (1996) 46-58.

2 D.S. Martula, R.T. Bonnecaze, and D.R. Lloyd, *The effects of viscosity on coalescence-induced coalescence*, International Journal of Multiphase Flow, 29 (2003) 1265-1282.
3 D.S. Martula, T. Hasegawa, D.R. Lloyd, and R.T. Bonnecaze, *Coalescence-induced coalescence of inviscid droplets in a viscous fluid*, Journal of Colloid and Interface Science, 232 (2000) 241-253.
4 P.L. Hanks and D.R. Lloyd, *Deterministic model for matrix solidification in liquid-liquid thermally induced phase separation*, Journal of Membrane Science, 306 (2007) 125-133.
5 G.T. Caneba and D.S. Soong, *Polymer membrane formation through the thermal-inversion process. 2. Mathematical modeling of membrane structure formation*, Macromolecules, 18 (1985) 2545-2555.
6 K.S. McGuire, *Membrane formation via liquid-liquid thermally induced phase separation*, Dissertation, The University of Texas at Austin, 1995.
7 B.F. Barton and A.J. McHugh, *Modeling the Dynamics of Membrane Structure Formation in Quenched Polymer Solutions.*, Journal of Membrane Science, 166 (2000) 119-125.
8 M. Sahimi, *Flow and Transport in Porous Media and Fractured Rock: From Classical Methods to Modern Approaches*, VCH, Weinheim, Germany, 1995. pages 482.
9 D.S. Martula, *Coalesence-Induced Coalescence in Polymeric Membrane Formation*, Dissertation (2000) 261.
10 W.F. Kern and J.R. Bland, *Solid Mensuration with Proofs*, 2nd ed, Wiley, New York, 1948.
11 A. Sheludko, *Thin liquid films*, Advances in Colloid and Interface Science, 1 (1967) 391-464.
12 A.K. Chesters, *The modelling of coalescence processes in fluid-liquid dispersions: a review of current understanding*, Transactions of the Institute of Chemical Engineers, 69 (1991) 259-270.

Chapter 5: ZeoTIPS Formation Methods

5.1 INTRODUCTION

Polymeric membranes have long been made by interfacial polymerization [1], phase inversion [2], and evaporative casting [3]. More recently, mixed matrix membranes have been made most often by evaporative casting and phase inversion [4, 5]. However, none of these methods are useful for the production of the zeolite-containing microporous mixed matrix membranes discussed in the previous four chapters. To prepare these membranes it is necessary to utilize the L–L TIPS method of making microporous membranes; thus the name ZeoTIPS membranes.

In this research, a variety of methods for producing ZeoTIPS membranes on a laboratory scale were attempted. Small samples were prepared using a hot stage to investigate phase separation characteristics and affinities between polymer, diluent, and zeolite. Larger membrane samples were prepared via extrusion and compression molding to test the performance of ZeoTIPS membranes.

5.2 MATERIALS

Poly(ethylene co-vinyl alcohol) was purchased from EVALCA (Houston, TX) with ethylene contents of 32 (product code F101B), 38 (product code H101A), and 44 (product code E151A) mol-% ethylene (EVAL32, EVAL38, EVAL44). Udel P-3500 poly(ether sulfone) (PES) was obtained from Solvay Advanced Polymers (Alpharetta, GA). Poly(methyl methacrylate) (PMMA) with a weight average molecular weight M_w of 105,400 g/mole was obtained in the form of Plexiglas from Rohm & Haas (Philadelphia, PA). Escorene Ultra 7760 poly(ethylene co-vinyl acetate) (EVAc, 26.7

wt-% vinyl acetate), Escor 5200 poly(ethylene co-acrylic acid) (EAA, 15 wt-% acrylic acid), and Escor 5100 poly(ethylene co-acrylic acid) (EAA, 11 wt-% acrylic acid) were generously provided by ExxonMobil Chemical (Houston, TX). Isotactic polypropylene (iPP) with a reported weight average molecular weight M_w of 340,000 g/mole was obtained from ExxonMobil Chemical. Cellulose Triacetate (CA-435-75S) was obtained from Eastman Chemical (Kingsport, TN), and polystyrene (M_n = 170,000, M_w = 350,000) was purchased from Sigma-Aldrich (St. Louis, MO).

Polyethylene glycol samples with average molecular weights of 200, 300, 400, and 600 g/mol, glycerol, 1,4-butanediol, cyclohexanol, dodecanol, tetradecanol, diphenyl ether, 2-ethyl-1,3-hexanediol, mineral oil, dioctyl phthalate, bisphenol-A, methanol, isopropyl alcohol, trimethylchlorosilane, aminopropyldimethylethoxysilane, bromobenzene, and copper(II) sulfate were purchased from Fischer Scientific (Pittsburgh, PA) and were used as received. Hexamethylbenzene was purchased from Eastman Kodak and used as received.

5.3 EXPERIMENTAL METHODS

Two non-continuous or batch methods and one continuous method of making membranes were used in this work. The small scale batch method using test tubes, microscope slides, and a hot stage is described in detail in Chapter 3. The second batch method using a compression mold was found to be irreproducible despite various improvements to the established equipment and procedure. Zeolite particle settling and insufficient mixing led to this irreproducibility; consequently, this method will not be discussed here. Details on the compression molding process are included in Appendix C, along with images of membranes produced with this method. The most effective method of forming ZeoTIPS membranes appears to be via continuous extrusion of a zeolite-

containing melt blend, in which good mixing can be achieved and particle settling does not occur due to short processing times.

5.3.1 Extrusion

The apparatus used for extrusion in this research was a Leistritz Micro-18 twin-screw extruder equipped with a Zenith PEP II 1.2 CC/rev gear pump and Leistritz Model AL-04 Flexible Lip 4 inch film die. The extruder barrel is divided into eight heating zones, with flow occurring from Zone 1 to Zone 8. Diluent was fed at a desired rate to Zone 5 from a temperature-controlled pot (Leistritz design using Zenith model H-9000, 0.6 CC/rev gear pump and ZeDrive 2000 DC Motor Speed Controller) onto the screws where it mixes with polymer fed to Zone 1 by a K-Tron Soder (Model K2MVT20). Dried zeolite powder was added to the screws in the same location as the polymer pellets (Zone 1) on a per minute basis from pre-measured vials. The polymer, diluent, and zeolite were mixed by turning the screws at 200 rpm at temperatures ranging from 120ºC to 210ºC, depending on the system involved. Die temperatures ranged from 50ºC to 160ºC, and also depend on the phase separation characteristics of the polymer−diluent system used.

Downstream processing was accomplished with equipment designed and built in the laboratory (shown in Figure 5.1). In order to achieve the desired ZeoTIPS structure discussed in the previous chapters, it is necessary to make sure that the polymer does not pull away from the zeolite surfaces due to stresses occurring in the solidification process. The solidification process involves the expulsion of diluent from the polymer matrix, leading to shrinkage of the matrix. To minimize these stresses and prevent polymer from pulling away from the zeolite, the extrudate or nascent membrane must cool slowly. Cooling too quickly does not allow the polymer enough time to adjust to the resulting

stresses. Furthermore, the cells in a ZeoTIPS membrane must be sufficiently large as to satisfy the requirements outlined in Chapter 4, where the optimum particle size to cell diameter ratio, W/D, was shown to be one. Kinetic studies performed in our laboratory and elsewhere [6-8] have shown that slow cooling is required to achieve cells of the desired size. Finally, it was found in preliminary experiments that the extrudate cannot come into contact with a smooth surface until after solidification. If the hot extrudate contacted a smooth surface of aluminum, Teflon, copper, or fiberglass, a smooth non-porous skin on the surface of the ZeoTIPS membrane resulted.

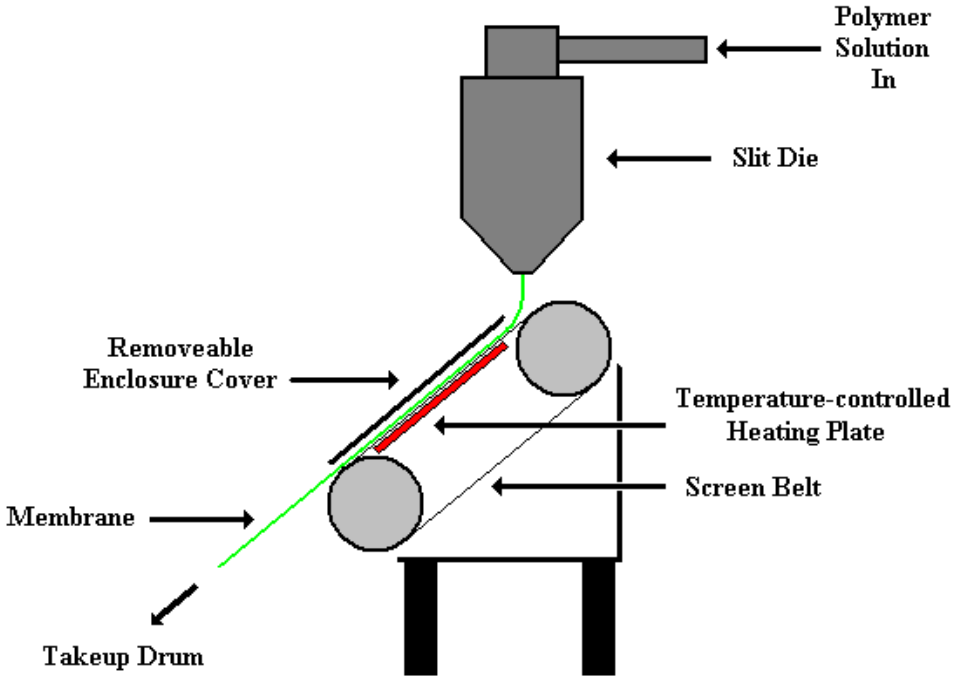

Figure 5.1: Downstream processing equipment for twin-screw extrusion

These requirements were all taken into account when designing the apparatus shown in Figure 5.1. A fiberglass screen belt was used to ensure at least 50% of the lower membrane surface comes into contact only with air, allowing diluent droplets to

reach the surface. No surfaces with which the nascent membrane came into contact were porous. SEM images of a membrane surface are shown in Figure 5.2.

The mesh belt was stretched around motor-driven rollers that controlled the speed of the belt. The belt passed over a heating plate consisting of two steel sheets with heating tape sandwiched between them. The temperature of these plates was monitored and controlled with a thermocouple. The speed of the belt was selected to make sure the membrane had solidified before leaving the belt and being wound on a take-up drum. The belt apparatus was enclosed by Plexiglas sheets that prevent large amounts of convective flow across the membrane surfaces and maintain a diluent vapor atmosphere around the membrane.

Solidified membranes were extracted and dried as described in Chapter 3. Figure 5.3 shows the difference in iPP membrane structure when the heating plate is not used compared to when the plate is used and is set to a high temperature. The heating plate greatly slows the cooling rate of the membrane, resulting in larger cells.

A variety of polymer−diluent systems were extruded in addition to iPP−DPE. EVAL38−PEG400 was found to be of too low viscosity to be extruded on the equipment described above. EVAc−DPE was too soft upon solidification to be extracted without collapsing the structure, due to the plasticizing effect of DPE. EAA−DPE was not able to cool quickly enough on the above apparatus, even without the use of the heating plate, due to its low phase separation temperature [9]. Cellulose triacetate−2-ethyl-1,3-hexanediol could not be cooled quickly enough to achieve the necessary cell size. Finally, EVAL38−glycerol was not able to cool slowly enough to achieve the desired cell size or the desired polymer−zeolite affinity (see discussion in Section 5.6).

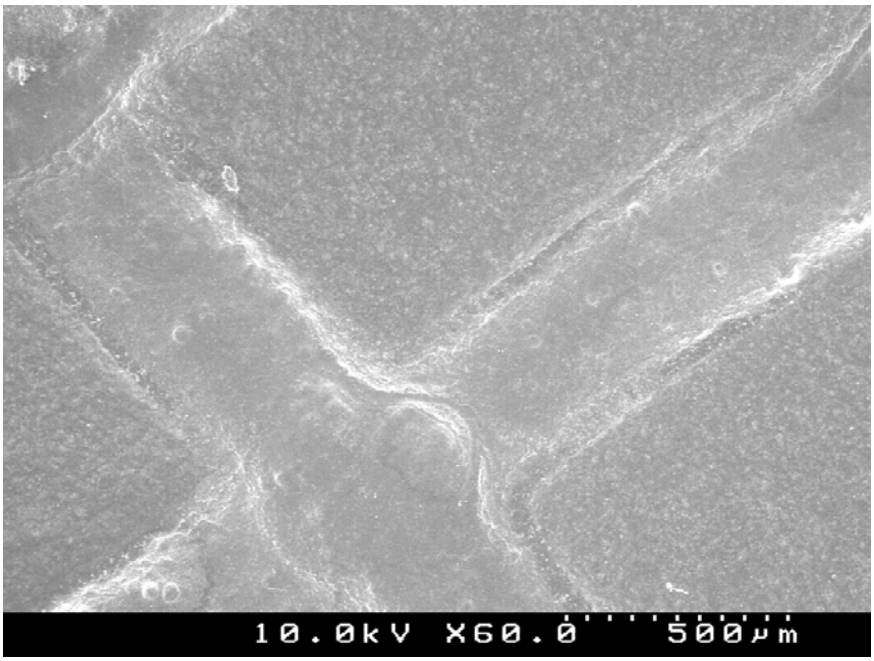

(a)

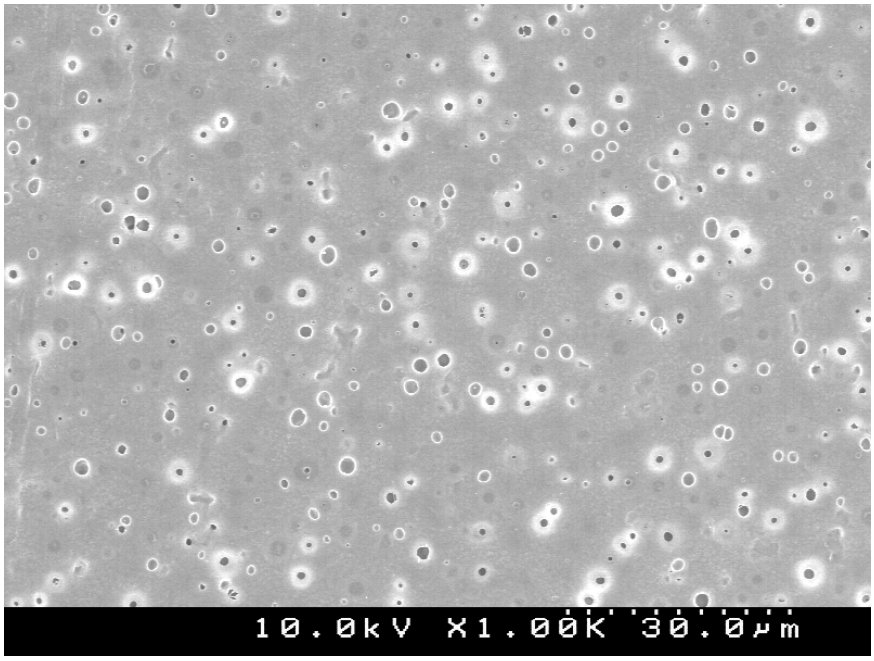

(b)

Figure 5.2: (a) SEM image of an extruded membrane surface showing the imprint of the fiberglass screen belt. Areas of the membrane in contact with the belt resulted in ~0% surface porosity. (b) Magnified image of the surface not in contact with the belt.

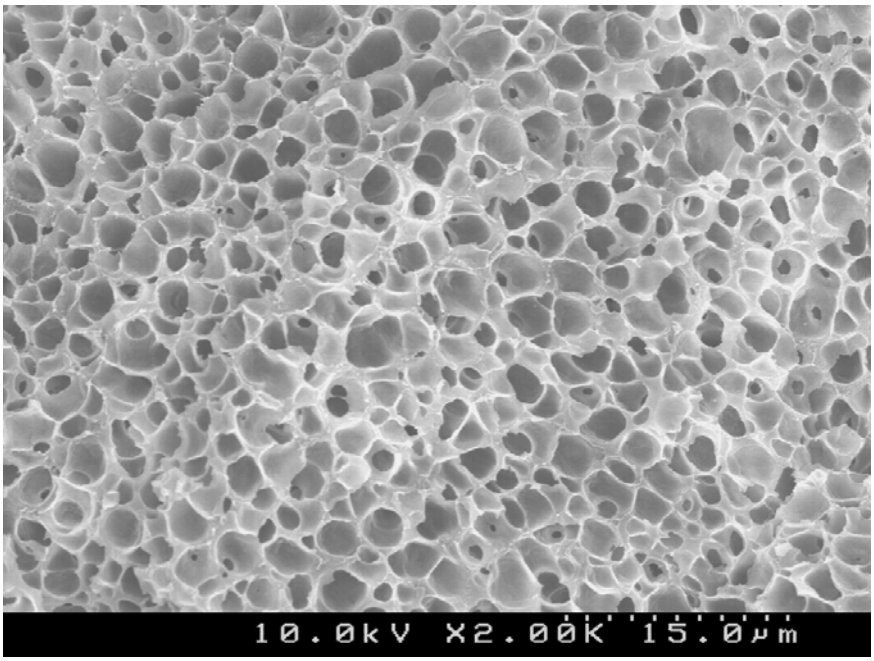

(a)

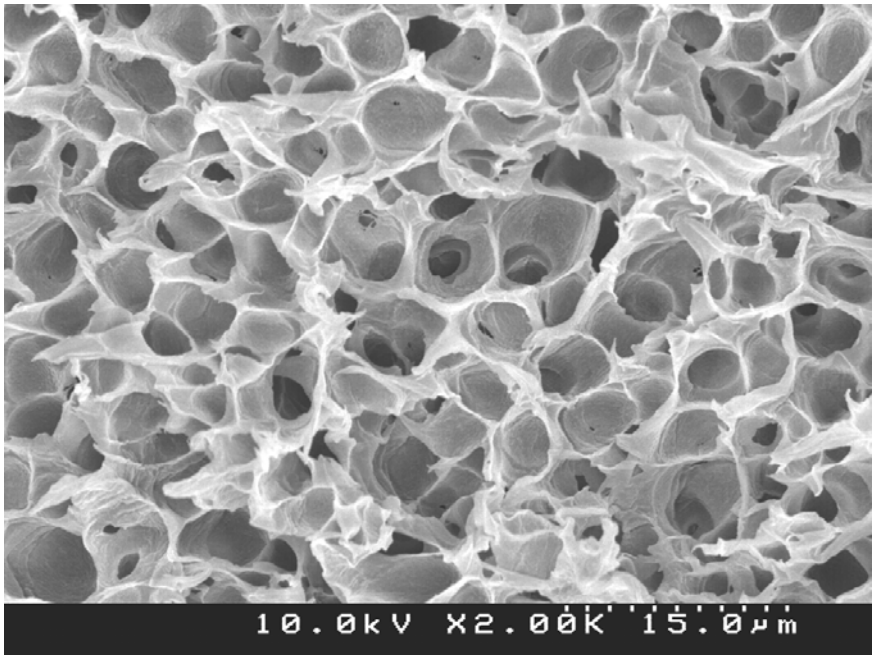

(b)

Figure 5.3: SEM image of a 30 wt-% polymer iPP−DPE membrane extruded on the fiberglass belt (a) without the heating plate and (b) with the heating plate set to 100ºC.

5.4 POLYMER AND DILUENT SELECTION

5.4.1 Cell Size Control by Polymer and Diluent Selection

In Section 4.2.2 it was shown that the zeolite loading is minimized when the cell diameter is equal to the zeolite particle diameter. When designing a membrane for a particular application, the first step is to select a zeolite of desired pore size. That choice may dictate the particle size; consequently, the remaining task is to control the L–L TIPS process to control the cell size in such a way so that the cell size equals the particle size. Pore size can be controlled via processing conditions (cooling rates – as discussed in sections 3.5 – and by selection of the polymer–diluent pair as discussed in this section.) Of course, as pointed out in Chapter 2, the choice of polymer and diluent will also influence the thickness of the polymer coating around the zeolite particle. Section 5.4.2 addresses the relationship between polymer–diluent–zeolite affinity and the presence of a polymer coating on the zeolite particles; the current section focuses on the influence of polymer and diluent on cells size control.

Once a suitable zeolite has been chosen for a separation, a polymer must be chosen to provide the necessary mechanical and chemical properties. Unfortunately, once the polymer is selected, it is not a simple task to select a diluent for that polymer due to a variety of factors that affect the phase separation characteristics for a given system. However, the Hildebrand solubility parameter can be used as a guideline in selecting diluents. Different diluents have different Hildebrand solubility parameters, which are a measure of how the diluents will interact with the polymer, taking into account dispersive, polymer, and hydrogen bonding forces [10]. The Hildebrand solubility parameter, δ [$(J/m^3)^{1/2}x10^{-3}$], is defined in Equation (5.1).

$$\delta^2 = \delta_d^2 + \delta_p^2 + \delta_h^2 \tag{5.1}$$

For instance, one can easily manipulate the cell size of a membrane by changing the diluent, which changes the shape of the phase diagram, changing the droplet coarsening time at a given cooling rate. Such is the case with PMMA, where several diluents can be used to form L−L TIPS membranes. These diluents include (but are not limited to) dioctyl phthalate, polyethylene glycol (PEG), cyclohexanol, and 1,4-butanediol. Additionally, mixed diluents composed of glycerol and 1,4-butanediol can be used to form TIPS membranes. For example, Figures 5.4 and 5.5 show how the cell sizes of PMMA TIPS membranes produced under identical conditions decrease as the diluent is changed from cyclohexanol to PEG. Notice that the two images are at different magnifications. Throughout the discussion presented here, the magnification of the images was selected such that the cells and pores are clearly visible. Membranes formed with 1,4-butanediol produce much larger cells, but diluent migration that occurs during the hot stage formation process makes it difficult to compare cell sizes, and so an example of such a membrane is not shown (this phenomenon occurs to a much lesser extent when zeolite particles are present). The ability to change the cell sizes in a TIPS system is quite useful for ZeoTIPS membrane formation since the zeolite particle size dictates the desired cell size.

Furthermore, one can change the molecular weight of the diluent to change its solubility parameter. For example, polyethylene glycol (PEG200) with an average molecular weight of 200 g/mol has a Hildebrand parameter of 24.3 $(J/m^3)^{1/2}x10^{-3}$, whereas PEG600 has a Hildebrand parameter of 20.8 $(J/m^3)^{1/2}x10^{-3}$. This change in molecular weight also changes the viscosity of the polymer−diluent solution, and both of these factors influence the final cell size in the membrane. Figure 5.6 shows a PMMA−PEG600 membrane formed under the same conditions as the PMMA−PEG200

membranes in Figure 5.5. The change in diluent resulted in cells too small for use in ZeoTIPS membranes.

The choice of polymer in a ZeoTIPS membrane can also be adjusted to yield the desired cell size. Varying the ethylene content of EVAL greatly affects the phase separation characteristics of L−L TIPS with glycerol as the diluent. Figures 5.7 and 5.8 show the resulting cell sizes of EVAL44 and EVAL38 membranes formed with glycerol using identical processing conditions. The cells of the EVAL44 membranes are much larger, due to a larger difference in solubility parameter between EVAL44 and glycerol than between EVAL38 and glycerol. This difference results in a larger liquid−liquid region of the phase diagram [11]. EVAL32−glycerol membranes with the same polymer content undergo solid−liquid TIPS and are not shown.

It is important to note that this investigation into changing the polymer and diluent to manipulate cell sizes is not an exhaustive study of the phenomena occurring during formation. There are many factors affecting cell sizes in TIPS membranes includes those mentioned above, such as solubility parameter and viscosity, but also cooling rate and polymer−zeolite interaction (discussed in Chapter 3 and below). The methods described in this section are only a brief description of the tools at one's disposal when developing a ZeoTIPS membranes system.

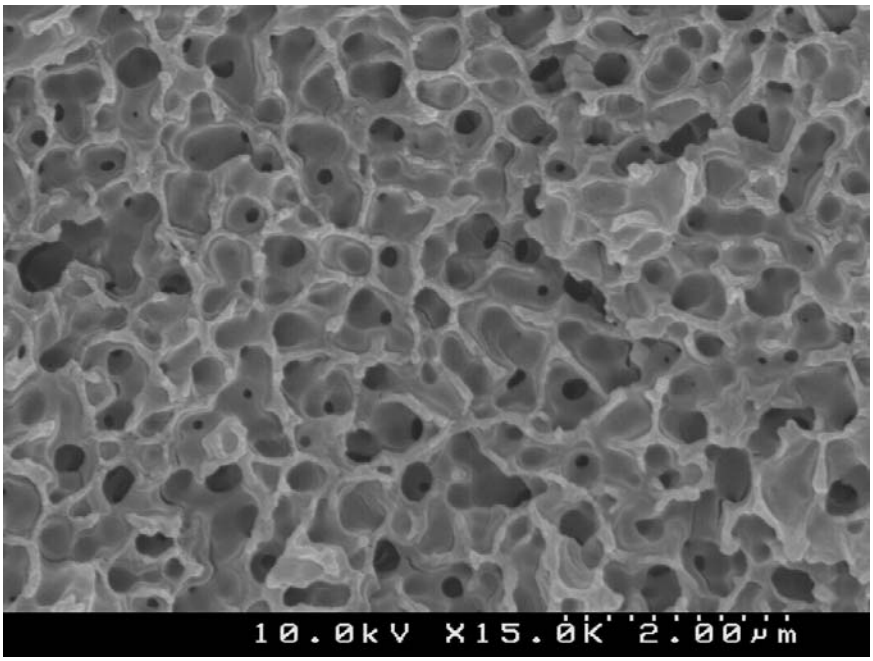

Figure 5.4: SEM image of a 27.5 wt-% polymer PMMA−cyclohexanol membrane cooled at 125ºC/min.

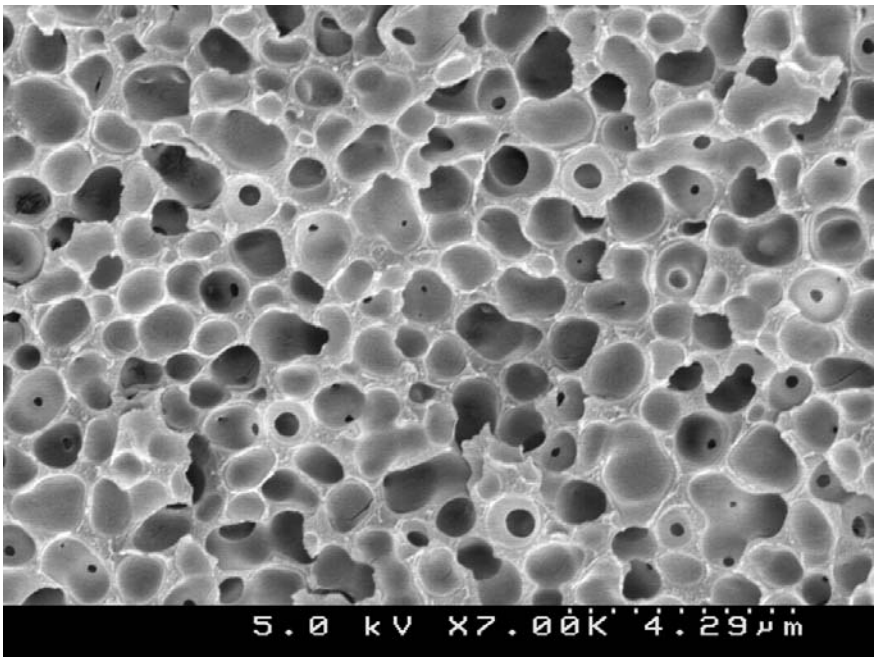

Figure 5.5: SEM image of a 27.5 wt-% polymer PMMA−PEG200 membrane cooled at 125ºC/min.

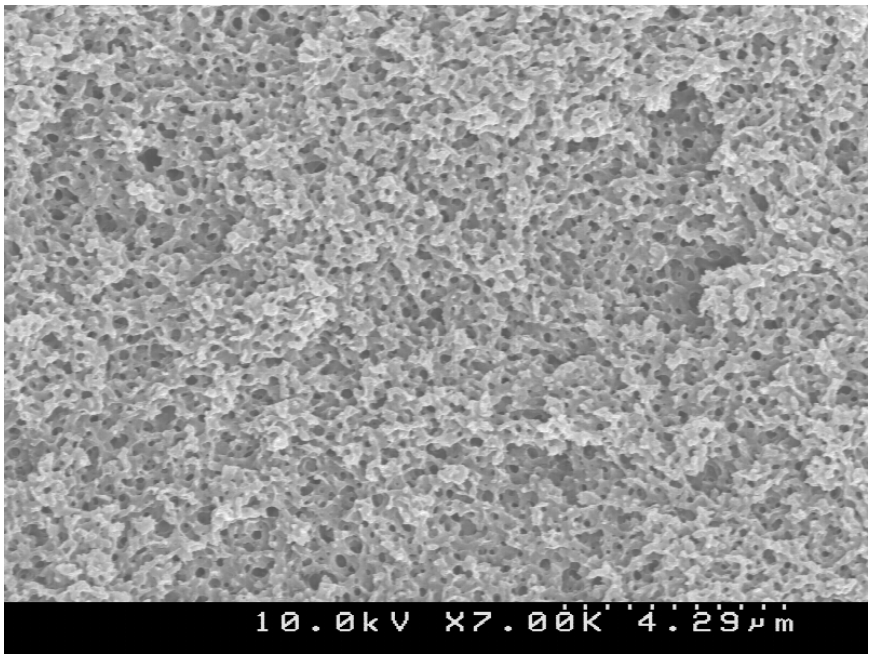

Figure 5.6: SEM image of a 27.5 wt-% polymer PMMA−PEG600 membrane cooled at 125°C/min.

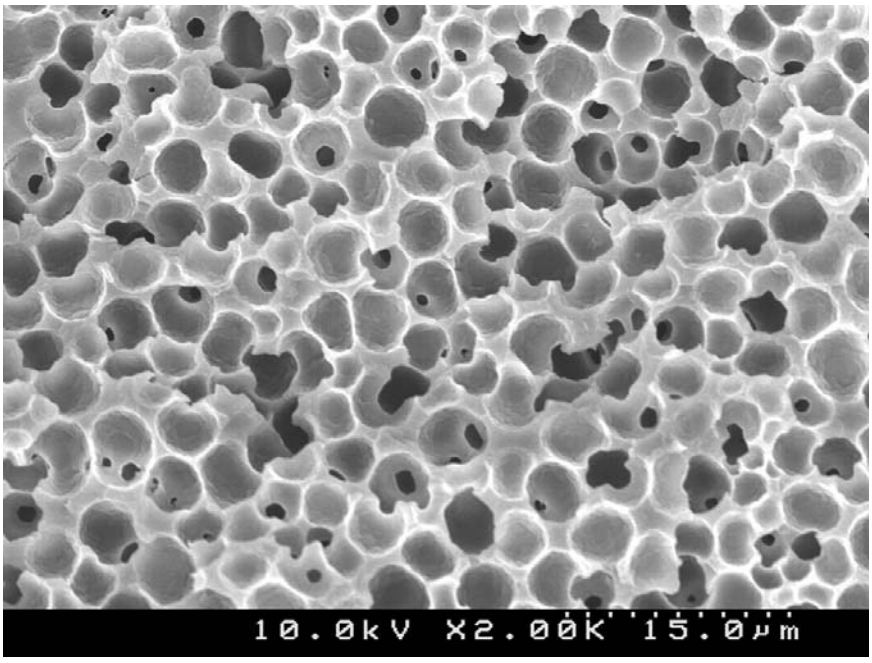

Figure 5.7: SEM image of a 20 wt-% polymer EVAL44−glycerol membrane cooled at 125°C/min.

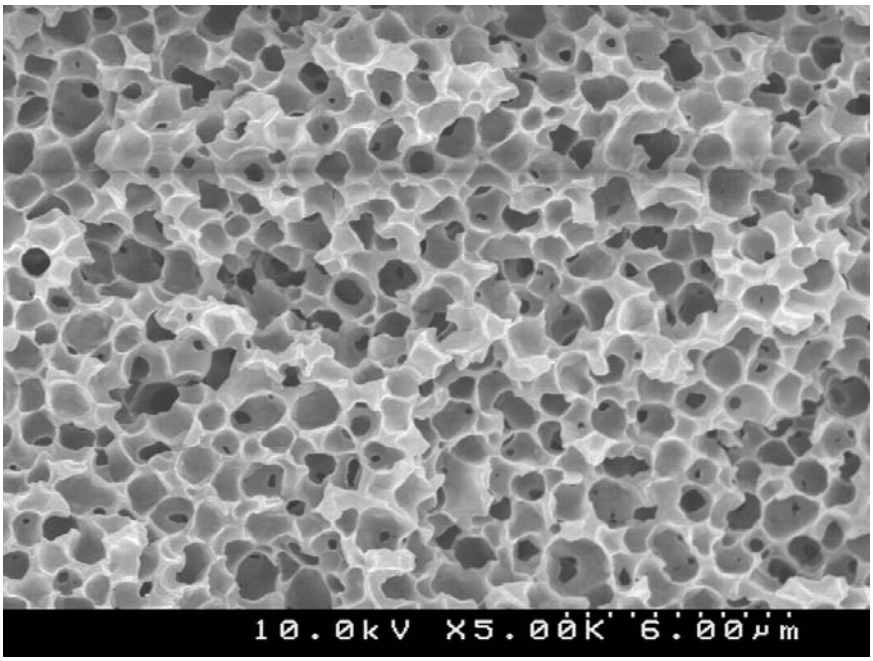

Figure 5.8: SEM image of a 20 wt-% polymer EVAL38−glycerol membrane cooled at 125°C/min.

5.4.2 Polymer−Diluent−Zeolite Interaction Analysis

Whether one achieves the *ideal* or *non-ideal* structures (that is, absence or presence of a polymer coating on the zeolite particle) and the thickness of the polymer coating depend on the polymer–zeolite affinity *and* the diluent–zeolite affinity. By balancing the affinities of the zeolite for the polymer and diluent, one can hopefully control the thickness of the polymer coating in the resulting ZeoTIPS membrane. The objective is to minimize the polymer coating thickness (that is, to minimize β as defined in Chapter 2) if the polymer is permeable, or to avoid the coating completely if the polymer is impermeable. The discussion presented in this section outlines methods of controlling the presence / absence of the polymer layer coating the zeolite particle

through polymer and diluent selection. Section 5.5 below presents an additional method of controlling the polymer–diluent–zeolite affinity.

An understanding of the affinities between polymer, diluent, and zeolite is paramount to controlling the structure of ZeoTIPS membranes. The strength of these interactions is not easily measured experimentally. However, they can be approximated using suitable theoretical considerations such as the Hildebrand solubility parameters defined above in Equation (5.1). These parameters have not been reported for 4A zeolite specifically, but by approximating 4A zeolite as silica, one can use Equation (5.2) to estimate the values [10].

$$\varepsilon = -0.519 + 0.043 * \delta \tag{5.2}$$

The Hildebrand solubility parameter for the zeolite can be used in Equation (5.2) to determine the strength of the interaction, ε $[(J/m^3)^{1/2} x 10^{-3}]$, between a solution component and the zeolite surface.

The solubility parameter data for the polymers and diluents used in this study are listed in Table 5.1. In Table 5.1, Hildebrand solubility parameters are given in parentheses. Values followed by an asterisk have been calculated using group contributions given in Van Krevelen [12]. Unless otherwise noted, values denoted as approximate were estimated from values given in the Polymer Handbook [13]. The data from Table 5.1 along with the solid−liquid interaction strength parameters estimated using Equation (5.2) were used to prepare Figure 5.8 and 5.9, which shows the interaction strength between the diluent and zeolite versus that between the polymer and zeolite for each of these systems. In Figures 5.8 and 5.9, “strong” polymer−zeolite affinity refers to a membrane formed where the polymer contacts the zeolite, and “weak” polymer−zeolite

affinity refers to a zeolite preference or affinity for the diluent, which yields membranes with voids around the zeolite.

Table 5.1: Polymers and diluents used in the interaction strength analysis.

Polymer (δ, $(J/m^3)^{1/2}x10^{-3}$)	**Diluents (δ, $(J/m^3)^{1/2}x10^{-3}$)**
EVAL44 (25.9*)	Glycerol (33.1), 1,4-butanediol/glycerol mixtures
EVAL38 (26.8*)	Glycerol (33.1), PEG300 (22.5*), PEG400 (21.6*), PEG600 (20.8*)
EVAL32 (27.6*)	Glycerol (33.1), PEG300 (22.5*), PEG400 (21.6*), PEG600 (20.8*)
Polystyrene (~18)	Dodecanol (20.1), Tetradecanol (19.5*)
iPP (~19)	Diphenyl Ether (20.7), Hexamethylbenzene (18.4*)
LDPE (~17)	Diphenyl Ether (20.7)
EAA11 (18.7*)	Diphenyl Ether (20.7), Mineral Oil (~19)
EAA15 (19.2*)	Diphenyl Ether (20.7)
EVAc26.7 (18.1*)	Diphenyl Ether (20.7), Phenyl Benzoate (~20)
Cellulose Triacetate (~27.5)	2-ethyl,1,3-hexanediol (19.2)
PMMA (~22)	Cyclohexanol (23.3), 1,4-butanediol (24.8), PEG200 (24.3*), PEG300 (22.5*), PEG400 (21.6*), PEG600 (20.8*), Dioctyl Phthalate (16.2), 1,4-butanediol/glycerol mixtures
Poly(ether sulfone) (~20.8) [14]	Cyclohexanol (23.3), Bisphenol-A (19.7)

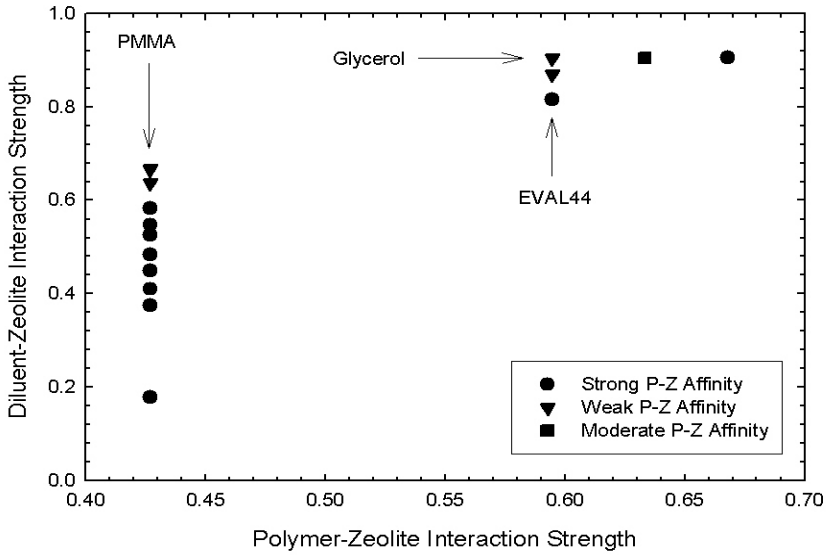

Figure 5.9: Interaction strength behavior for various polymers and diluents. Data for PMMA and for EVAL44 show the transition between weak and strong affinity as the diluent interaction strength is decreased. Data for the diluent glycerol show the transition between weak and strong affinity as the polymer interaction strength is increased.

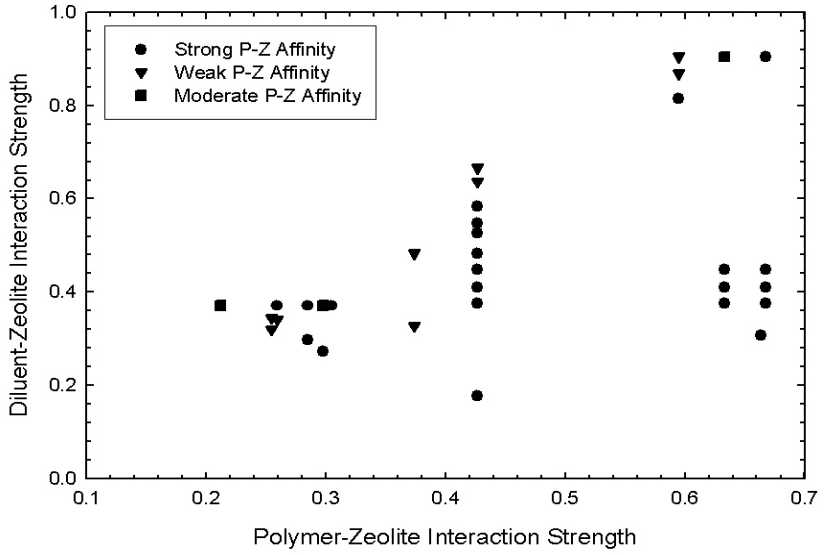

Figure 5.10: Interaction strength behavior for all polymers and diluents investigated.

For a particular diluent such as glycerol (see Figure 5.9), there exists a point where the polymer−zeolite affinity transitions from strong to weak as the polymer−zeolite interaction strength is decreased. Poly(ethylene-co-vinyl alcohol) is the polymer used with glycerol in Figure 5.9, and the ethylene contents used include 44, 38, and 32 mol-%. Additional potential adjustable polymers include poly(ethylene co-vinyl acetate) and poly(ethylene co-acrylic acid). A variety of ethylene contents in these polymers was not available for this research, so an investigation of the necessary monomer composition was not undertaken. Furthermore, Figure 5.9 shows that there exists a point where the polymer−zeolite affinity transitions from strong to weak as the diluent−zeolite affinity is increased for PMMA. One possible way to adjust the diluent−zeolite affinity is through the use of mixed diluents; for example, mixtures of 1,4-butanediol and glycerol (top four PMMA data points, the uppermost point having the greatest glycerol content) resulted in changing the affinities in the PMMA–diluent–zeolite system.

Additionally, Figure 5.9 shows that by adding 1,4-butanediol to the EVAL44−glycerol system, one can decrease the diluent−zeolite interaction strength enough to go from weak affinity to strong affinity. In Figure 5.11 it can be seen that the zeolite particles reside within cells, rather than in contact with the polymer, for EVAL44. In contrast, Figure 5.12 shows that by adding 1,4-butanediol to the EVAL44−1,4-butanediol solution, the polymer is also allowed to come into contact with the zeolite particles. Figure 5.13 shows that by decreasing the ethylene content of the EVAL to 38 mol-%, the polymer is allowed to come into contact with the particles under the same conditions.

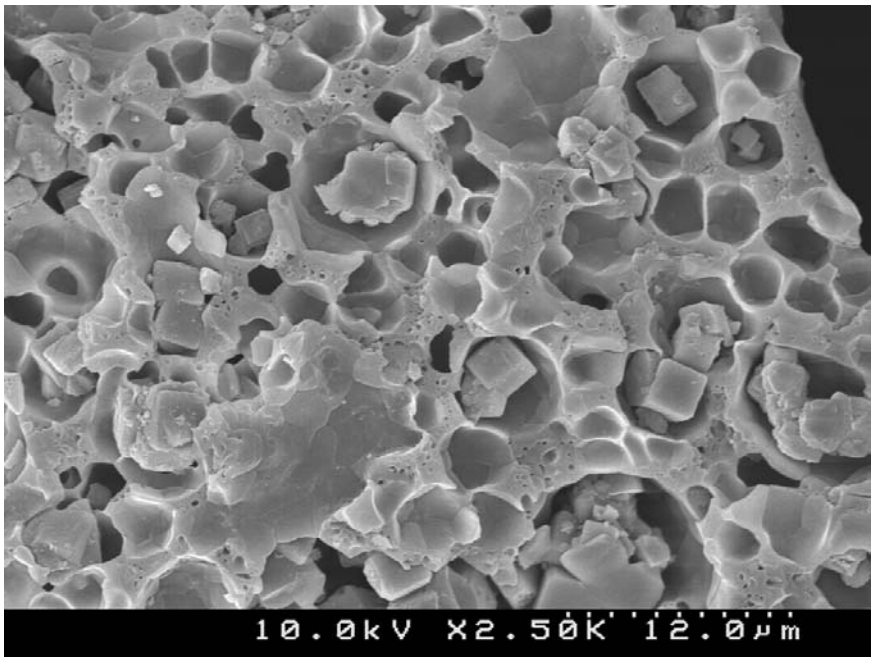

Figure 5.11: SEM image of a 20 wt-% polymer EVAL44−glycerol membrane containing zeolite particles that were surrounded by diluent in the formation process.

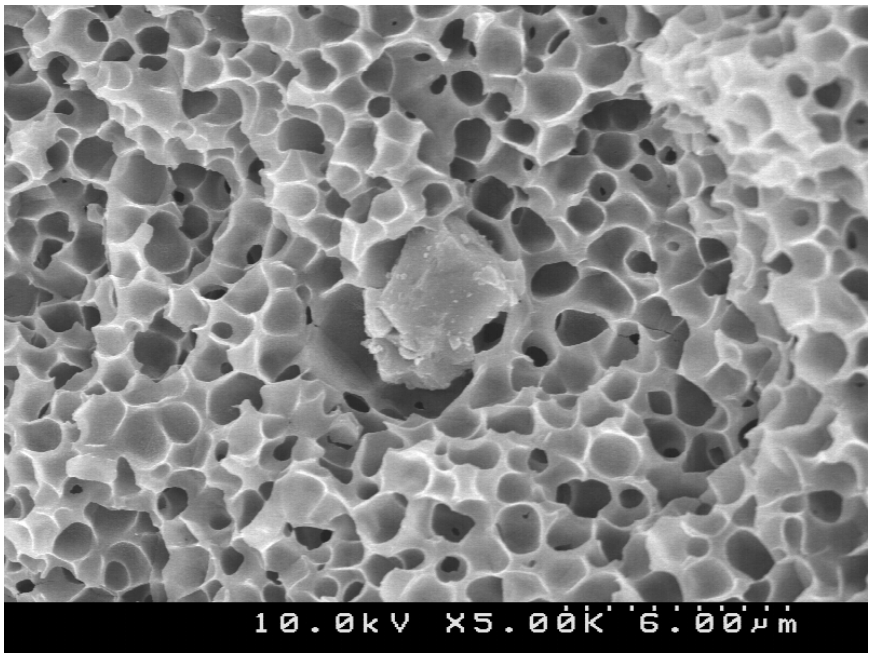

Figure 5.12: SEM image of a 30 wt-% polymer EVAL44−(90/10 glycerol/1,4-butanediol mixture) membrane containing zeolite particles.

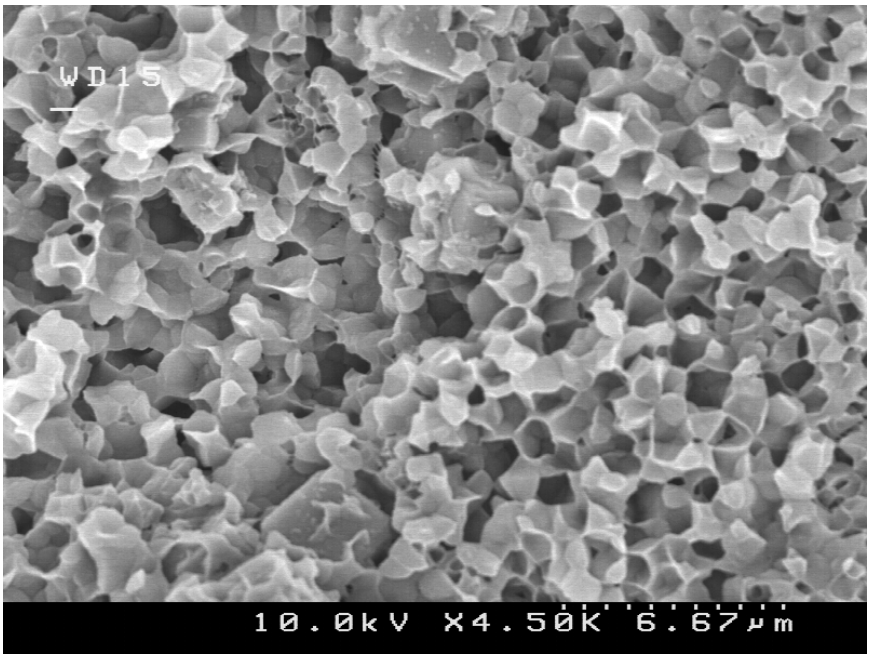

Figure 5.13: SEM image of a 20 wt-% polymer EVAL38−glycerol membrane containing zeolite particles and cooled at 125ºC/min.

Some systems shown in Figures 5.9 and 5.10 resulted in moderate affinity in which the attachment of polymer to zeolite was found to depend on cooling rate. These kinetic effects are discussed briefly in Section 5.6.

It is near the transitions from strong to weak polymer−zeolite affinity that the ideal ZeoTIPS membrane should be formed. Figure 5.10 does not show a clear delineation between strong and weak affinity that transcends all polymer−diluent systems with 4A zeolite; however, Figures 5.9 and 5.10 do illustrate that for a particular polymer or diluent, there is a possibility that a complement exists that will lead to ideal polymer−zeolite affinity. In all cases of adjustable polymers and diluents, the change in solubility parameter does have an effect on the phase separation of the system. It is important to take this into account and adjust processing conditions in order to keep the resulting cells at approximately the same size when changing polymers or diluents.

5.5 ZEOLITE SURFACE MODIFICATION

5.5.1 Literature overview

If one has selected a polymer–diluent combination from which ZeoTIPS membranes are to be formed, the only ways to control the strength of interactions between the three membrane components are either by choosing a zeolite with the perfect surface hydrophobicity, or, more realistically, by modifying the surface of the zeolite. The literature reports several ways of modifying zeolite surface chemistry, including Grinard treatment, where methyl groups are added in place of surface hydroxyls in order to reduce the surface hydrophilicity [4]. Other modifications include the addition of functionalized silane groups, some designed for further reaction with the polymer chains in the membrane [4, 15, 16]. These treatments have been performed with the goal of achieving greater polymer−zeolite affinities in dense mixed matrix membranes.

5.5.2 Experimental procedure

To determine if silane additions could be used to control the structure of ZeoTIPS membranes, silane additions were made to 4A zeolites by reacting trimethylchlorosilane (TMCS) with a stirred suspension of zeolite in toluene in a flask for up to 24 hours. This reaction is shown below.

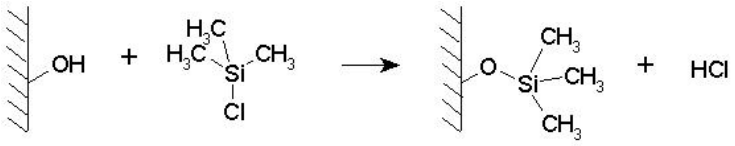

(5.3)

Before carrying out this reaction, the glassware was exposed to the TMCS to silylate all surfaces and prevent future reaction. The reaction shown in Equation (5.3) was attempted three times. First, the reaction was conducted for 2 hours at room

temperature with 10 grams of zeolite powder in a solution of 10 μL of TMCS and 100 mL of toluene dried over molecular sieves. The second experiment was performed similarly with a solution of 1.0 mL TMCS and 100 mL of toluene for 24 hours. The third attempt used 2.0 mL of TMCS and 100 mL of toluene and was reacted for 24 hours before increasing the reaction temperature to 50ºC for 24 hours to achieve the greatest extent of reaction possible. Following each of these reactions, the zeolites were filtered, washed with isopropyl alcohol, and dried under 25 inHg vacuum at 180ºC for 24 hours.

An additional method involved reacting aminopropyldimethylethoxysilane (APDMES) with the zeolites, thereby grafting a different group to the surface, as shown in Equation (5.4).

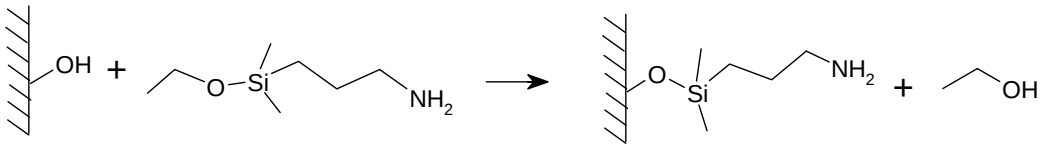

(5.4)

This reaction was conducted for 2 hours at room temperature with five grams of zeolite, 1 mL of APDMES, and 50 mL of dry toluene, as suggested by Husain and Koros [4]. The zeolites were then filtered, washed, and dried as above.

These modified zeolites were then added to polymer−diluent solutions with known polymer−zeolite affinities to determine if modification of the zeolite surfaces can lead to control of the polymer−diluent−zeolite interaction.

An attempt was made to react the APDMES-modified zeolites further in order to add a phenyl group to the surface of the zeolite in the presence of copper catalyst [17, 18].

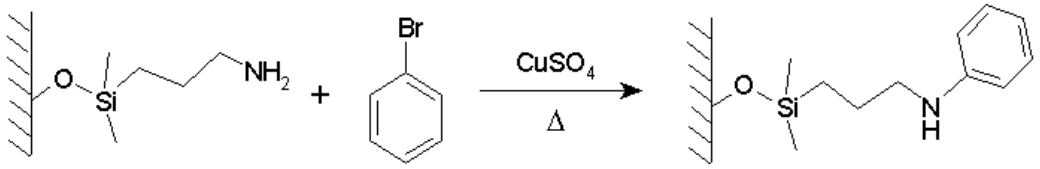

(5.5)

According to the literature, this reaction can be accomplished with heterogeneous or homogeneous catalysis. However, it was not anticipated that heterogeneous catalysis would work, since the amine is itself a heterogeneous reactant. Furthermore, the presence of a heterogeneous catalyst adds a difficult separation step to the process in which the catalyst powder must be removed from the zeolite powder. Therefore, the homogeneous catalysis route in Equation (5.5) was investigated whereby the modified zeolite was suspended in an aqueous solution of bromobenzene, and copper (II) sulfate. The suspension was heated to 100ºC for 2 hours. Unfortunately, the amine led to the precipitation of copper hydroxide, which prevented the reaction from occurring. Addition of acid to the reaction solution to prevent the formation of $Cu(OH)_2$ would only lead to the protonation of the amine, preventing the amine from acting as a nucleophile in the reaction.

5.5.3 Results of the Zeolite Modification Studies

To determine the success of zeolite surface modifications, X-ray photoelectron spectroscopy (XPS) was used to verify the presence of the attached silane groups. XPS uses a beam of x-rays that irradiates a sample under high vacuum, causing electrons to escape from the surface. The spectrometer directly measures the number and kinetic energy of these electrons, and by using Equation (5.6), determines the binding energy of those electrons.

$$h\nu = E_k + E_b + q\phi \qquad (5.6)$$

The electron binding energy, E_b, is related to the x-ray energy, $h\upsilon$, the electron kinetic energy measured by the machine, E_k, and the product of a reference charge and the work function of the material, $q\phi$ [19]. Due to the low concentration of silane groups added, it is difficult to detect their presence, distinguishing between the desired signal and instrumental noise. However, the results from XPS can be used to help interpret results seen in SEM image of membranes.

Carbon–carbon bonds can be detected by looking for a binding energy peak at 284 eV. Nitrogen bonded to carbon produces peaks at around 398 eV [20]. Figures 5.14 and 5.17 show evidence of the surface additions.

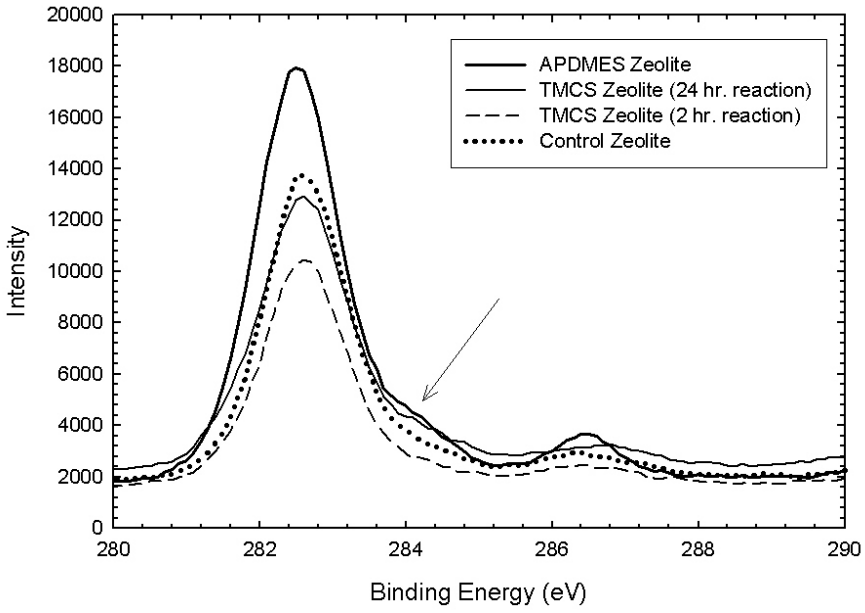

Figure 5.14: XPS spectrum showing the presence of carbon from the silane additions. The shoulder (284 eV) of the large peak suggests that the APDMES and 24hr TMCS reactions were successful.

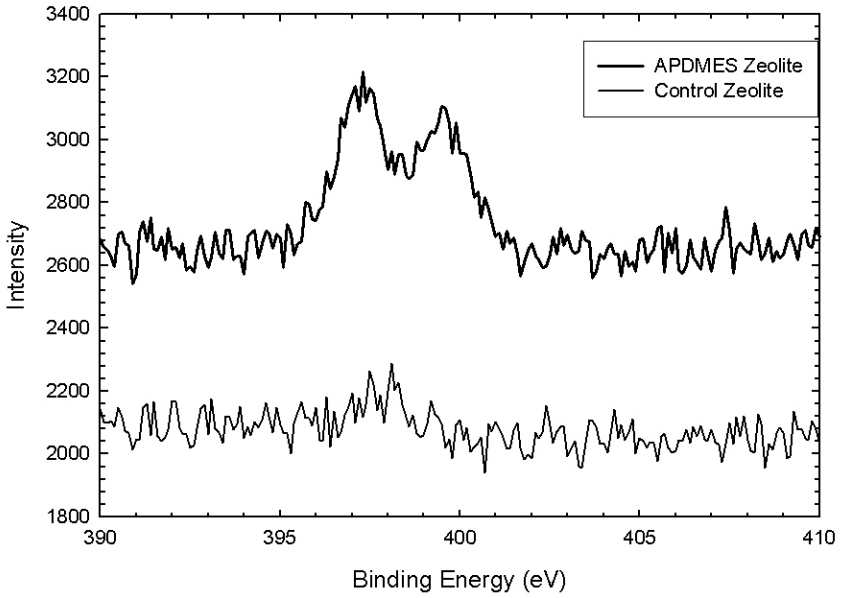

Figure 5.15: XPS spectrum showing the presence of nitrogen from the APDMES reaction.

Figure 5.14 shows a peak shoulder at 284 eV for both the APDMES and 24 hr. TMCS reactions, suggesting the reactions were successful. The large peaks at 282.5 eV are a result of an unknown contaminant present in all samples. Neither the unmodified control zeolite sample nor the 2 hr. TMCS reaction showed this shoulder. Furthermore, Figure 5.15 indicates the presence of nitrogen on the surface of the APDMES zeolites due to the peaks at around 398 eV [20], which is also proof of the addition.

The TMCS-modified zeolites were then added to four polymer−diluent systems: polystyrene−dodecanol, EVAL44−glycerol, PES−cyclohexanol, and PMMA−cyclohexanol. The first three systems exhibited poor polymer−zeolite affinity with unmodified zeolites. The use of modified zeolites was intended to change the surface hydrophilicity such that the polymer could better compete with the diluent and polymer−zeolite affinity would become strong. This was not the case in the first three systems. In Figure 5.16, it is shown that modified and unmodified zeolites in the

EVAL44−glycerol system reside in the diluent droplets due to strong diluent−zeolite affinity. The same result is shown in Figure 5.17 for the polystyrene−dodecanol system.

The system of PES−cyclohexanol (Figure 5.18) did not show strong polymer−zeolite affinity, but appeared to have had that interaction during the membrane formation process only to have the polymer pull away from the zeolite surfaces during solidification, drying, or the freeze fracturing process. This is suggested by the fact that the zeolite particles do not reside within diluent droplets and are not coated by polymer. By making the zeolite surfaces more hydrophobic, the PES appears to have been better able to compete with the cyclohexanol, although the affinity of the PES for the hydrophobic surface was not strong enough to maintain contact.

The fourth system, PMMA−cyclohexanol, exhibited strong polymer−zeolite affinity, and this did not change when the modified zeolites were added (see Figure 5.19).

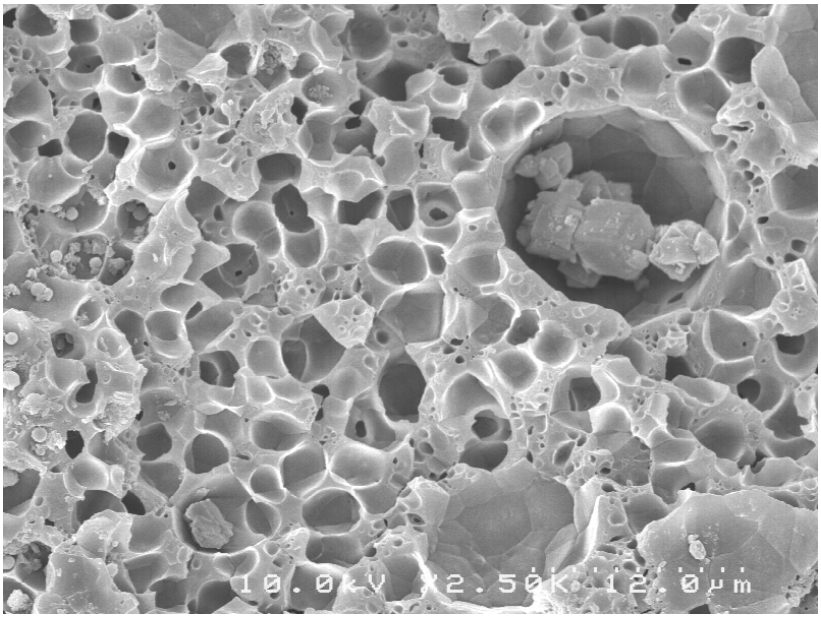

Figure 5.16: EVAL44−glycerol membrane containing TMCS-modified zeolite particles with poor polymer−zeolite affinity. Figure 5.12 shows the same system with unmodified particles.

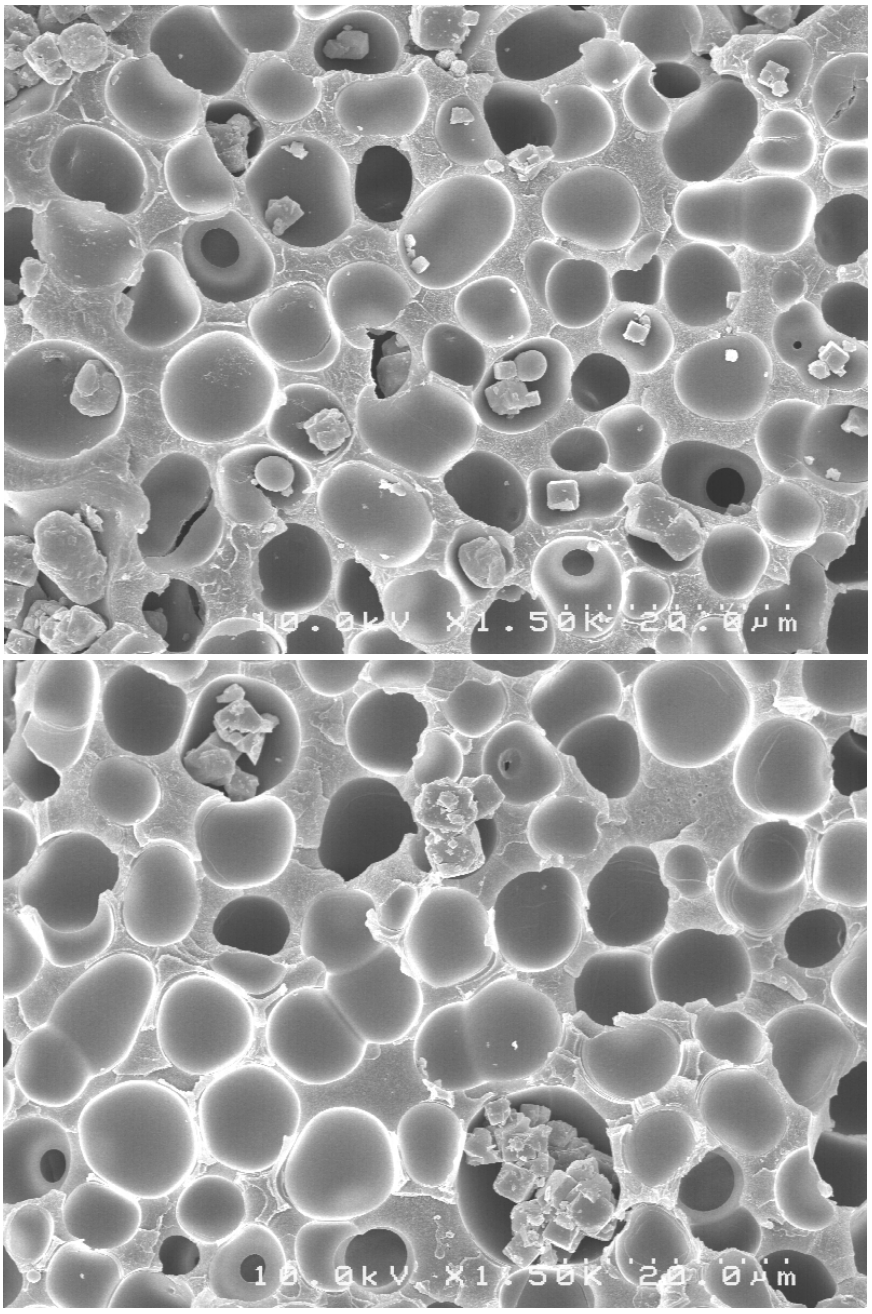

(a)

(b)

Figure 5.17: Polystyrene−dodecanol membrane (a) containing unmodified zeolite particles and (b) containing TMCS-modified zeolite particles. Both show weak polymer−zeolite affinity.

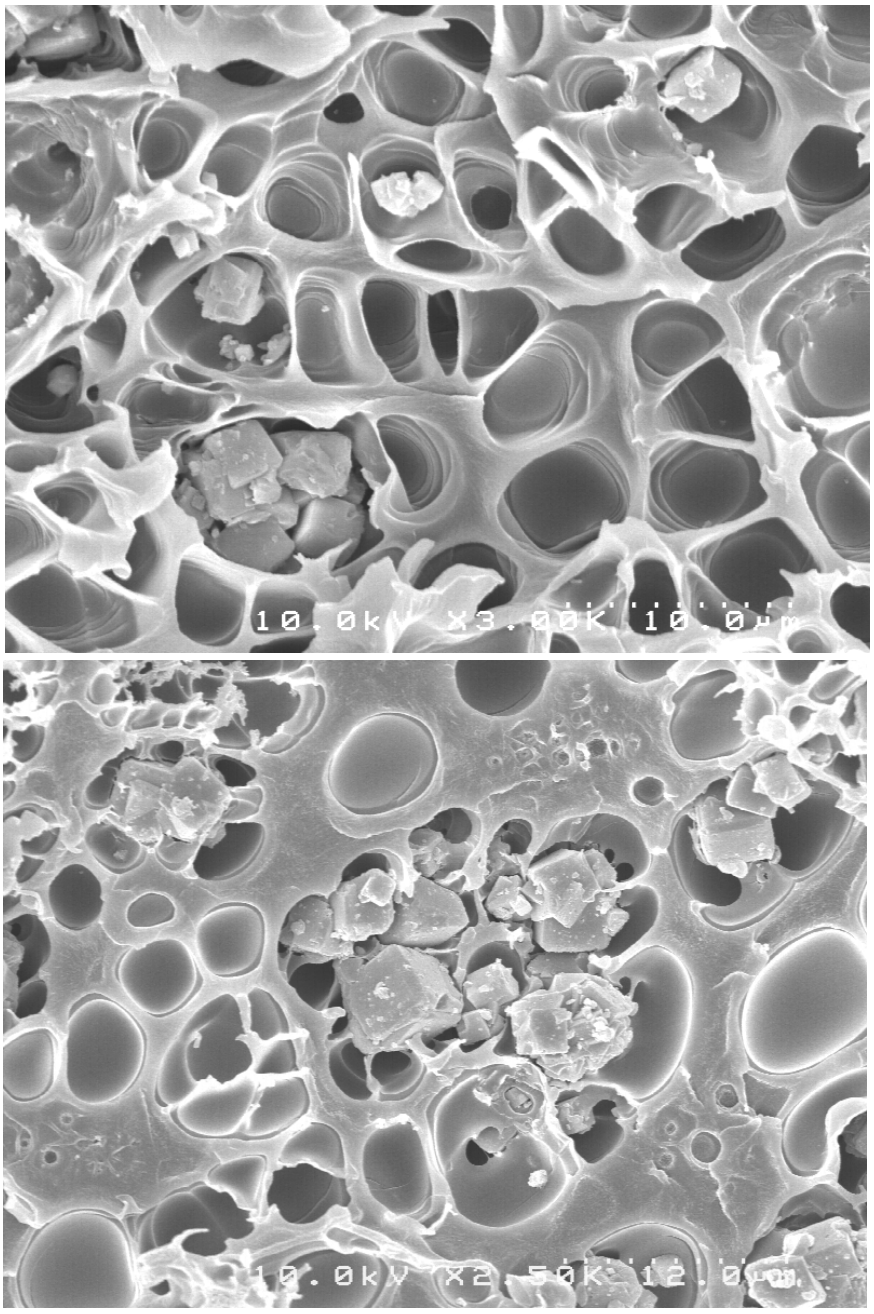

(a)

(b)

Figure 5.18: (a) PES−cyclohexanol membrane containing unmodified zeolite particles and showing weak polymer−zeolite affinity (b) The same type of membrane containing TMCS-modified zeolite particles.

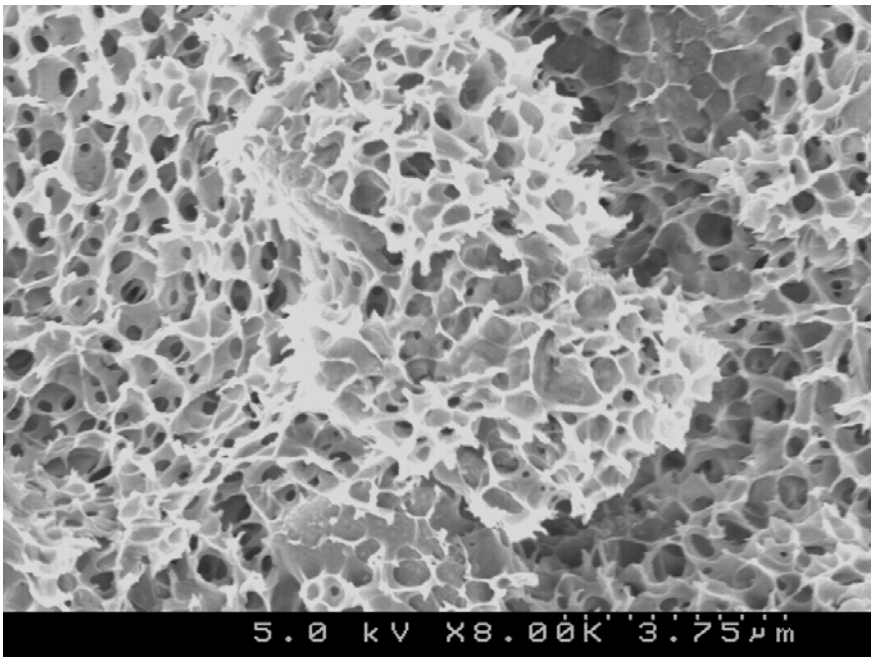

(a)

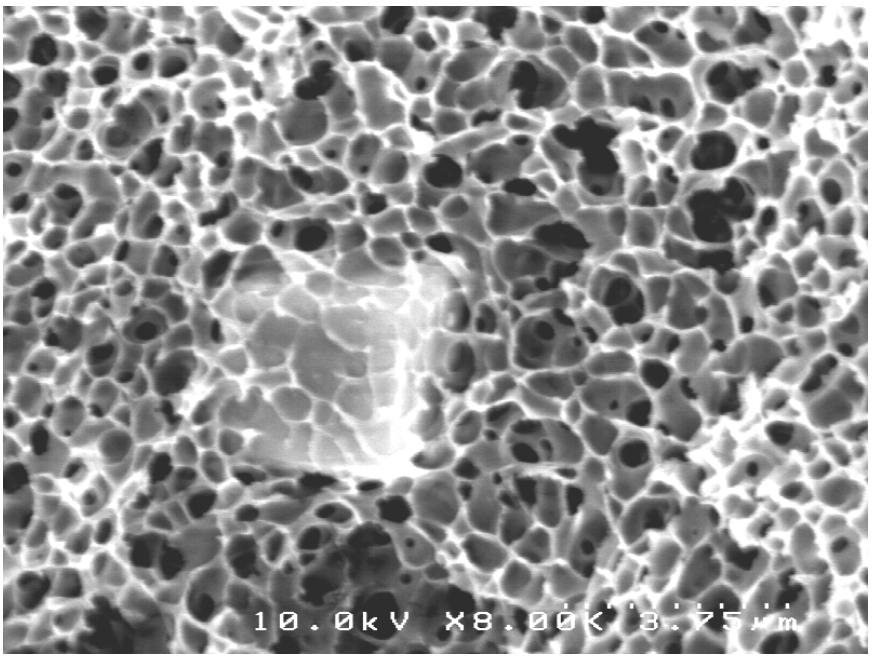

(b)

Figure 5.19: PMMA−cyclohexanol membranes (a) containing unmodified zeolite particles and (b) containing TMCS-modified zeolite particles. Both show strong polymer−zeolite affinity.

It is possible that the zeolite surface modification did not fully modify the surfaces, still allowing the system component with the stronger affinity to coat the zeolite surfaces. As suggested by the PES−cyclohexanol results shown in Figure 5.18, it is possible that a hydrophobic zeolite is also unfavorable for interaction with the polymers chosen. The methods attempted were successful in the literature because they were intended in improve the affinity of a polymer for a zeolite surface. However, the addition of a third component, the diluent, complicated the formation process to the extent that the methods of zeolite modification used were unsuccessful.

Given the above results, it appears that the zeolite modifications described are not the best methods of influencing ZeoTIPS membrane structure, although other methods of modification may be more beneficial. In order to maintain good contact of the polymer with the zeolite, hydrophilic polymers that can hydrogen bond to zeolite surfaces will likely be the most effective. Also, selection of the proper polymer and diluent could lead to more success in balancing interactions.

5.6 EFFECTS OF COOLING RATE ON POLYMER−ZEOLITE ADHESION

The effects of polymer, diluent, and zeolite selection and the effects of zeolite surface modification on polymer−zeolite adhesion discussed above are thermodynamic in nature. However, as mentioned in Section 5.4.2, polymer−zeolite adhesion is also influenced by cooling rate. These kinetic effects can be illustrated by looking at two of the systems shown in Figure 5.10 to have moderate polymer−zeolite affinity. Figure 5.20 shows the EVAL38−glycerol system for comparison to Figure 5.13 (the smaller cells in Figure 5.20 compared to those in Figure 5.13 are evidence of a greater cooling rate), and Figure 5.21 shows this phenomenon in the iPP−DPE system. A fast cooling rate resulted

in the polymers pulling away from the zeolite surfaces, and a slow cooling rate resulted in a nearly ideal structure.

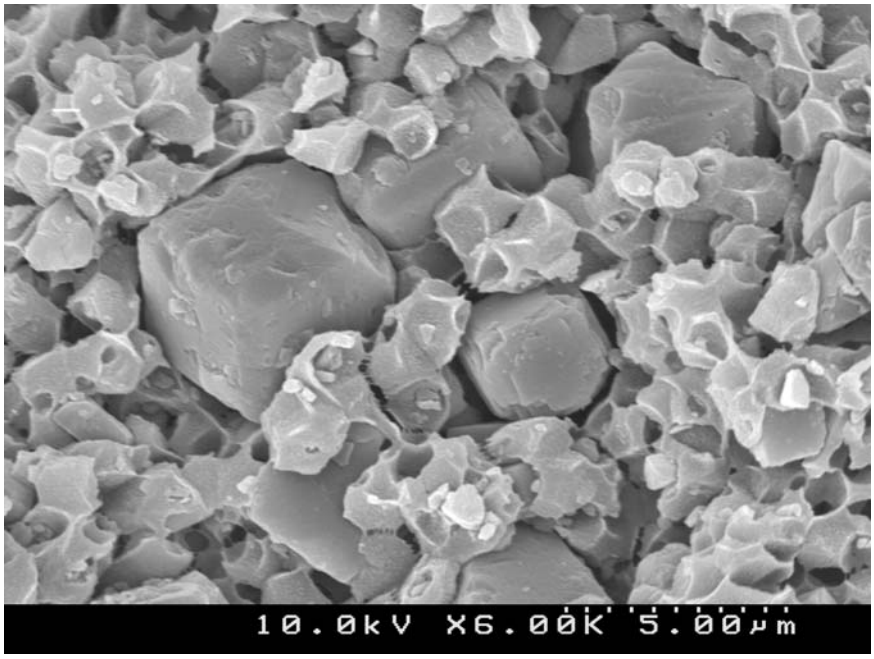

Figure 5.20: SEM image of an extruded 20 wt-% polymer EVAL38−glycerol membrane containing zeolite particles and cooled using the system described in Figure 5.1 (belt temperature = 80ºC). Cooling occurred too quickly for the polymer to remain in contact with the zeolite particles.

A similar result was also seen in work performed by Mahajan, et al [21]. Here it was observed that by forming mixed matrix membranes at room temperature, polymers were more likely to delaminate from the zeolite surfaces than at high temperatures due to shrinkage during solidification. It was necessary for the polymer to adjust to these stresses, and that was not possible at low temperatures. Raising the temperature of formation alleviated this problem. Similarly, in the ZeoTIPS formation process, by cooling quickly, the polymer does not have sufficient time to adjust to the stresses

occurring during solidification, and shrinkage causes a similar delamination in certain polymer−diluent systems that lack a strong polymer−zeolite affinity.

Cooling rate has a major effect on cell size in L−L TIPS membranes, as discussed in Section 5.4.1. The results shown in Figure 5.20 and 5.21 are evidence that the cooling rate in ZeoTIPS membrane processing is of even greater importance.

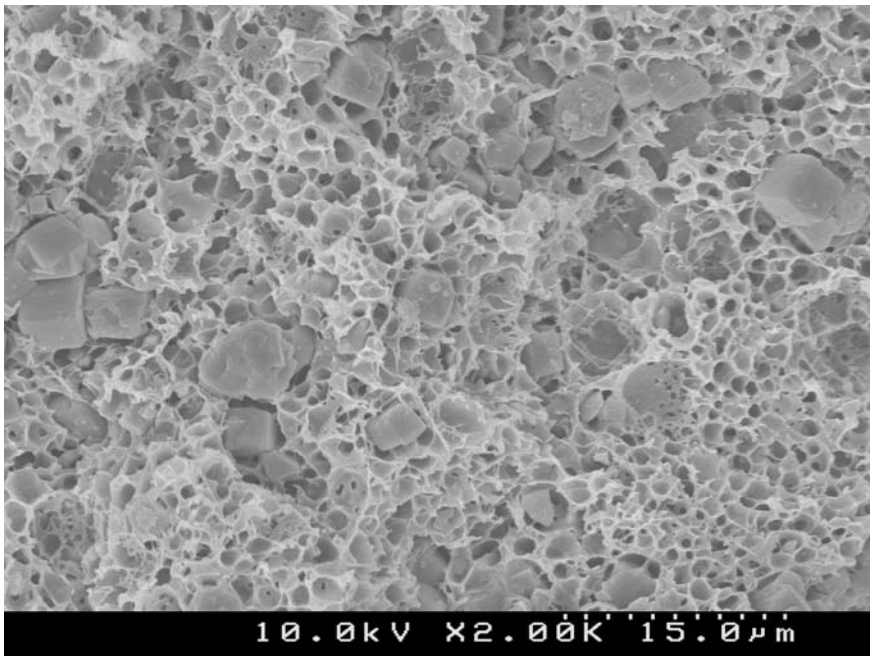

(a)

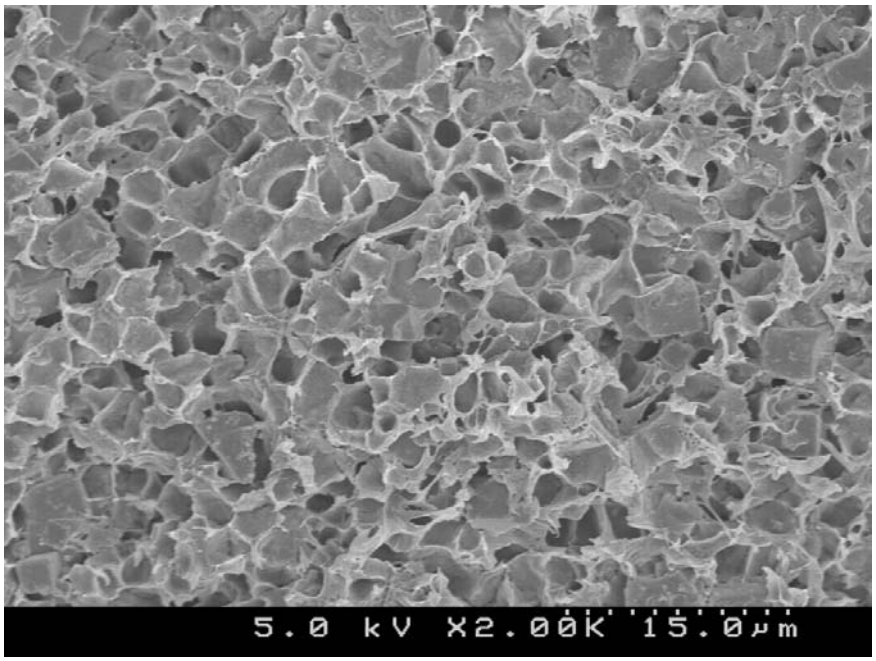

(b)

Figure 5.21: Extruded iPP−DPE membranes cooled (a) quickly, resulting in small cells and poor polymer−zeolite affinity and (b) slowly, resulting in large cells and strong polymer−zeolite affinity.

5.7 SUMMARY OF CHAPTER 5

The best method of formation for ZeoTIPS membranes appears to be extrusion, due to the need for vigorous mixing and short processing times that will limit the settling of the zeolite particles. Compression molding lacks the repeatability of a continuous extrusion process, and the hot stage method does not produce large enough samples to test.

Experiments discussed in this chapter have shown that selecting a polymer and diluent for ZeoTIPS membranes is more complicated than simply determining the polymer's solubility in the chosen diluent. Affinities between those two components and the zeolite powder will determine whether or not one will achieve ideal or non-ideal behavior. It has been shown that by adjusting the system's solubility parameters, it is possible to adjust the affinity of the polymer for the zeolite particles and approach $\beta = 0$, the ideal behavior. Furthermore, experiments with zeolite surface modification suggest that changing the zeolite surface hydrophilicity is another way to accomplish this goal, although experiments discussed here were not successful.

While a variety of encouraging membrane structures were formed, successful membranes were not produced in this research. However, this is not due to limitations in the ZeoTIPS concept, but stems from limitations in the available extrusion equipment. The experimental equipment lacked the necessary downstream processing and control, preventing the use of desired cooling rates and systems with low suspension viscosities.

5.8 REFERENCES

1 P.W. Morgan, *Interfacial Polymerization*, in: J.I. Kroschwitz (Ed.), Encyclopedia of Polymer Science and Engineering, 8, Wily, New York, 1987, pp. 221-237.

2 I.M. Wienk, R.M. Boom, M.A.M. Beerlage, A.M.W. Bulte, C.A. Smolders, and H. Strathmann, *Recent advances in the formation of phase inversion membranes made from amorphous or semi-crystalline polymers.*, Journal of Membrane Science, 113 (1996) 361-371.

3 B. Kunst and S. Sourirajan, *Effect of casting conditions on the performance of porous cellulose acetate membranes in reverse osmosis*, Journal of Applied Polymer Science, 14 (1970) 723-733.

4 S. Husain and W.J. Koros, *Mixed matrix hollow fiber membranes made with modified HSSZ-13 zeolite in polyetherimide polymer matrix for gas separation*, Journal of Membrane Science, 288 (2007) 195-207.

5 R. Mahajan and W.J. Koros, *Factors controlling successful formation of mixed-matrix gas separation materials*, Industrial & Engineering Chemistry Reasearch, 39 (2000) 2692-2696.

6 D.R. Lloyd, S.S. Kim, and K.E. Kinzer, *Microporous membrane formation via thermally-induced phase separation. II. Liquid-liquid phase separation*, Journal of Membrane Science, 64 (1991) 1-11.

7 K.S. McGuire, D.R. Lloyd, and G.B.A. Lim, *Microporous membrane formation via thermally-induced phase separation. VII. Effect of dilution, cooling rate, and nucleating agent addition on morphology*, Journal of Membrane Science, 79 (1993) 27-34.

8 H. Matsuyama, S. Berghmans, M.T. Batarseh, and D.R. Lloyd, *Effects of thermal history on anisotropic and asymmetric membranes formed by thermally induced phase separation*, Journal of Membrane Science, 142 (1998) 27-42.

9 H. Matsuyama, S. Berghmans, and D.R. Lloyd, *Formation of hydrophilic microporous membranes via thermally induced phase separation*, Journal of Membrane Science, 142 (1998) 213-224.

10 A.F.M. Barton, *CRC Handbook of solubility parameters and other cohesion parameters*, CRC Press, Boca Raton, Florida, 1983.

11 M.X. Shang, H. Matsuyama, M. Teramoto, D.R. Lloyd, and N. Kubota, *Preparation and membrane performance of poly(ethylene-co-vinyl alcohol) hollow fiber membrane via thermally induced phase separation*, Polymer, 44 (2003) 7441-7447.

12 D.W. Van Krevelen, *Properties of Polymers*, 3rd ed, Elsevier, New York, 1990. pages 427.

13 J. Brandrup and E.H. Immergnt, (Eds.), Polymer Handbook, New York, 1975.

14 S. Zhu, Y. Dun, and Q. Wang, *Determination of solubility parameter of phenolphthalein-based poly(ether sulfone)*, Huagong Xinxing Cailiao, 33 (2005) 21-23.

15 I.F.J. Vankelecom, S.V.d. broeck, E. Merckx, H. Geerts, P. Grobet, and J.B. Uytterhoeven, *Silylation to improve incorporation of zeolites in polyimide films*, Journal of Physical Chemistry, 100 (1996) 3753-3758.

16 R. Mahajan and W.J. Koros, *Mixed matrix membrane materials with glassy polymers. Part 1*, Polymer Engineering and Science, 42 (2002) 1420-1431.

17 A.J. Paine, *Mechanisms and Models for Copper Mediated Nucleophilic Aromatic Substitution. 2. A Single Catalytic Species from Three Different Oxidation States*

of Copper in an Ullmann Synthesis of Triarylamines, Journal of the American Chemical Society, 109 (1987) 1496-1502.

18 L.D.S. Yadav, B.S. Yadav, and V.K. Rai, *Active-Copper-Promoted Expeditious N-Arylations in Aqueous Media under Microwave Irradiation*, Syntheis, 11 (2006) 1868-1872.

19 T.L. Barr, *Modern ESCA: The Principles and Practice of X-Ray Photoelectron Spectroscopy*, CRC Press, Boca Raton, 1994.

20 B.V. Crist, *Handbook of monochromatic XPS spectra*, Wiley, Chichester, New York, 2000.

21 R. Mahajan, R. Burns, M. Schaeffer, and W.J. Koros, *Challenges in forming successful mixed matrix membranes with rigid polymeric materials*, Journal of Applied Polymer Science, 86 (2002) 881-890.

Chapter 6: Liquid−Solid Thermally Induced Phase Separation for ZeoTIPS Membranes [2]

6.1 INTRODUCTION

As introduced in Chapter 1 and in earlier literature from this laboratory [1-3], L–S TIPS can lead to unique microporous structures. In L–S TIPS, there are several ways of controlling microporous membrane morphology, including cooling rate, diluent concentration, and diluent crystal structure (*i.e.,* triclinic, monoclinic, orthorhombic, etc.). Consequently, when forming membranes via L–S TIPS, selection of the diluent requires careful consideration of the crystal form. Proper control of the kinetics of crystal growth through control of the cooling rate may lead to a tight pore size distribution, which would have considerable impact in biological separations in which a narrow size cut-off is needed. Furthermore, a L−S TIPS membrane can be made into hollow fiber form, an important advantage over track-etch membranes, which characteristically have narrow pore size distributions useful for biological separations but cannot be formed as hollow fibers.

Many L−S TIPS systems can produce porous structures of short, randomly oriented cavities upon diluent extraction. Such structures may or may not be useful as membranes for separations, depending on the connectivity of the porous structure. A more useful morphology would result if the crystals could be grown as long, continuous, aligned needles that span or traverse the membrane thickness. Upon diluent extraction, the result would be non-tortuous paths across the membrane, thereby limiting trans-membrane pressure drop and maintaining good throughput. The ideal crystallizable

[2] Portions of this chapter are based on: C.V. Funk, P.L. Hanks, K.J. Kaczorowski, and D.R. Lloyd, *Diluent Crystal Alignment in the Formation of Membranes via Liquid−Solid Thermally Induced Phase Separation*, J. Porous Mat., (2008) submitted.

diluent would produce a structure similar to that of a track-etch membrane with straight pores that span from the feed to permeate side of the membrane. The advantage of the L–S TIPS approach is that through the use of a high diluent concentration, there is the potential to produce highly selective membranes with vastly greater porosity than track-etch membranes. This chapter suggests a method for producing L−S TIPS membranes with *aligned* crystals and thus aligned pores.

The possibility of using L−S TIPS systems in the formation of ZeoTIPS membranes is also suggested below. Trans-membrane crystal alignment is not a useful property in ZeoTIPS membranes, but the same properties that make a diluent useful for crystal alignment may also prove helpful in forming successful ZeoTIPS structures.

6.2 MATERIALS AND METHODS

6.2.1 Materials

Udel P-3500 poly(ether sulfone) (PES) was obtained from Solvay Advanced Polymers. Poly(methyl methacrylate) (PMMA) with a M_w of 105,400 g/mole was obtained in the form of Plexiglas from Rohm & Haas (Philadelphia, PA). Escorene Ultra 7760 poly(ethylene co-vinyl acetate) (EVAc, 26.7 wt-% vinyl acetate) and Escor 5100 poly(ethylene co-acrylic acid) (EAA, 11 wt-% acrylic acid) were generously provided by ExxonMobil Chemical (Houston, TX). Isotactic polypropylene (iPP) with a reported M_w of 138,000 g/mole was obtained from ExxonMobil Chemical. Ultem polyetherimide (PEI) was obtained from GE Plastics (Pittsfield, MA). Hexamethylbenzene purchased from Eastman Kodak and benzoic acid, adipic acid, resorcinol, bisphenol-A, phenyl benzoate, dioctyl phthalate, sodium hydroxide, and methanol purchased from Fisher Chemical (St. Louis, MO) were used as received without further purification.

6.2.2 Membrane Systems and Phase Diagrams

Research on a few L–S TIPS systems has been published in the literature to date; systems reported include iPP–hexamethylbenzene, LDPE−hexamethylbenzene, LDPE−tetrachlorobenzene, poly(L-lactic acid)−p-hydroxybenzoic acid, and PLLA−hexamethylbenzene [1, 4, 5]. Systems investigated in the research reported here include: PES–benzoic acid, EAA–benzoic acid, EVAc–benzoic acid, PMMA–benzoic acid, PEI−benzoic acid, and PES−resorcinol. All of these systems exhibit thermodynamic behavior similar to that shown in Figure 6.1 for EVAc−benzoic acid and Figure 6.2 for PES–benzoic acid. These two systems are used in this chapter to illustrate the concept of crystal alignment in L-S TIPS.

The EVAc−benzoic acid system is a relatively simple one for producing a complete phase diagram because the polymer is semi-crystalline and its crystallization can be monitored by differential scanning calorimetry (DSC) using a Perkin-Elmer DSC 7. Homogeneous samples of 10, 20, 30, 40, 50, and 60 wt-% polymer were produced in sealed test tubes according to the procedure outlined in Chapter 3. These test tubes were broken, and ~10 mg portions of these samples were sealed into aluminum volatile sample pans. These samples were then heated in the DSC from 25ºC to 170ºC at a rate of 50ºC/min, held for 10 minutes to erase thermal history, and then cooled to room temperature at a rate of 10ºC/min while monitoring the crystallization temperatures of the polymer and diluent. Due to the high degree of supercooling (that is, the cooling of a substance below its crystallization temperature without solidifying), the crystallization temperatures for benzoic acid were somewhat erratic, as indicated in Figure 6.1 by the error bars on each point representing ± 1 standard deviation.

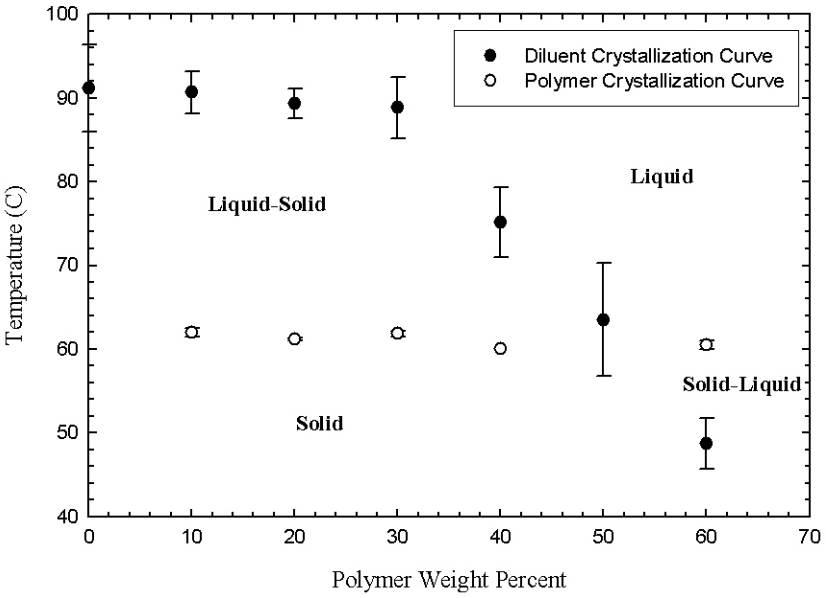

Figure 6.1: Phase diagram for the EVAc−benzoic acid system showing the diluent crystallization curve and polymer crystallization curve, both determined calorimetrically (error bars = ±1 standard deviation)

Although PES is not crystalline and thus its solidification cannot be monitored by DSC, the system of PES−benzoic acid is nonetheless important and the diluent crystallization curve is shown in Figure 6.2. Again, due to the high degree of supercooling, there was a large data spread for each polymer weight fraction. At a polymer concentration of 50 wt-%, the pore morphology observed microscopically changed dramatically, indicating that the polymer solidified before the diluent and that the eutectic temperature for this system is around 80ºC. However, it was not possible to determine the exact eutectic temperature experimentally.

These phase diagrams will be used to explain membrane morphologies discussed in Section 6.3.2.

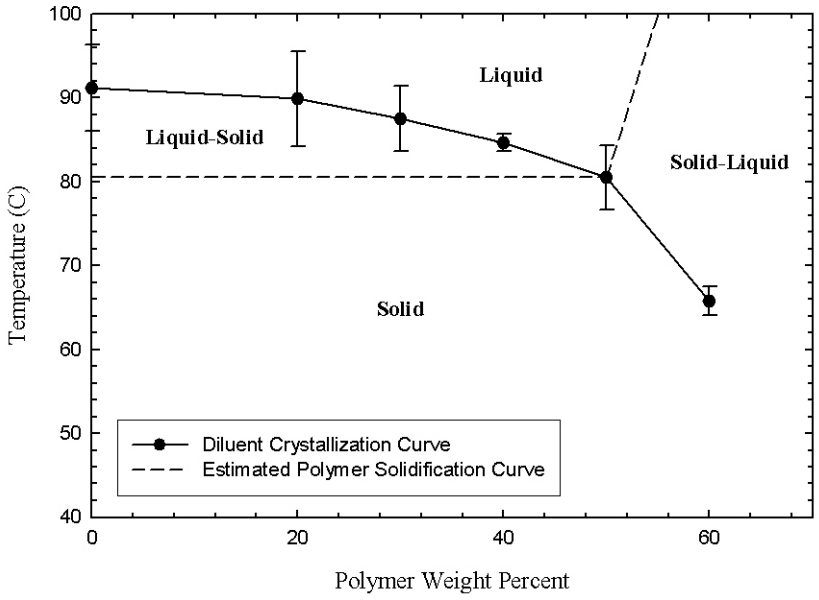

Figure 6.2: Phase diagram for the PES−benzoic acid system showing the diluent crystallization curve (determined calorimetrically) and estimated polymer solidification curve (error bars = ±1 standard deviation)

6.2.3 Membrane Formation

Membranes were formed by the two experimental procedures described herein. The first procedure, conducted to assess solution behavior, involved forming small membranes on a hot stage between glass coverslips in a controlled environment. Polymer–diluent samples were prepared as outlined in Chapter 3. The heated hot stage samples were cooled at rates of 10, 50, or 125ºC/min. They were then removed from the slides and extracted as described below.

The second procedure for making membranes involved spinning hollow fibers using a batch extruder. A 200–300 gram sample of polymer and diluent was sealed in a stainless steel vessel under nitrogen atmosphere. The vessel was heated to 180°C for 24 hours with agitation from an impellor to ensure homogeneity. The solution was pumped

via a metering pump at 40–60 cc/min through a spinneret (3 mm ID, 4 mm OD) heated to approximately 10ºC above the crystallization temperature of the diluent. The bore fluid used was air heated to the temperature of the clad. The fibers passed through an air gap and into a water bath to complete the polymer solidification before being taken up on a drum and then extracted.

After solidification, membranes produced by both methods were extracted in a two-step process. Aqueous solutions of sodium hydroxide were used to remove benzoic acid crystals from the membranes. A second wash of methanol was used to replace the water, preventing large amounts of shrinkage during the drying process. Methanol was used because preliminary experiments using water as the final extractant resulted in considerable shrinkage of the membrane upon drying. All samples were air dried at room temperature without restraint.

6.3 RESULTS AND DISCUSSION

Since upon extraction the hole left by the crystal forms the pore, there are two main factors that influence the effectiveness of a polymer−diluent system when forming membranes via L−S TIPS — crystal shape and crystal alignment. In terms of crystal shape, needle-like crystals are more desirable than sheet-like crystals because they will provide the narrower pore size distribution required for high selectivity. In terms of crystal alignment, uni-directional crystal growth from one membrane surface to the other is ideal for reducing tortuosity and pressure drop across a membrane, in addition to helping to maintain regularity in surface pore size and shape.

6.3.1 Crystal and Pore Shape

Hexamethylbenzene has been shown in previous studies to exhibit regular rectangular crystals when used in a L−S TIPS system with polyolefins [1, 5]. These regular crystals are highly desirable, since they could lead to a high porosity, high selectivity microporous membrane with low tortuosity. The membranes formed by Alwattari by quenching an iPP−HMB solution at elevated temperatures for long periods resulted in short, wide crystals. Conversely, Alwattari found that by quenching at fast rates, it was possible to produce much longer, thinner crystals [1]. However, these crystals nucleated freely and did not result in well-aligned pore structures upon diluent extraction. Furthermore, the faster the cooling rate, the less regular the HMB crystal shape [8].

Benzoic acid, with its relatively low cost and low toxicity, is a favorable choice of diluent for making L−S TIPS membranes. It was found in the research reported here that benzoic acid can be used as a diluent for the polymers EVAc, EAA, PMMA, and PES. In the case of PMMA, EVAc and EAA, low cooling rates (~50ºC/min) resulted in benzoic acid crystals forming a sheet morphology that is not conducive to membranes for separations applications. These membranes lacked durability and probably the desired selectivity. An example of such an EVAc−benzoic acid membrane cooled at 50ºC/min is shown in Figure 6.3.

However, when benzoic acid crystallizes in EVAc at cooling rates of 125ºC/min the result is needle-shaped crystals similar to those shown in Figure 6.4. The structure shown in Figure 6.4 also resulted when benzoic acid was crystallized in PES at all cooling rates studied here. These structures are more useful as membranes, although the shape of the crystals shown in Figure 6.4 was less regular than those reported by Alwattari for HMB in iPP [8].

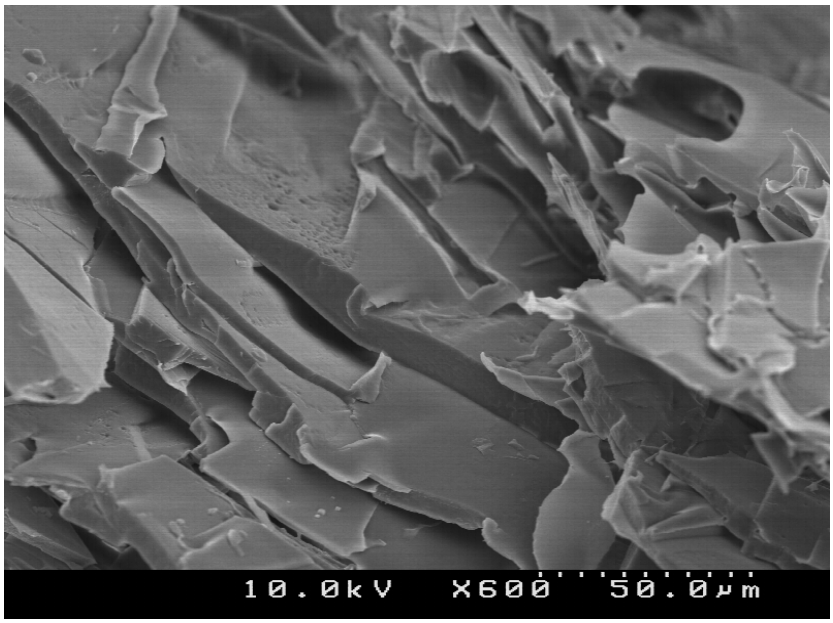

Figure 6.3: EVAc−benzoic acid membrane showing pores formed from crystals in a sheet morphology

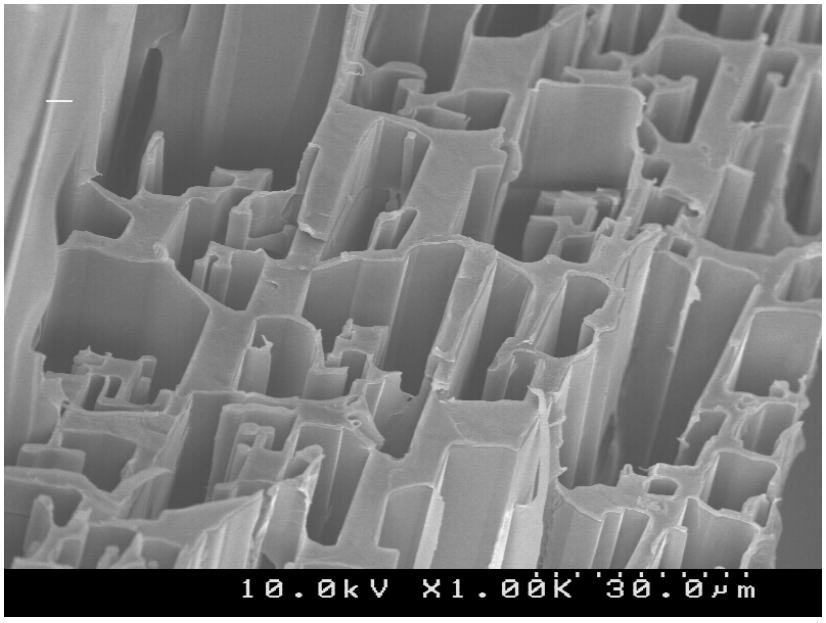

Figure 6.4: PES−benzoic acid membrane cross section (break perpendicular to direction of crystal growth) showing randomly shaped pores due to irregular crystals

6.3.2 Crystal Alignment

The ideal membrane morphology consists of a narrow pore size distribution with aligned pores traversing the membrane. Such a structure provides low tortuosity, leading to low pressure drop and lower internal fouling, and good selectivity. Membranes formed using PES and benzoic acid were found to exhibit a nearly ideal alignment under certain conditions to be described below.

Benzoic acid dissolves PES at temperatures far below the PES glass transition temperature of 200ºC, making this L−S TIPS system a simple one to utilize. It was observed that when membranes were formed as flat sheets using the first procedure outlined above, phase separation started at the edges of the sample and progressed to the sample center. This progression from the sample edges is attributed to a slight concentration gradient near the perimeter of the sample, which results from diluent migration toward the perimeter during the preparation and cooling of the sample. This area with higher diluent concentration crystallized first, as suggested by the phase diagrams in Figures 6.1 and 6.2. The observed crystal alignment behavior is due to the degree of supercooling of the PES−benzoic acid system as the benzoic acid cools below its crystallization temperature prior to crystallization. Crystals first began to grow near the outside because of the higher diluent concentration. These crystals along the perimeter act as seed crystals, and allow for subsequent phase separation that progresses towards the interior of the sample. Such a phenomenon occurs more often with asymmetric molecules such as benzoic acid due to a lack of molecular regularity [9]. HMB, with its high degree of symmetry, does not exhibit a large degree of supercooling, since it can more easily form a regular crystal lattice [9].

Differential scanning calorimetry experiments revealed the supercooling behavior of both benzoic acid and HMB. By heating a sample of HMB at 10ºC/min above its

melting point and then cooling the sample at the same rate, a 2ºC difference resulted between the temperature at which the sample melted and the temperature at which the sample crystallized. The same experiment with pure benzoic acid showed a 30ºC difference between the melting and crystallization temperatures. These results, along with the above observations, show that benzoic acid (unlike HMB) is much more likely to crystallize in the presence of seed crystals (which may have formed due to concentration gradients at the edges of the membrane) than it is to begin nucleating crystals throughout the sample. This behavior is ideal for producing membranes, since such a phenomenon will result in long, aligned pores, like those in Figure 6.5, which grew parallel to the glass coverslips.

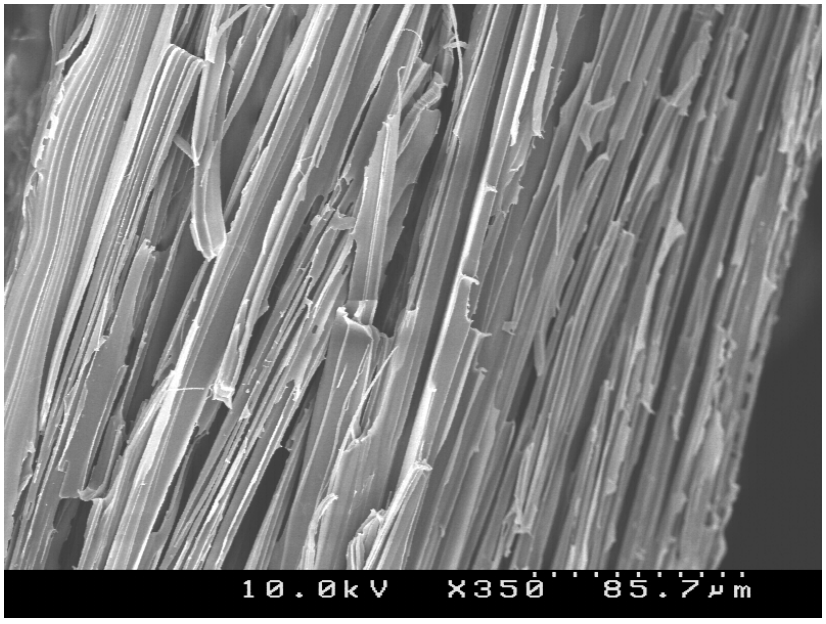

Figure 6.5: PES−benzoic acid flat sheet membrane cross section (break parallel to direction of crystal growth) showing well-aligned pores

While concentration gradients were shown to be useful in inducing uni-directional crystal growth in these small, flat sheet membranes, gradients in temperature can be

equally useful. To demonstrate this point, hollow fiber membranes were formed as described above. Typically in the formation of hollow fibers, cooling occurs from the exterior of the membrane to the interior. Taking advantage of the seeding phenomenon, one can cool the outside of a PES−benzoic acid fiber, thereby beginning phase separation and growing crystals radially from the outer surface to the inner surface. Figure 6.6 shows a cross section of such a hollow fiber and exhibits reasonably well-aligned crystals. In this figure, cooling occurred from left (outside of the fiber) to right (lumen of the fiber).

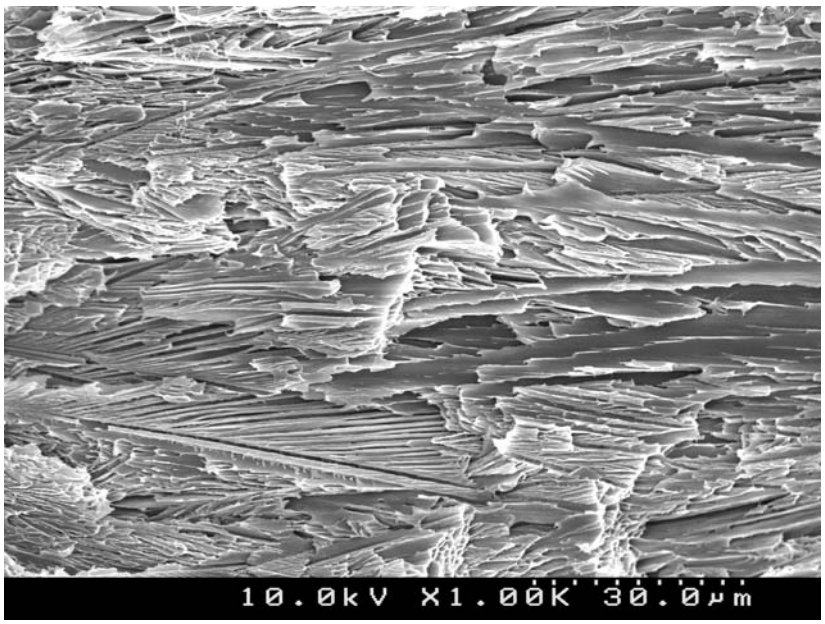

Figure 6.6: PES−benzoic acid hollow fiber membrane cross section (break perpendicular to the spinline) showing well-aligned pores

6.4 PROCESSING CHALLENGES

In TIPS membrane production, the one phase homogeneous liquid phase is cooled at a given rate to induce phase separation. The amount of time in the phase separated

region prior to polymer solidification impacts the morphology of the membrane. Taking a typical composition of 30 wt-% polymer, Figure 6.2 indicates that PES-benzoic acid has a phase separated region of approximately 8ºC between diluent crystallization and polymer solidification. On the other hand, Figure 6.1 shows that at 30 wt-% polymer the EVAc−benzoic acid system has an L–S region of approximately 30ºC between crystallization of polymer and diluent. If both systems are extruded under the same conditions, the PES–benzoic acid system has a much shorter time period during which drawdown of the nascent membrane can occur prior to fiber solidification. Consequently, in the PES–benzoic acid system there is less of a tendency of the benzoic acid crystals to be re-oriented from an orientation perpendicular to the spinline (induced by concentration / temperature gradients) to an orientation parallel to the spinline (induced by flow fields due to drawdown). Thus, in the formation of L–S TIPS hollow fibers, selection of systems with small phase separated gaps is preferred. In addition, one can minimize re-orientation of the crystals during the drawdown of the nascent hollow fiber by using short air gaps.

Additionally, the extrusion process needs to be controlled in such a way as to minimize diluent evaporation from the outer surface of the fiber. The loss of benzoic acid at the outer surface of the nascent fiber will drive up the polymer concentration in the outermost region of the fiber. According to the phase diagrams in Figure 6.1 and Figure 6.2, at high polymer concentrations the system may undergo S–L TIPS rather than L–S TIPS. If this occurs in the outer region of the fiber, then the final structure of the hollow fiber membrane will have undesirable polymer crystals on the outer surface. Such a structure is not suitable for separations applications. Thus, in the formation of L–S TIPS hollow fibers one should select diluents with low volatility at its melting point, or

consider options such as co-extrusion of a sacrificial layer of diluent or non-volatile liquid on the outside of the membrane fiber.

6.5 APPLICATION OF L−S TIPS TO ZEOTIPS MEMBRANES

As discussed in Section 6.3.2, a diluent's ability to supercool is the key factor in producing aligned crystals. Without a seed, the diluent prefers to remain in solution below its melting point. This behavior may lead to useful behavior when zeolite particles are present in solution. By using a hydrophilic diluent, one may be able to induce crystallization at the hydrophilic particle surfaces, yielding a structure like that in Figure 6.7, where the light grey regions represent polymer supporting the dark grey zeolite particles. The white areas represent the pores after diluent extraction. The use of a hydrophilic diluent leads to hydrogen bonding at the surface of the zeolite, making the surface a favorable location to seed crystals.

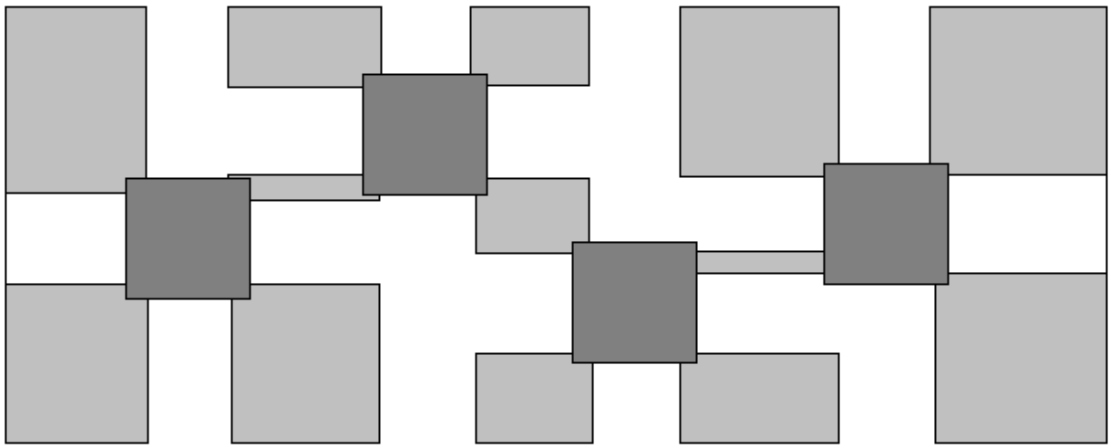

Figure 6.7: Proposed structure of a L−S ZeoTIPS membrane. Crystals grow from the particle surfaces in all directions, some leading to the membrane surface.

Benzoic acid was the most successful diluent in aligning crystals in section 6.3.2 above. Optical microscopy showed that it also had the ability to seed on 4A zeolite particle surfaces. Figures 6.8(a) and 6.8(b) show benzoic acid crystals formed under 10ºC/min cooling between glass slides without zeolite present and with zeolite, respectively. The full width of the pure benzoic acid crystal image is 280 μm, whereas the crystals formed in the presence of zeolite were much smaller. The full width of the image in Figure 6.8(b) is 60 μm.

Benzoic acid was not a successful diluent in forming needle-like crystals when polymer and zeolite were present. It is known that zeolites can be used to catalyze reactions with benzoic acid. In the presence of RE-Y and H-β zeolites, benzoic acid reacts to form a reactive benzoyl cation [10, 11]. This cation is free to react with the polymer in solution and this behavior was observed in attempts to form ZeoTIPS membranes. Solutions of benzoic acid with EVAc, EAA, PES, or PEI containing 4A zeolite particles resulted in this reaction between polymer and diluent, causing the polymer to fall out of solution, coating the zeolite particles. The resulting membranes resembled dense mixed matrix membranes. Adipic acid, although not a suitable L−S TIPS diluent, also underwent a zeolite-catalyzed reaction with the polymer, leading to the conclusion that carboxylic acids in general cannot be used in ZeoTIPS membranes when 4A zeolite is used.

The iPP−hexamethylbenzene system was also used in an attempt to make a successful ZeoTIPS membrane. However, the polymer had a greater affinity for the zeolite surface than did the diluent, and since the diluent crystals nucleated in the bulk solution, the resulting structure was not useful.

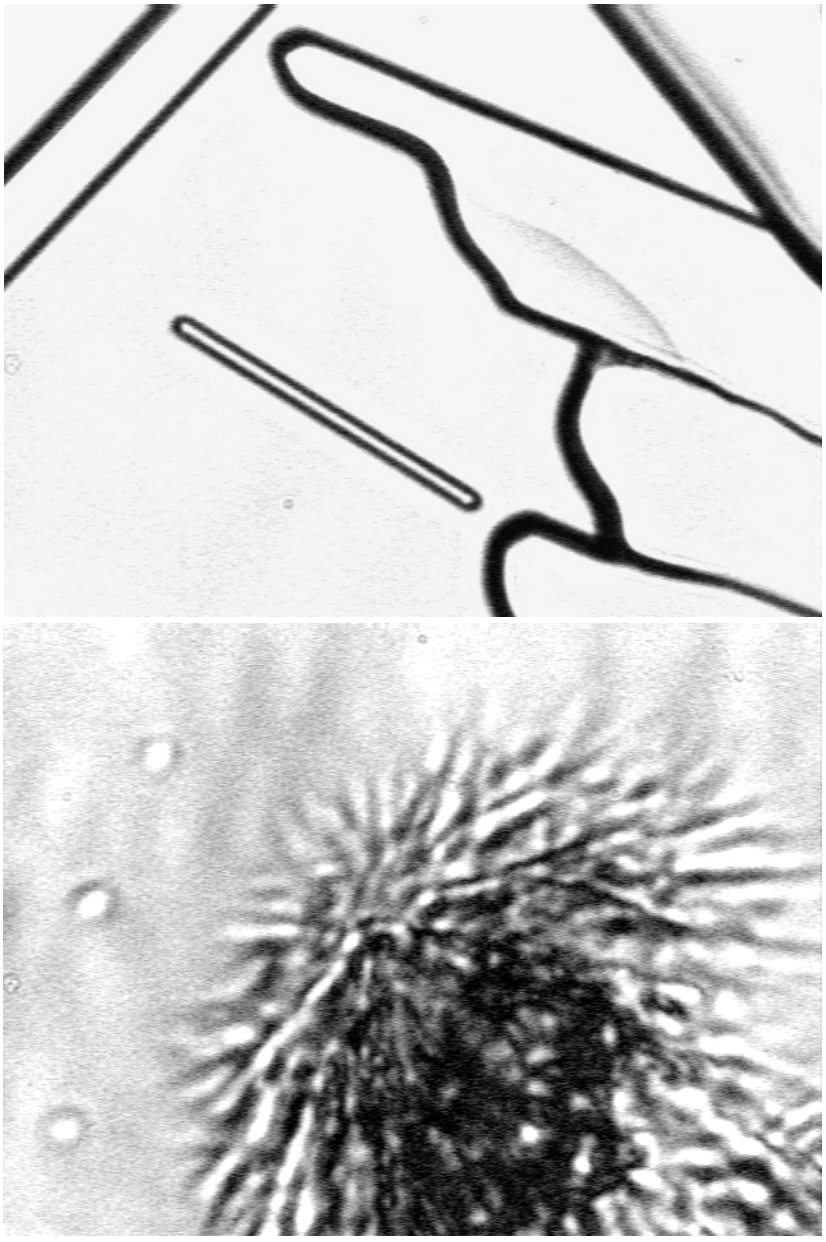

Figure 6.8: Benzoic acid crystals grown at 10ºC/min cooling (a) in the absence of zeolite (full image width = 280 µm), and (b) in the presence of zeolite (full image width = 60 µm).

A proper diluent for a L−S ZeoTIPS membrane must be one that has a reasonable degree of supercooling to prevent nucleation in the bulk solution. The diluent crystals must only nucleate on the zeolite particle surfaces, and therefore, as discussed in Section 6.3.2, the diluent must be asymmetric in structure. Additionally, if 4A zeolite is to be used, the diluent must have the capacity to hydrogen bond to the surface, since a non-polar diluent like hexamethylbenzene will not nucleate on the zeolite particles.

Three additional diluents were investigated for this purpose: bisphenol-A, resorcinol, and phenyl benzoate. All had the necessary supercooling ability, and had low toxicity. Their melting points and structures are shown in Table 6.1.

The use of bisphenol-A for L−S TIPS was not fruitful as the diluent failed to phase separate from the five polymers used – PMMA, EAA, EVAc, EVAL, and PES. Resorcinol was unable to dissolve the grades of EVAc and EAA used, but did undergo L−S TIPS with PMMA and PES. However, the phase separation was unique in that the diluent crystallized at such low temperatures that the solution became quite viscous. The subsequent crystal growth was extremely slow due to the supercooling ability of resorcinol and the resistance to diluent diffusion of the viscous solution. The resulting morphology lacked order and was not useful to achieve the goals of this investigation (see Figure 6.9).

This result suggests that a final criterion for selecting a L−S TIPS diluent is that its melting point must be sufficiently high to undergo supercooled crystallization at a temperature well above room temperature. Crystallization at room temperature in these experiments occurred in high viscosity solutions, preventing porous structures like that shown in Figures 6.4, 6.5, and 6.6.

Phenyl benzoate did not undergo L−S TIPS with EAA or EVAc. Instead, L−L TIPS occurred, forming liquid droplets before the phenyl benzoate crystallized.

Table 6.1: Selected polar diluents for use in L−S ZeoTIPS membranes

Diluent	Structure	Melting Point	L−S TIPS Polymers	Result
Benzoic Acid	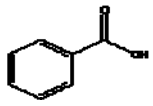	122ºC	PMMA, EVAc, EAA, PES, PEI	Reacted with zeolite and polymer
Adipic Acid	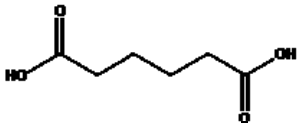	152ºC	–	Did not undergo L−S TIPS with polymers tested; reacted with zeolite and polymer
Bisphenol-A	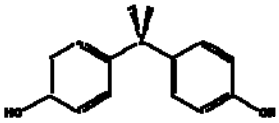	155ºC	–	Did not undergo L−S TIPS with polymers tested
Resorcinol	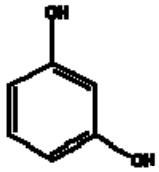	110ºC	PES	Structure was not useful; did not nucleate on zeolite surface
Phenyl Benzoate	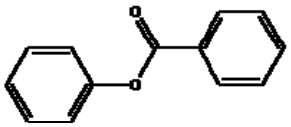	70ºC	EAA, EVAc	Underwent L−L TIPS

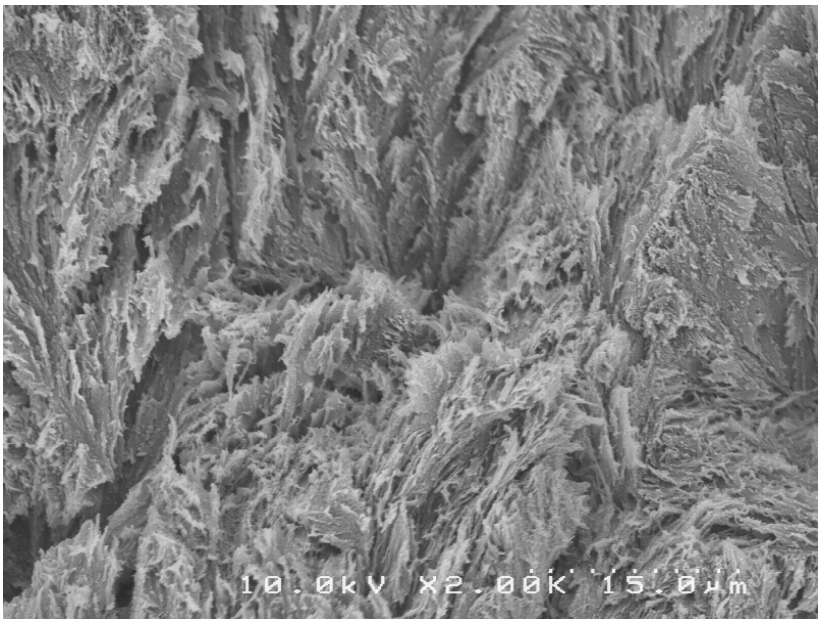

Figure 6.9: SEM image of a PES−resorcinol membrane made with 30 wt-% polymer and cooled at 10ºC/min.

Zeolite surface modifications discussed in Chapter 5 could be useful in producing L−S ZeoTIPS membranes. First, modifications could be used to prevent the reaction between benzoic acid and the zeolite. When a hydrophobic zeolite is chosen, modifications could also be performed to increase the affinity of hydrophilic diluents for the zeolite surface, causing them to seed on the particle surfaces. The same could be said for a hydrophilic zeolite when a hydrophobic diluent and polymer are used. However, it is unlikely that any of the polymer−diluent−zeolite systems described in this chapter in conjunction with the modifications described in Chapter 5 will be successful.

6.6 SUMMARY OF CHAPTER 6

Liquid−solid thermally induced phase separation appears to be a viable method of producing hollow fiber microporous membranes that have the potential to be highly

porous and selective. Under appropriate processing conditions, concentration and/or temperature gradients can be induced across the nascent fiber wall, which in turn can cause the crystals to align in that direction. When the diluent crystals are extracted from the membrane, the resulting pores are aligned from one surface of the hollow fiber to the other. The ability of the polymer–diluent system to be supercooled strongly impacts the ability of the crystals to align. Asymmetric molecules, such as benzoic acid, are more readily supercooled than symmetric molecules, such as HMB, and thus benzoic acid crystals are more readily aligned. Other factors such as diluent volatility impact the ability to form hollow fiber membranes with diluent crystals aligned across the entire fiber wall. Phase separation characteristics, such as L−S versus S−L phase separation and the size of the L−S region of the phase diagram, not only affect the crystal size and shape in the final structure, but also influence their orientation in an extruded membrane. Finally, diluent crystallization must occur within a relatively low viscosity solution to prevent resistance to mass transfer.

The use of L−S TIPS for ZeoTIPS membranes also appears promising. Hydrophilic diluents can crystallize on zeolite particles and grow radially from those surfaces, although this was not proven in the presence of polymer. Future work is required to determine the best ways to control diluent evaporation and to find diluents that provide more regular crystal shape without reacting with zeolite filler.

6.7 REFERENCES

1 A.A. Alwattari and D.R. Lloyd, *Microporous membrane formation via thermally-induced phase separation. VI. Effect of diluent morphology and relative crystallization kinetics on polypropylene membrane structure*, Journal of Membrane Science, 64 (1991) 55-68.

2 A.A. Alwattari and D.R. Lloyd, *Isothermal crystallization of isotactic polypropylene-hexamethylbenzene blends: crystal morphology*, Polymer, 35 (1994) 2710-2715.
3 A.A. Alwattari and D.R. Lloyd, *Isothermal crystallization of isotactic polypropylene - hexamethylbenzene blends: kinetics analysis*, Polymer, 39 (1998) 1129-1137.
4 R.J.M. Zwiers, S. Gogolewski, and A.J. Pennings, *General crystallization behavior of poly(L-lactic acid) PLLA. 2. Eutectic crystallization of PLLA*, Polymer, 24 (1983) 167-174.
5 P. Smith and A.J. Pennings, *Eutectic crystallization of pseudo binary systems of polyethylene and high melting diluents*, Polymer, 15 (1974) 413-419.
6 S.S. Kim and D.R. Lloyd, *Microporous membrane formation via thermally-induced phase separation. III. Effect of thermodynamic interactions on the structure of isotactic polypropylene membranes*, Journal of Membrane Science, 64 (1991) 13-29.
7 D.R. Lloyd, S.S. Kim, and K.E. Kinzer, *Microporous membrane formation via thermally-induced phase separation. II. Liquid-liquid phase separation*, Journal of Membrane Science, 64 (1991) 1-11.
8 A. Alwattari, *Thermally induced phase separation of isotactic polyproylene and hexamethylbenzene*, Dissertation, The University of Texas at Austin, 1990.
9 D. Vorlander, *Investigation of the molecular form by means of crystalline liquids*, Z. Physik Chem., 105 (1923) 211-54.
10 S.R. Schmidt, *Catalysis of Organic Reactions*, CRC Press, Boca Raton, FL, 2006.
11 Y. Ding, R. Wu, and Q. Lin, *The chemoselective preparation of the substituted phenyl benzoates using RE-Y zeolite as catalyst.* , Synthetic Communications, 32 (2002) 2149-2153.

Chapter 7: Conclusions and Recommendations

7.1 CONCLUSIONS

The goal of this research, gaining fundamental understanding of the ZeoTIPS membrane formation process and separation capabilities, was accomplished through both theoretical and experimental means. Successful ZeoTIPS membranes were not formed in this study due to equipment limitations, as discussed in Chapter 5. However, the information obtained does provide a strong basis for future ZeoTIPS membrane development. Conclusions from the work presented here are as follows:

1. Mathematical modeling was used in Chapter 2 to show that ZeoTIPS membranes offer the opportunity for significant improvements in both selectivity and permeability over dense mixed matrix membranes with both the ideal and non-ideal ZeoTIPS structures.
2. As reported in Section 3.5.1, the main factors affecting droplet growth in ZeoTIPS membranes are cooling rate, polymer concentration, zeolite loading. Increased polymer concentration leads to decreased cell sizes because of an increase in viscosity and a decrease in diluent volume. Increased cooling rate leads to decreased cell sizes due to lower coarsening time for droplets. Zeolite loading affects droplet sizes by inhibiting coalescence and, depending on the polymer−zeolite interaction, by influencing the bulk diluent concentration.
3. It was shown in Section 3.5.2 that polymer−zeolite interaction has a significant effect on ZeoTIPS droplet growth and coalescence. Strong interaction leads to increased cell sizes, and this counteracts coalescence inhibition by the particles to varying degrees. Weak polymer−zeolite affinity, which is useless for the purposes of ZeoTIPS membranes, leads to varied

results, depending on the W/D ratio of the membrane. Zeolite surface modification may be used to adjust this polymer−zeolite affinity, as discussed in Section 5.4.2.

4. As shown in Figure 4.8 and discussed in Section 4.22, the minimum required zeolite loading can be achieved when the average zeolite particle size is equal to the average cell diameter. Thus, when producing a ZeoTIPS membrane, a zeolite of the desired pore size must first be obtained. Then, processing conditions should be adjusted to manipulate the final membrane cell size according to the zeolite particle size that is used, as particle sizes may change from zeolite to zeolite.
5. Extrusion is the most feasible method of continuous formation of ZeoTIPS membranes. Compression molding does not provide sufficient mixing and requires long processing times.
6. Liquid−solid TIPS, in which the diluent crystallizes prior to the polymer solidification, can be used to obtain unique and useful structures. The pores in these membranes are straight and narrow, showing potential for high selectivity microporous membranes if the crystals can be aligned. Diluent crystal alignment in L−S TIPS membranes can be achieved by the use of diluents such as benzoic acid with the ability to supercool and applying a concentration or temperature gradient across the membrane, as discussed in Section 6.3.2.
7. L−S ZeoTIPS membranes can be made if a suitable inert diluent, one that will not react with the zeolite surfaces, can be found.

7.2 RECOMMENDATIONS FOR FUTURE WORK

The main goal of this research was not to produce successful ZeoTIPS membranes, but to gain the necessary fundamental understanding of ZeoTIPS membrane formation for developing them in the future. Important information was gained from the studies described in Chapters 3 and 4, and although expanding the work described there would be beneficial, more immediate benefit would be gained by focusing on extensions of the more applied studies of Chapters 5 and 6. Expanding the work in Chapter 3 would require the use of a polymer−diluent system that yields weak polymer−zeolite interaction, but does not lead to diluent migration in the hot stage method of formation, a source of irreproducibility. Such a system was not found in this research. Expanding the work in Chapter 4 would require the ability to model sphere deformation in the two-phase suspension, and methods to model that phenomenon are not yet described in the literature.

The work discussed in Chapters 5 and 6, specifically development of formation methods and understanding of phenomena involved in formation, is an important basis for future development of ZeoTIPS membranes. Additional work in those areas could lead to successful ZeoTIPS membranes capable of high separation efficiencies.

7.2.1 ZeoTIPS Membrane Extrusion Downstream Processing Development

One of the greatest obstacles to producing ZeoTIPS membranes was the control of cooling rate in the extrusion process. The equipment described in Chapter 5 was insufficient in two ways. First, for some polymer−diluent systems such as EVAL38−glycerol, it was not able to cool the membrane slow enough to reach the necessary cell size. For systems such as cellulose triacetate−2-ethyl-1,3-hexanediol, the equipment was unable to handle low viscosity suspensions and extrude them into sheets.

Future work should involve the development of downstream processing equipment fulfilling the following requirements:

1. The equipment must be able to cool the extruded suspension very slowly, most likely by heating to temperatures just below the solidification temperature of the membranes.
2. The equipment must also have the capacity to cool the suspension quickly, as this will be required for some polymer−diluent systems.
3. The equipment must not allow the nascent membrane to contact a smooth surface.
4. As membrane development leads to very thin ZeoTIPS membranes, the equipment must either supply a porous support, such as paper, onto which the membrane can be applied, or be equipped to process a co-extruded membrane.

7.2.2 Liquid−Liquid ZeoTIPS Investigation

The next steps in developing L−L ZeoTIPS membranes should involve the formation of membranes with permeable polymers, such as cellulose triacetate, polyimides, or polyamides. Formation of membranes with these materials will be the simplest route due to their affinity for hydrophobic zeolite surfaces. With these materials successfully made, it will be possible to partially validate the permeation model in Chapter 2.

Next, using either zeolite surface modification or adjustable polymers or diluents, efforts should be made to reduce the thickness of the polymer layer on the zeolite particles until an ideal or nearly ideal structure is obtained. Because it will be difficult to measure that thickness, permeation tests could be used to track the effectiveness of these

efforts. At constant W/D ratio and zeolite loading, the greater the separation efficiency, the thinner the polymer layer has become.

Once suitable methods of formation have been established, the final step in development of these types of membranes is to attempt to produce ideal membranes with impermeable polymers. Such membranes will have the greatest performance and, most likely, the greatest durability and chemical stability.

7.2.3 Liquid−Solid ZeoTIPS Investigation

As discussed in Chapter 6, L−S ZeoTIPS membranes have potential to perform successful separations. In order to form these membranes through L−S TIPS, a diluent must first be identified that does not react at the surface of the zeolite, as does benzoic acid. This diluent must fulfill the following requirements:

1. It must be easily dissolved by a low boiling point extractant.
2. It should be asymmetric in nature, which will lead to supercooling ability.
3. It should have an affinity for the zeolite used, giving the ability to seed crystals on the zeolite surfaces, rather than in the bulk polymer solution.
4. It must have a high enough melting point that its crystallization temperature in the polymer solution is well above room temperature.

Further development of this membrane technology will require an analysis of crystal growth and the control of crystal shape for the chosen diluent. Additionally, it will be necessary to develop processing equipment which can form the membranes in a thin film on a porous support. This will lead to each pathway through the membrane only

requiring passage through a single zeolite particle. With this knowledge base, it will be possible to develop a ZeoTIPS membrane using L−S TIPS.

Appendix A: Nomenclature

Symbol	**Definition** (Equation), units
A	Hamaker constant (4.1), kg*m^2/s^2
a_{eq}	Equivalent radius of merging droplets (4.1), m
a_1	Radius of droplet 1 (4.1), m
a_2	Radius of droplet 2 (4.1), m
E_b	Electron binding energy (5.6), kg*m^2/s^2
E_k	Electron kinetic energy (5.6), kg*m^2/s^2
h_{cr}	critical inter-droplet distance (4.1), m
$h\upsilon$	X-ray energy (5.6), kg*m^2/s^2
P^{II}	Permeability of Path II (2.1), barrer
P^{III}	Permeability of Path III (2.1), barrer
P_{O2}	Permeability of oxygen (2.13), barrer
P_{N2}	Permeability of nitrogen (2.13), barrer
P_P	Permeability of polymer (2.1), barrer
P_V	Permeability of void or diluent (2.1), barrer
P_Z	Permeability of zeolite (2.2), barrer
$q\phi$	Work function (5.6), kg*m^2/s^2
β	Percentage of total polymer in the membrane that contributes to the coating of the zeolite particles (2.5)
γ	Surface tension (4.1), kg/s^2
δ	Hildebrand solubility parameter (5.1), (J/m^3)$^{1/2}$x10^{-3}

δ_d	Solubility parameter component due to dispersion forces (5.1), $(J/m^3)^{1/2}x10^{-3}$
δ_p	Solubility parameter component due to polar forces (5.1), $(J/m^3)^{1/2}x10^{-3}$
δ_h	Solubility parameter component due to hydrogen bonding (5.1), $(J/m^3)^{1/2}x10^{-3}$
ε	Solid−liquid interaction strength parameter (5.2), $(J/m^3)^{1/2}x10^{-3}$
ϕ^I	Overall volume fraction of Path I (2.10)
ϕ^{II}	Overall volume fraction of Path II (2.10)
ϕ_P^{II}	Volume fraction of polymer in Path II (2.1)
ϕ_P^{III}	Volume fraction of polymer in Path III (2.2)
ϕ_V^{II}	Volume fraction of void or diluent in Path II (2.1)
ϕ_Z^{II}	Volume fraction of zeolite in Path II (2.3)
ϕ_Z^{III}	Volume fraction of zeolite in Path III (2.2)
ϕ_P^o	Overall volume fraction of polymer (2.5)
ϕ_V^o	Overall volume fraction of void or diluent (2.5)
ϕ_Z^o	Overall volume fraction of zeolite (2.5)
ϕ_P^*	Volume fraction of polymer in original solution (2.7)
ϕ_V^*	Volume fraction of diluent in original solution (2.8)

Appendix B: Matlab Code

The files listed below are available electronically on a CD enclosed with this dissertation. Copies of the disk are available from D.R. Lloyd at *drl@che.utexas.edu* or by mail at:

Professor D.R. Lloyd
1 University Station, C0400
Austin, TX 78712-0231

All of these programs were coded in Matlab. Extensive comments are also included within each program.

B.1 2-DIMENSIONAL LATTICE MODEL CODE

Percolation2D.m

1. User-defined variables are input
2. Cells are placed into 2-D space
3. Pores are placed around cells
4. Cells are related to their neighboring cells through pores
5. Pores are closed to reach desired starting pores/cell value
6. Zeolite particles are added
7. Connectivity determination is performed either visually by plotting or mathematically with percolation theory.

B.2 3-DIMENSIONAL LATTICE MODEL CODE

Percolation3D.m

1. User-defined variables are input
2. Cells are placed into 3-D space

3. Pores are placed around cells
4. Cells are related to their neighboring cells through pores
5. Pores are closed to reach desired starting pores/cell value
6. Zeolite particles are added
7. Connectivity determination is performed either visually by plotting or mathematically with percolation theory.

B.3 3-DIMENSIONAL RANDOM DROPLET PLACEMENT MODEL CODE

RandomDroplet3D.m

1. User-defined variables are input
2. Particles are placed into 3-D space
3. Particles are randomly oriented by a 3-step coordinate transform process.
4. Small droplets are placed around zeolite particles according to constraints that they cannot overlap with each other
5. Small droplets grow according to constraints

neighbor1.m

1. Coordinates of all pores are calculated and all pores are related to their respective cells
2. Random pores are closed to reach the desired pores/cell limit

upperlower.m

1. Coordinations of starting and ending cells in the connectivity determination are found.

2. Number of starting and ending cells are calculated for use in the connectivity determination.

connectivity1.m

1. Stepping through the list of starting cells, one million attempts are made to connect from cell to cell through open pores.
2. If a cell in the list of ending points is reached, program prints "connected"
3. If one million attempts fail, program prints "not connected"
4. Program repeats for y- and z-directions.

neighbornew.m

1. Cells are related to neighbors through open pores (determined in neighbor1.m)
2. Cells are related to neighboring particles by looking at particles as if they are actually cells themselves, thus increasing the number of neighbors each cell has.

connectivity2.m

1. Stepping through the list of starting cells, one million attempts are made to connect from cell to cell or cell to particle.
2. If a cell in the list of ending point is reached, program prints "connected".
3. If one million attempts fail, program prints "not connected"
4. Program repeats for y- and z-directions

Appendix C: Compression Molding

C.1 Compression Molding Procedure

To produce samples large enough for flux tests, compression molding was attempted. Previous work on compression molding TIPS membranes had one major drawback – diluent evaporation [1]. By heating a sample in an environment that is not saturated with diluent vapor, large amounts of diluent are lost, changing the phase separation characteristics of the membranes to an irreproducible extent.

In this work, slices of polymer−diluent−zeolite sample were taken from a test tube prepared as described in Section 3.4 (see Section 3.2 for material description), and were placed between two aluminum plates lined with 0.13 mm Teflon sheets. One side of the mold had a 0.25 mm recess in which the membrane forms. The plates were clamped together with two large binder clips and placed in a large glass dessicator that had been preheated to the necessary formation temperature with a small amount of diluent inside the dessicator to produce a saturated vapor atmosphere. Once the mold was placed into the dessicator and the dessicator sealed, the dessicator was placed back in the oven where the solid sample can melt and homogenize for about 30 minutes. The dessicator was then removed from the oven, the mold was removed from the dessicator, and allowed to cool either in air or in a water bath, depending on the desired membrane cell sizes. Solidified membranes were removed from the mold, extracted, and dried in air without restraint.

The drawbacks to this batch processing method begin with processing time. A long period of time was required to make the membranes, even if 3 or 4 membranes were made in the dessicator at a time, since the samples must first be mixed in a test tube for at least 24 hours. Furthermore, the mixing of the samples could not take place in the mold and the zeolites settled to the bottom of the mold once the sample had melted. The result

was a lack of repeatability from sample to sample. Despite this irreproducibility, the compression molding process was useful in screening a variety of potential systems for use to form ZeoTIPS structures.

C.2 COMPRESSION MOLDING MEMBRANE IMAGES

Poly(ethylene co-acrylic acid) (EAA) produced promising ZeoTIPS structures via compression molding when diphenyl ether (DPE) was used as diluent (see Figure C.1). Extrusion was used to mimic these results, but the cooling rate in the extrusion process was too fast relative to the compression mold and produced membranes with cells of diameter significantly smaller than desired.

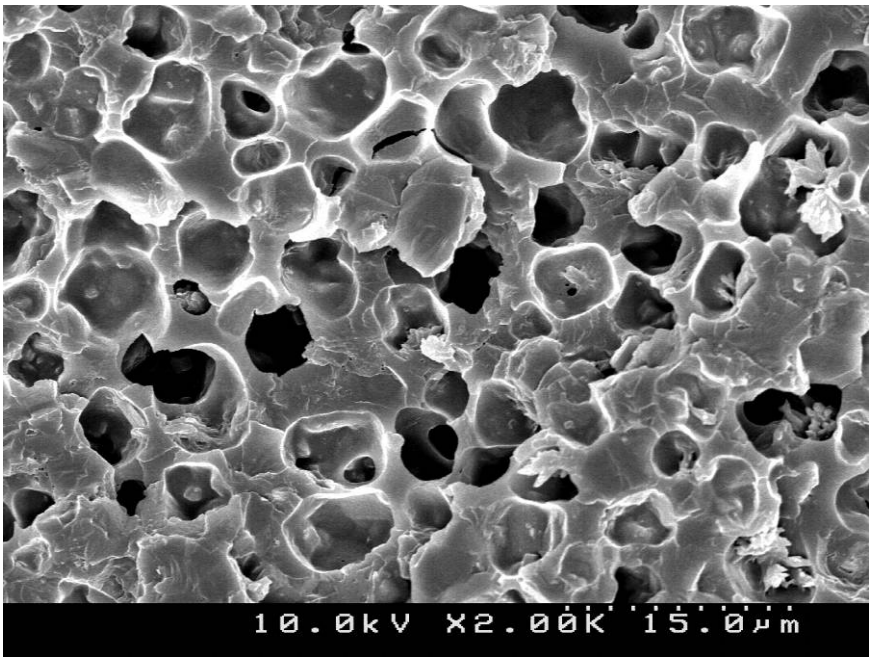

Figure C.1: SEM image of a 25 wt-% polymer EAA15−DPE ZeoTIPS membrane with 30 wt-% zeolite loading formed in a compression mold and air-cooled.

The system of poly(methyl methacrylate)−1,4-butanediol produced favorable ZeoTIPS structures via the compression molding process, as shown in Figure C.2. However, these membranes were extremely brittle and were impossible to test.

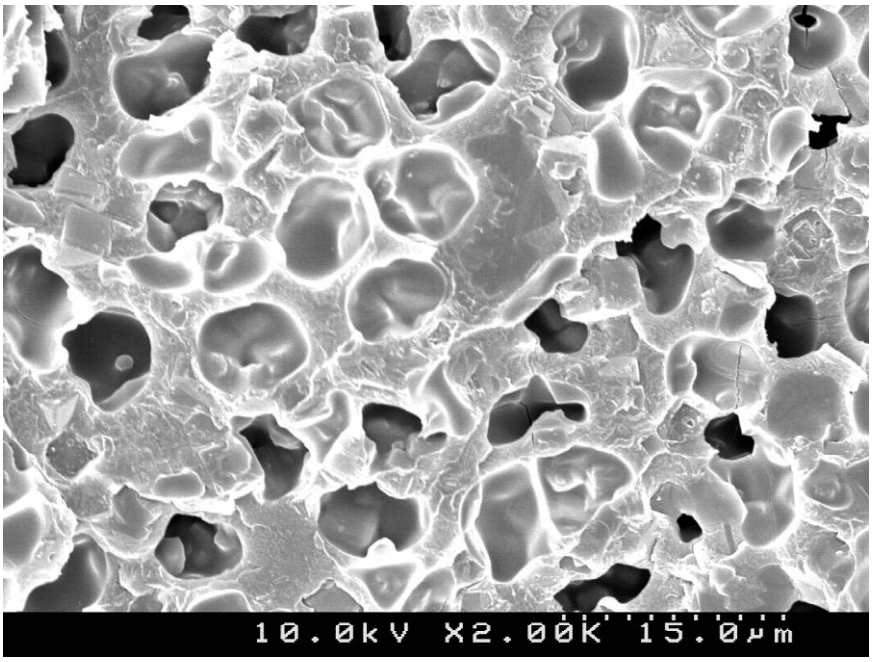

Figure C.2: SEM image of a 30 wt-% polymer poly(methyl methacrylate)−1,4-butanediol ZeoTIPS membrane with 30 wt-% zeolite loading formed in a compression mold and air-cooled.

The best ZeoTIPS structure (see Figure C.3) was obtained with cellulose triacetate, which is a water permeable polymer. Attempts were made to extrude this system, but were unsuccessful because the equipment was unable to process a system of such low viscosity.

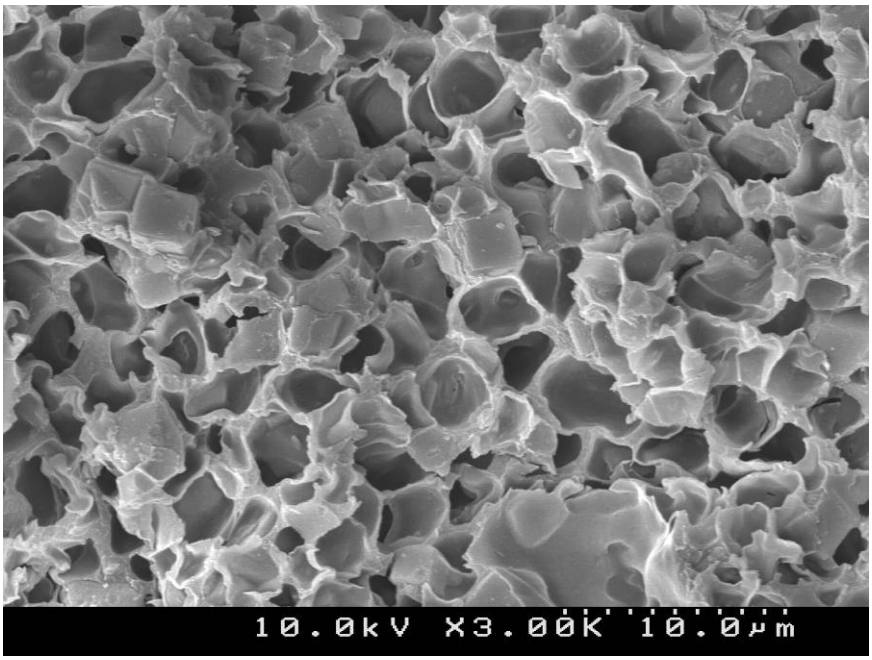

Figure C.3: SEM image of a 25 wt-% polymer cellulose triacetate−2-ethyl-1,3-hexanediol ZeoTIPS membrane with 30 wt-% zeolite loading formed in a compression mold and air-cooled.

C.3. REFERENCES

1 D.S. Martula, *Coalesence-Induced Coalescence in Polymeric Membrane Formation*, Dissertation (2000) 261.

Appendix D: Thermally Induced Phase Separation Polymer−Diluent Systems Used in This Research

D.1 Liquid−Liquid Thermally Induced Phase Separation Systems

The following polymer−diluent systems were found to undergo L−L TIPS upon cooling. To the best of the author's knowledge, these systems have not been mentioned in the literature prior to this work. While phase diagrams were not produced for all of these systems, images of each are included to illustrate the characteristics of each system.

The system of poly(ethylene-co-acrylic acid)−mineral oil (see Section 3.2 for material descriptions) is a very inexpensive system that homogenizes quickly. It is also somewhat unique in that it involves a hydrophilic polymer and hydrophobic diluent. The membrane shown in Figure D.1 was formed using the hot stage method outlined in Chapter 3 and was heated to 150ºC and held for 10 minutes before cooling at 50ºC/min.

The system of polyethersulfone(PES)−cyclohexanol is also easily formed and the membrane has good durability. The membrane shown in Figure D.2 was formed using the hot stage method outlined in Chapter 3 and was heated to 160ºC and held for 10 minutes before cooling at 50ºC/min. It should be noted that the boiling point of cyclohexanol is too low to form this membrane at atmospheric pressure.

The system of poly(methyl methacrylate)−polyethylene glycol (PMMA−PEG) is very interesting because membranes can be formed from a range of PEG molecular weights, and as shown in Figure D.3, the system forms very regular cell sizes. The membrane shown in Figure D.3 was formed using the hot stage method outlined in Chapter 3 and was heated to 160ºC and held for 10 minutes before cooling at 50ºC/min.

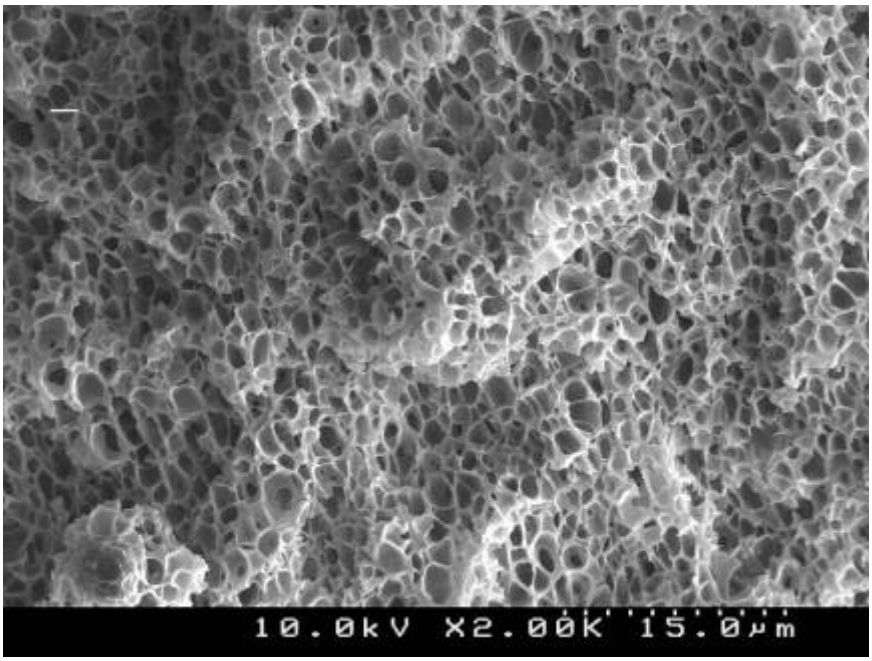

Figure D.1: SEM image of a 25 wt-% polymer EAA(15 wt-% acrylic acid)−mineral oil membrane cooled at 50ºC/min.

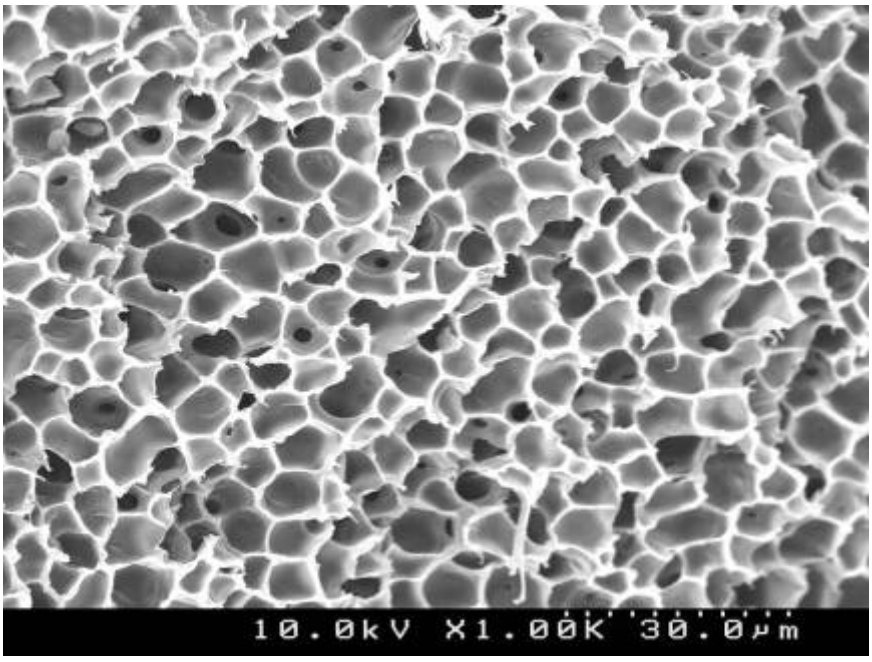

Figure D.2: SEM image of a 25 wt-% polymer polyethersulfone−cyclohexanol membrane cooled at 50ºC/min.

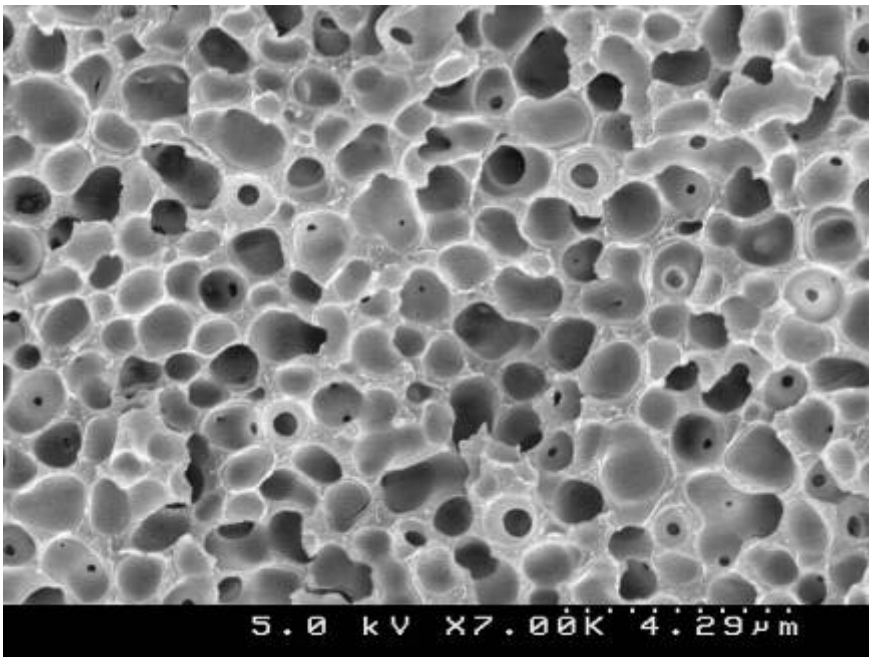

Figure D.3: SEM image of a 25 wt-% polymer PMMA−PEG200 membrane cooled at 50ºC/min.

The system of PMMA−dioctyl phthalate was investigated to determine if a small amount of dioctyl phthalate could remain in the PMMA matrix and plasticize sufficiently to give the membrane some flexibility. This was not the case; using IPA as the extractant, enough dioctyl phthalate was removed to leave a very brittle membrane. The membrane shown in Figure D.4 was formed using the hot stage method outlined in Chapter 3 and was heated to 150ºC and held for 10 minutes before cooling at 125ºC/min.

Additional L−L TIPS systems of which micrographs were not taken but exhibit cellular structures include PES−phenyl benzoate and PES−bisphenol-A.

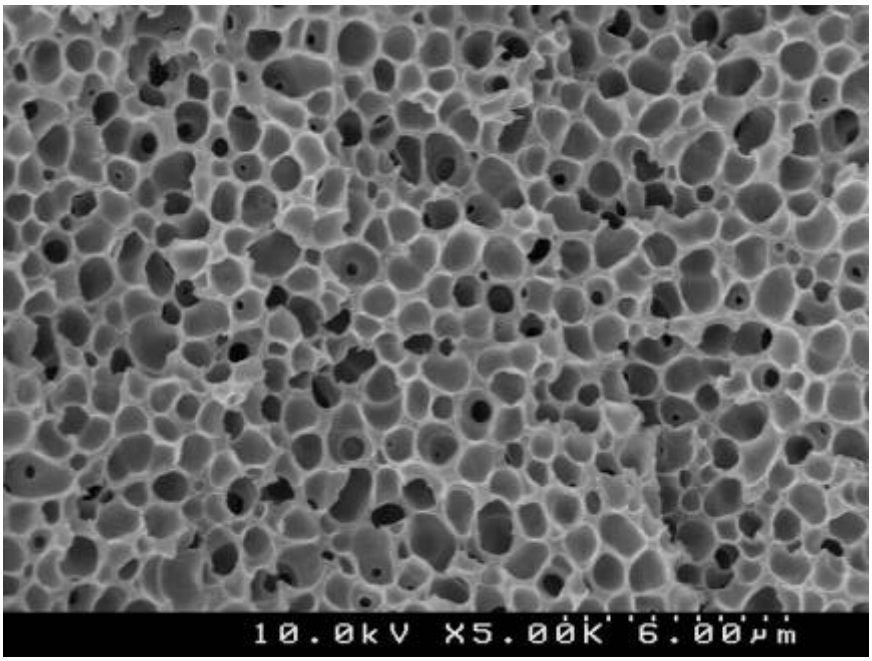

Figure D.4: SEM image of a 30 wt-% polymer PMMA−dioctyl phthalate membrane cooled at 125ºC/min.

D.2 LIQUID−SOLID THERMALLY INDUCED PHASE SEPARATION SYSTEMS

A variety of L−S TIPS systems were found during the course of this research, and they are described below. To the best of the author's knowledge, these systems have not been reported in the literature prior to this work.

The PES−benzoic acid system was well documented in Chapter 6, although additional images are included here for comparison to other L−S TIPS systems. The membranes shown in Figure D.5 was formed using the hot stage method outlined in Chapter 3 and was heated to 180ºC and held for 10 minutes before cooling at 125ºC/min.

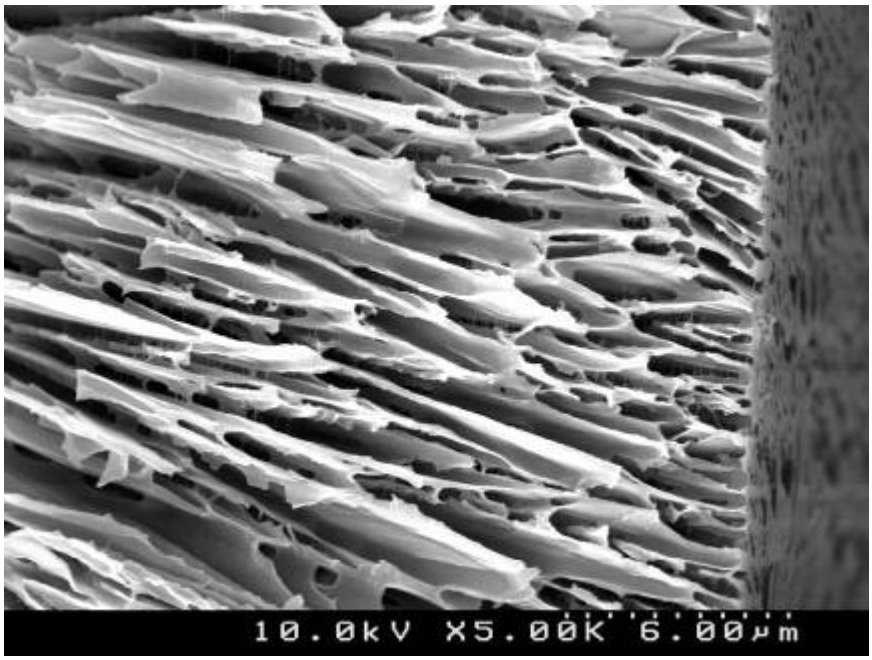

(a)

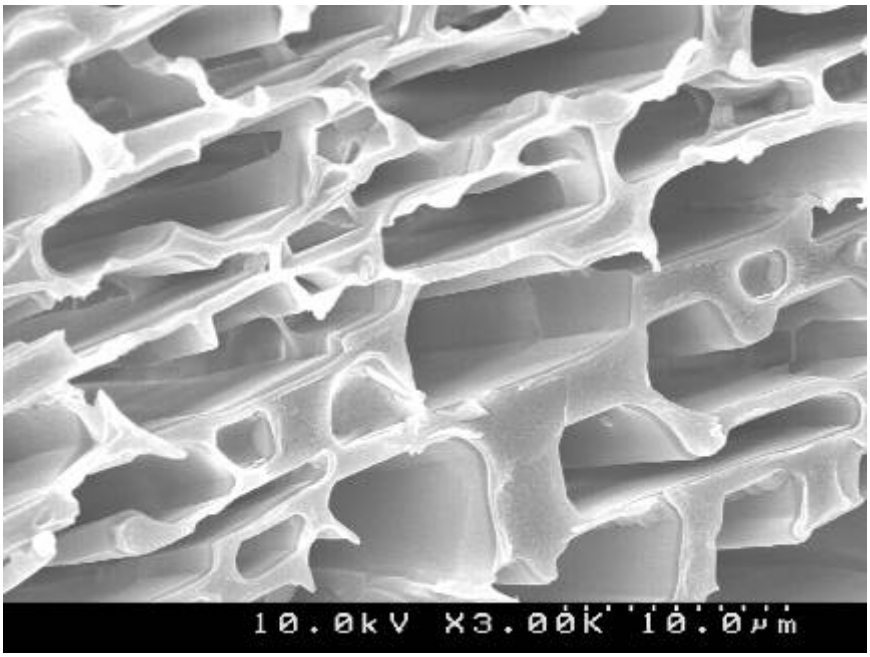

(b)

Figure D.5: SEM image of a 30 wt-% polymer PES−benzoic acid membrane cooled at 125ºC/min and broken (a) parallel to the direction of crystal growth and (b) perpendicular to the direction of crystal growth.

Ultem, a polyetherimide, is a commercial gas separation polymer that was found to be soluble in benzoic acid at high temperatures as well. The result was a more regular crystal shape, although of an oblong nature. This structure may yield good selectivity and less flux decline during filtration than a membrane with circular pores, since a particle large enough to be stopped by the pore will not fully block flux through the pore. The membrane shown in Figure D.6 was formed using the hot stage method outline in Chapter 3 and was heated to 180ºC and held for 10 minutes before cooling at 50ºC/min.

Less successful L−S TIPS membranes were formed with EVAc and PMMA with benzoic acid, with PES−resorcinol, as shown in Figure C.7-C.9. It is important to note that the crystals in the EVAc−benzoic acid system were not sheet-like under all processing conditions. Under the fast cooling rates of extrusion, these membranes had much more narrow crystals. Benzoic acid in PMMA membranes formed large, irregular sheets under all conditions studied, and PES−resorcinol membranes are discussed in Chapter 6. All of these membranes were formed using the hot stage method outline in Chapter 3 and were heated to 160ºC and held for 10 minutes before cooling.

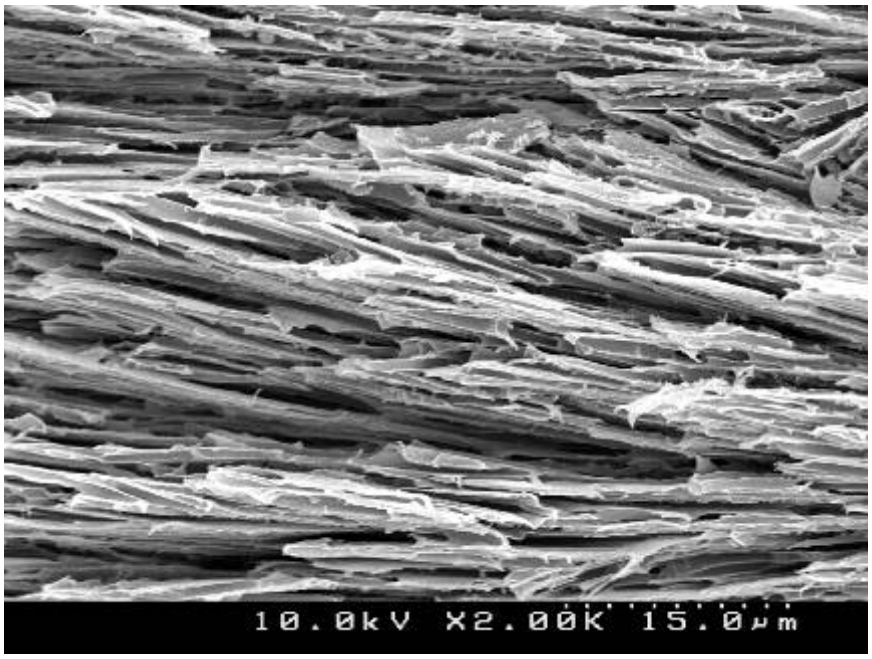

(a)

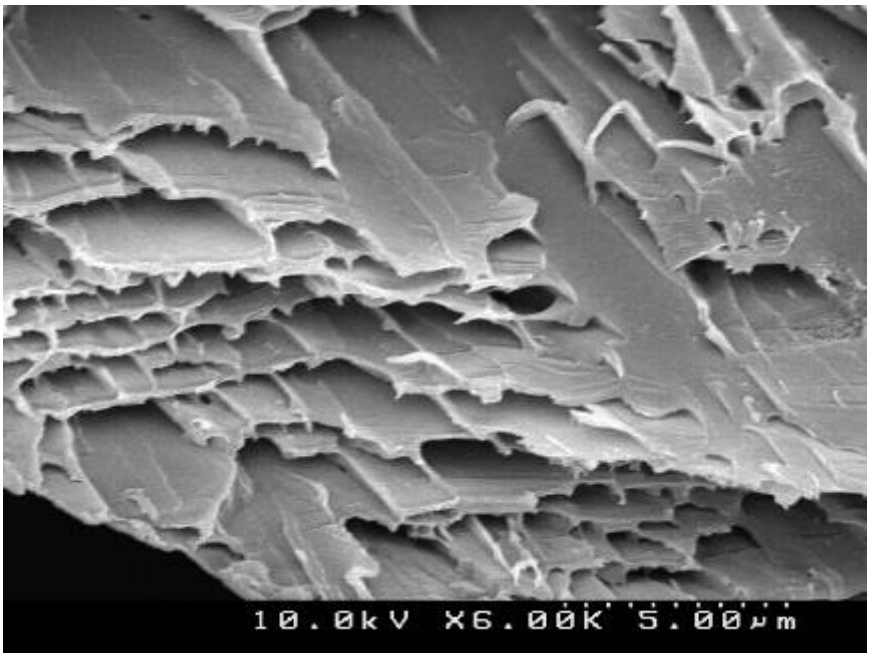

(b)

Figure D.6: SEM images of a 30 wt-% polymer polyetherimide(Ultem)−benzoic acid membrane cooled at 50ºC/min.

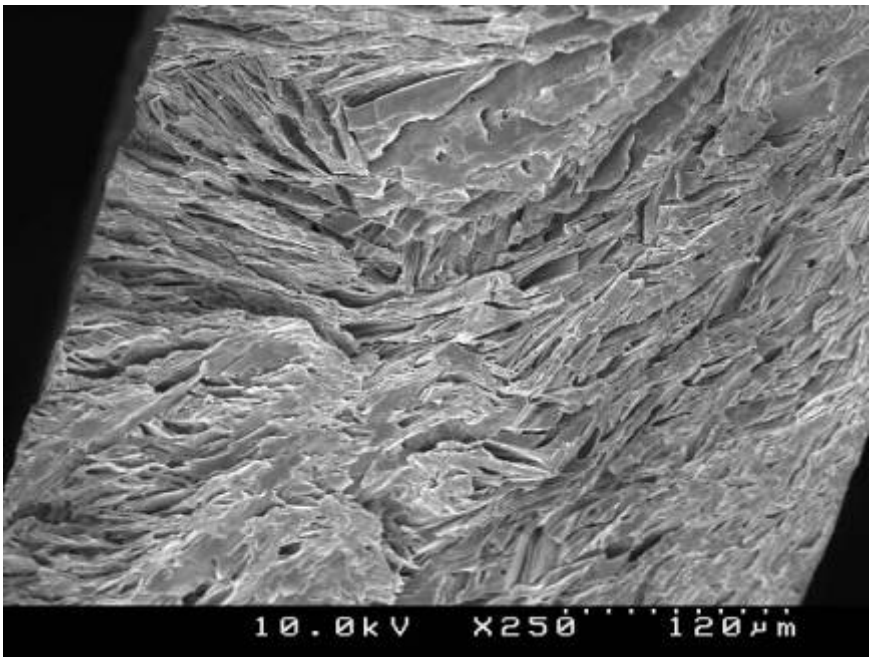

Figure D.7: SEM image of a 30 wt-% polymer EVAc(26.7 wt-% vinyl acetate)−benzoic acid membrane cooled at 50ºC/min.

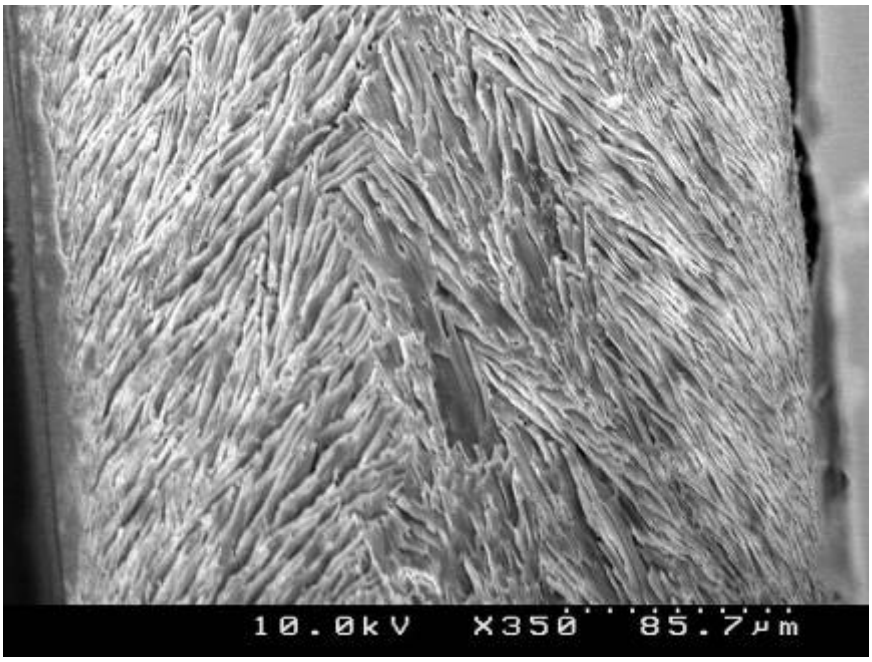

Figure D.8: SEM image of a 50 wt-% polymer PMMA−benzoic acid membrane cooled at 50ºC/min.

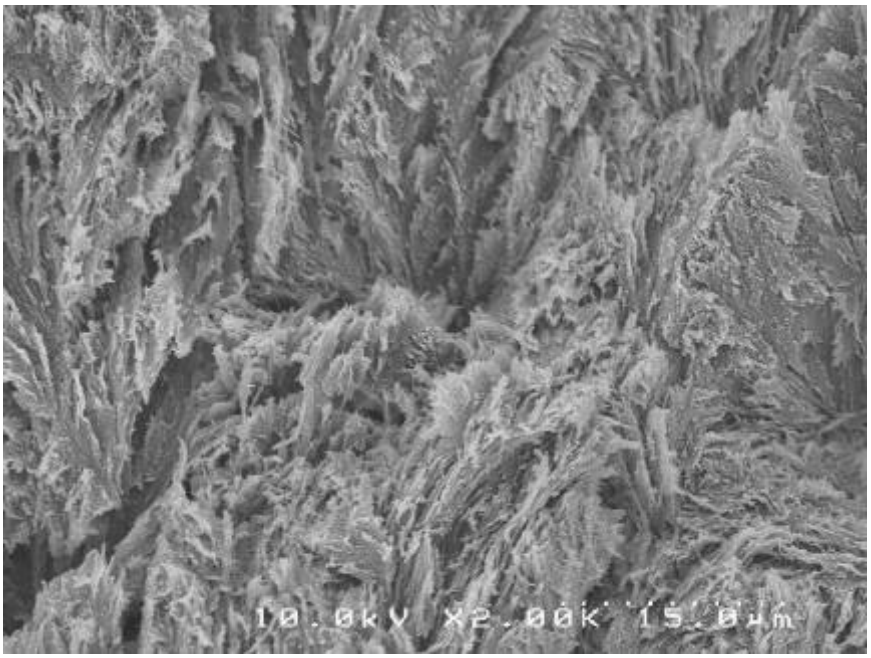

Figure D.9: SEM image of a 30 wt-% polymer PES−resorcinol membrane cooled at 1ºC/min.

References

A. Alwattari, *Thermally induced phase separation of isotactic polyproylene and hexamethylbenzene*, Dissertation, The University of Texas at Austin, 1990.

A.A. Alwattari and D.R. Lloyd, *Isothermal crystallization of isotactic polypropylene-hexamethylbenzene blends: crystal morphology*, Polymer, 35 (1994) 2710-2715.

A.A. Alwattari and D.R. Lloyd, *Isothermal crystallization of isotactic polypropylene - hexamethylbenzene blends: kinetics analysis*, Polymer, 39 (1998) 1129-1137.

A.A. Alwattari and D.R. Lloyd, *Microporous membrane formation via thermally-induced phase separation. VI. Effect of diluent morphology and relative crystallization kinetics on polypropylene membrane structure*, Journal of Membrane Science, 64 (1991) 55-68.

T.L. Barr, *Modern ESCA: The Principles and Practice of X-Ray Photoelectron Spectroscopy*, CRC Press, Boca Raton, 1994.

A.F.M. Barton, *CRC Handbook of solubility parameters and other cohesion parameters*, CRC Press, Boca Raton, Florida, 1983.

B.F. Barton and A.J. McHugh, *Modeling the Dynamics of Membrane Structure Formation in Quenched Polymer Solutions*, Journal of Membrane Science, 166 (2000) 119-125.

M.T. Batarseh, *Formation of anisotropic hollow fiber membranes via TIPS*, Dissertation, The University of Texas at Austin, 1999.

T. Bein, *Synthesis and Applications of Molecular Sieve Layers and Membranes*, Chemistry of Materials, 8 (1996) 1626-1653.

T.C. Bowen, R.D. Noble, and J.L. Falconer, *Fundamentals and applications of pervaporation through zeolite membranes*, Journal of Membrane Science, 245 (2004) 1-33.

J. Brandrup and E.H. Immergnt, (Eds.), Polymer Handbook, New York, 1975.

G.T. Caneba and D.S. Soong, *Polymer membrane formation through the thermal-inversion process. 2. Mathematical modeling of membrane structure formation*, Macromolecules, 18 (1985) 2545-2555.

C.R. Cannon, *Cellulose acetate reverse osmosis desalination membranes*, United States Patent 3285765, 1966.

A.J. Castro, *Methods for making microporous products*, US Patent 4,247,498, 1981.

A.K. Chesters, *The modelling of coalescence processes in fluid-liquid dispersions: a review of current understanding*, Transactions of the Institute of Chemical Engineers, 69 (1991) 259-270.

B.V. Crist, *Handbook of monochromatic XPS spectra*, Wiley, Chichester, New York, 2000.

Y. Ding, R. Wu, and Q. Lin, *The chemoselective preparation of the substituted phenyl benzoates using RE-Y zeolite as catalyst.* , Synthetic Communications, 32 (2002) 2149-2153.

L. Li, J. Dong, T.M. Nenoff, and R. Lee, *Reverse osmosis of ionic aqueous solutions on a MFI zeolite membrane*, Desalination, 70 (2004) 309-316.

P.D. Graham, A.J. Pervan, and A.J. McHugh, *The dynamics of Thermal-Induced Phase Separation in PMMA solutions*, Macromolecules, 30 (1997) 1651-1655.

H.-M. Guan, T.-S. Chung, Z. Huang, M.L. Chng, and S. Kulprathipanja, *Poly(vinyl alcohol) multilayer mixed matrix membranes for the dehydration of ethanol-water mixture*, Journal of Membrane Science, 268 (2006) 113-122.

P.L. Hanks and D.R. Lloyd, Deterministic model for matrix solidification in liquid-liquid thermally induced phase separation, Journal of Membrane Science, 306 (2007) 125-133.

T. Hasegawa, D.S. Martula, D.R. Lloyd, and R.T. Bonnecaze, *Coalescence-induced coalescence: calculation of the velocity field*, Physics of Fluids, in preparation (2000).

C.-C. Hu, T.-C. Liu, K.-R. Lee, R.-C. Ruann, and J.-Y. Lai, *Zeolite-filled PMMA composite membranes: influence of coupling agent addition on gas separation properties*, Desalination, 193 (2006) 14-24.

Z. Huang, Y. Li, R. Wen, M.m. Teoh, and S. Kulprathipanja, *Enhanced gas separation properties by using nanostructured PES-Zeolite 4A mixed matrix membranes*, Journal of Applied Polymer Science, 101 (2006) 3800-3805.

S. Husain and W.J. Koros, *Mixed matrix hollow fiber membranes made with modified HSSZ-13 zeolite in polyetherimide polymer matrix for gas separation*, Journal of Membrane Science, 288 (2007) 195-207.

M. Jia, K.V. Peinemann, and R.D. Behling, *Molecular sieving effect of the zeolite-filled silicone rubber membranes in gas permeation*, Journal of Membrane Science, 57 (1991) 289-96.

L.Y. Jiang, T.S. Chung, C. Cao, Z. Huang, and S. Kulprathipanja, *Fundamental understanding of nano-sized zeolite distribution in the formation of the mixed matrix single- and dual-layer asymmetric hollow fiber membranes*, Journal of Membrane Science, 252 (2005) 89-100.

J. Karger and D.M. Ruthven, *Diffusion in zeolites and other microporous solids*, Wiley-Interscience Publications, New York, 1992.

W.F. Kern and J.R. Bland, *Solid Mensuration with Proofs*, 2nd ed, Wiley, New York, 1948.

I. Kim, K. Lee, and T. Tak, *Preparation and characterization of integrally skinned uncharged polyetherimide asymmetric nanofiltration membrane*, Journal of Membrane Science, 183 (2001) 235-247.

S.S. Kim, G.B.A. Lim, A.A. Alwattari, Y.F. Wang, and D.R. Lloyd, *Microporous membrane formation via thermally-induced phase separation. V. Effect of diluent mobility and crystallization on the structure of isotactic polypropylene membranes*, Journal of Membrane Science, 64 (1991) 41-53.

S.S. Kim and D.R. Lloyd, *Microporous membrane formation via thermally-induced phase separation. III. Effect of thermodynamic interactions on the structure of isotactic polypropylene membranes*, Journal of Membrane Science, 64 (1991) 13-29.

S.S. Kim and D.R. Lloyd, *Thermodynamics of polymer–diluent systems for TIPS. III. Liquid–liquid phase separation systems*, Polymer, 33 (1992) 1047-1057.

S. Kulprathipanja, *Mixed Matrix Membrane Development*, Annals of the New York Academy of Sciences, 984 (2003) 361-369.

S. Kulprathipanja, *Separation of gases by means of mixed matrix membranes*, United States Patent 5127925, 1988.

S. Kulprathipanja, R.W. Neuzil, and N.N. Li, *Separation of fluids by means of mixed matrix membranes*, United States Patent 4740219, 1988.

I. Kumakiri, T. Yamaguchi, and S. Nakao, *Application of a zeolite A membrane to reverse osmosis process*, Journal of Chemical Engineering of Japan, 33 (2000) 333-336.

B. Kunst and S. Sourirajan, *Effect of casting conditions on the performance of porous cellulose acetate membranes in reverse osmosis.* , Journal of Applied Polymer Science, 14 (1970) 723-733.

J.M. Larson and S.H. Gryska, *Sorbent-filled polyolefin/wax membranes made via thermally induced phase separation process and adsorption properties.*, Polymer Materials Science and Engineering, 77 (1997) 361-362.

A. Laxminarayan, K.S. McGuire, S.S. Kim, and D.R. Lloyd, *Effect of initial composition, phase separation temperature, and polymer crystallization on the formation of microcellular structures via TIPS*, Polymer, 35 (1994) 3060-3068.

Y. Li, T.-S. Chung, C. Cao, and S. Kulprathipanja, *The effects of polymer chain rigidification, zeolite pore size and pore blockage on polyethersulfone (PES)-zeolite A mixed matrix membranes*, Journal of Membrane Science, 260 (2005) 45-55.

G.B.A. Lim, S.S. Kim, Q. Ye, Y.F. Wang, and D.R. Lloyd, *Microporous membrane formation via thermally-induced phase separation. IV. Effect of isotactic polypropylene crystallization kinetics on membrane structure*, Journal of Membrane Science, 64 (1991) 31-40.

B. Liu, Q. Du, and Y. Yang, *The phase diagrams of EVAL and PEG in relation to membrane formation*, Journal of Membrane Science, 180 (2000) 81-92.

D.R. Lloyd, J.W. Barlow, and K.E. Kinzer, *Microporous membrane formation via thermally-induced phase separation*, in: K.K. Sirkar and D.R. Lloyd (Eds.), New Membrane Materials and Processes for Separation, AIChE Symposium Series 261, New York, 1988.

D.R. Lloyd, K.E. Kinzer, and H.S. Tseng, *Microporous membrane formation via thermally-induced phase separation. I. Solid-liquid phase separation*, Journal of Membrane Science, 52 (1990) 239-261.

D.R. Lloyd, S.S. Kim, and K.E. Kinzer, *Microporous membrane formation via thermally-induced phase separation. II. Liquid-liquid phase separation*, Journal of Membrane Science, 64 (1991) 1-11.

R. Mahajan, R. Burns, M. Schaeffer, and W.J. Koros, *Challenges in forming successful mixed matrix membranes with rigid polymeric materials*, Journal of Applied Polymer Science, 86 (2002) 881-890.

R. Mahajan and W.J. Koros, *Factors controlling successful formation of mixed-matrix gas separation materials*, Industrial & Engineering Chemistry Reasearch, 39 (2000) 2692-2696.
R. Mahajan and W.J. Koros, *Mixed matrix membrane materials with glassy polymers. Part 1*, Polymer Engineering and Science, 42 (2002) 1420-1431.
R. Mahajan and W.J. Koros, *Mixed matrix membrane materials with glassy polymers. Part 2*, Polymer Engineering and Science, 42 (2003) 1432-1441.
D.S. Martula, *Coalesence-Induced Coalescence in Polymeric Membrane Formation*, Dissertation (2000) 261.
D.S. Martula, T. Hasegawa, D.R. Lloyd, and R.T. Bonnecaze, *Coalescence-induced coalescence of inviscid droplets in a viscous fluid*, Journal of Colloid and Interface Science, 232 (2000) 241-253.
D.S. Martula, R.T. Bonnecaze, and D.R. Lloyd, *The effects of viscosity on coalescence-induced coalescence*, International Journal of Multiphase Flow, 29 (2003) 1265-1282.
H. Matsuyama, S. Berghmans, and D.R. Lloyd, *Formation of hydrophilic microporous membranes via thermally induced phase separation*, Journal of Membrane Science, 142 (1998) 213-224.
H. Matsuyama, S. Berghmans, M.T. Batarseh, and D.R. Lloyd, *Effects of thermal history on anisotropic and asymmetric membranes formed by thermally induced phase separation*, Journal of Membrane Science, 142 (1998) 27-42.
H. Matsuyama, S. Berghmans, M.T. Batarseh, and D.R. Lloyd, *Formation of anisotropic and asymmetric membranes via thermally induced phase separation*, in: I. Pinnau and B.D. Freeman (Eds.), Membrane Formation and Modification, ACS Symposium Series, 744, ACS Press, Washington, DC, 2000, pp. 23-41.
C. Maxwell, *Treatise on Electricity and Magnetism*, 1, Oxford University Press, London, 1873.
K.S. McGuire, *Membrane formation via liquid-liquid thermally induced phase separation*, Dissertation, The University of Texas at Austin, 1995.
K.S. McGuire, A. Laxminarayan, and D.R. Lloyd, *Kinetics of droplet growth in liquid-liquid phase separation of polymer-diluent systems: experimental results*, Polymer, 36 (1995) 4951-4960.
K.S. McGuire, A. Laxminarayan, D.S. Martula, and D.R. Lloyd, *Kinetics of droplet growth in liquid-liquid phase separation of polymer-diluent systems: model development*, Journal of Colloid and Interface Science, 182 (1996) 46-58.
K.S. McGuire, D.R. Lloyd, and G.B.A. Lim, *Microporous membrane formation via thermally-induced phase separation. VII. Effect of dilution, cooling rate, and nucleating agent addition on morphology*, Journal of Membrane Science, 79 (1993) 27-34.
T.T. Moore, R. Mahajan, D.Q. Vu, and W.J. Koros, *Hybrid membrane materials comprising organic polymers with rigid dispersed phases*, AIChE Journal, 50 (2004) 311-321.
T.T. Moore and W.J. Koros, *Non-ideal effects in orgain-inorganic materials for gas separation membranes*, Journal of Molecular Structure, 739 (2005) 87-96.

M. Noack, P. Kolsch, R. Schafer, P. Toussaint, and J. Caro, *Molecular Sieve Membranes for Industrial Application: Problems, Progress, Solutions*, Chemical Engineering Technology, 25 (2002) 221-230.

S. Obst and H. Bradaczek, *Molecular dynamics study of the structure and dynamics of the hydration shell of alkaline and alkaline-earth metal cations*, Journal of Physical Chemistry, 100 (1996) 15677-15687.

E. Okumus, T. Gurkan, and L. Yilmaz, *Development of a mixed-matrix membrane for pervaporation*, Separation Science and Technology, 29 (1994) 2451.

A.J. Paine, *Mechanisms and Models for Copper Mediated Nucleophilic Aromatic Substitution. 2. A Single Catalytic Species from Three Different Oxidation States of Copper in an Ullmann Synthesis of Triarylamines*, Journal of the American Chemical Society, 109 (1987) 1496-1502.

D.R. Paul and D.R. Kemp, *The diffusion time lag in polymer membranes containing adsorptive fillers*, Journal of Polymer Science, 41 (1973) 79-93.

L.M. Robeson, *Correlation of separation factor versus permeability for polymeric membranes*, Journal of Membrane Science, 62 (1991) 165-185.

L.M. Robeson, A. Noshay, M. Matzner, and C.N. Merriam, *Physical property characteristics of pulysulfone/poly(dimethylsiloxane) block copolymers*, Angewandte Makromolekulare Chemie, 29 (1973) 47-62.

D.M. Ruthven and R.I. Derrah, *Diffusion of Monatomic and Diatomic Gases in 4A and 5A Zeolites*, Journal of the Chemical Society, Faraday Transactions, 71 (1975) 2031.

M. Sahimi, *Flow and Transport in Porous Media and Fractured Rock: From Classical Methods to Modern Approaches*, VCH, Weinheim, Germany, 1995. pages 482.

S.R. Schmidt, *Catalysis of Organic Reactions*, CRC Press, Boca Raton, FL, 2006.

M.X. Shang, H. Matsuyama, M. Teramoto, D.R. Lloyd, and N. Kubota, *Preparation and membrane performance of poly(ethylene-co-vinyl alcohol) hollow fiber membrane via thermally induced phase separation*, Polymer, 44 (2003) 7441-7447.

P. Shao and R.Y.M. Huang, *Polymeric membrane pervaporation*, Journal of Membrane Science, 287 (2007) 162-179.

J.A. Sheffel and M. Tsapatsis, *A model for the performance of microporous mixed matrix membranes with oriented selective flakes*, Journal of Membrane Science, 295 (2007) 50-70.

A. Sheludko, *Thin liquid films*, Advances in Colloid and Interface Science, 1 (1967) 391-464.

P. Smith and A.J. Pennings, *Eutectic crystallization of pseudo binary systems of polyethylene and high melting diluents*, Polymer, 15 (1974) 413-419.

Y. Song, F. Liu, and B. Sun, *Preparation, characterization, and application of thin film composite nanofiltration membranes*, Journal of Applied Polymer Science, 95 (2005) 1251-1261.

M.G. Suer., N. Bac, and L. Yilmaz, *Gas permeation properties of polymer-zeolite mixed matrix membranes*, Journal of Membrane Science, 91 (1994) 77.

J.S. Taylor and E.P. Jacobs, *Reverse osmosis and nanofiltration*, in: J. Mallevialle, P.E. Odendaal, and M.R. Wiesner (Eds.), Water Treatment Membrane Processes, McGraw-Hill, New York, 1996.

S.B. Teli, G.S. Gokavi, M. Sairam, and T.M. Aminabhavi, *Mixed matrix membranes of poly(vinyl alcohol) loaded with phosphomolybdic heteropolyacid for the pervaporation separation of water-isopropanol mixtures*, Colloids and Surfaces A, 301 (2007) 55-62.

P.C. van der Heijden, M.H.V. Mulder, and M. Wessling, *Phase behavior of polymer-diluent systems characterized by temperature modulated differential scanning calorimetry*, Thermochimica Acta, 378 (2001) 27-34.

I.F.J. Vankelecom, S.V.d. broeck, E. Merckx, H. Geerts, P. Grobet, and J.B. Uytterhoeven, *Silylation to improve incorporation of zeolites in polyimide films*, Journal of Physical Chemistry, 100 (1996) 3753-3758.

D.W. Van Krevelen, *Properties of Polymers*, 3rd ed, Elsevier, New York, 1990. pages 427.

M.E. van Leeuwen, *Derivation of Stockmayer potential parameters for polar fluids*, Fluid Phase Equilibria, 99 (1994) 1.

P.W. Voorhees, *Ostwald ripening of two-phase mixtures*, Annual Reviews of Materials Science, 22 (1992) 197-215.

D. Vorlander, *Investigation of the molecular form by means of crystalline liquids*, Z. Physik Chem., 105 (1923) 211-54.

H. Wang and R.H. Davis, *Droplet growth due to Brownian, Gravitational, or Thermocapillary motion and coalescence in dilute dispersions*, Journal of Colloid and Interface Science, 159 (1993) 108-118.

I.M. Wienk, R.M. Boom, M.A.M. Beerlage, A.M.W. Bulte, C.A. Smolders, and H. Strathmann, *Recent advances in the formation of phase inversion membranes made from amorphous or semi-crystalline polymers.*, Journal of Membrane Science, 113 (1996) 361-371.

L.D.S. Yadav, B.S. Yadav, and V.K. Rai, *Active-Copper-Promoted Expeditious N-Arylations in Aqueous Media under Microwave Irradiation*, Syntheis, 11 (2006) 1868-1872.

S. Zhu, Y. Dun, and Q. Wang, *Determination of solubility parameter of phenolphthalein-based poly(ether sulfone)*, Huagong Xinxing Cailiao, 33 (2005) 21-23.

C.M. Zimmerman, A. Singh, and W.J. Koros, *Tailoring mixed matrix composite membranes for gas separations*, Journal of Membrane Science, 137 (1997) 145-154.

R.J.M. Zwiers, S. Gogolewski, and A.J. Pennings, *General crystallization behavior of poly(L-lactic acid) PLLA. 2. Eutectic crystallization of PLLA*, Polymer, 24 (1983) 167-174.

Vita

Caleb Vincent Funk was born in Effingham, IL on March 4, 1982, son of Ted and Jan Funk. After graduating from Arcola High School in Arcola, IL in 2000, he entered The University of Illinois at Urbana/Champaign. While attending The University of Illinois, he studied Chemical Engineering, spent summers as an engineering intern for Baxter Healthcare International and Merck & Company, and performed undergraduate research under Dr. James Lisy in the UIUC Physical Chemistry Department. He graduated Magna Cum Laude and with Highest Honors in the Chemical Engineering Curriculum in May 2004. He began his graduate studies at The University of Texas at Austin in August 2004 and worked under Dr. Douglas Lloyd. He will work for The Dow Chemical Company upon graduation.

Permanent address: 1808 Lyndhurst Dr., Savoy, IL 61874

This dissertation was typed by the author.